SYNTHESIS OF VERTICALLY ALIGNED CNT ARRAYS USING LIQUID BASED PRECURSORS AND THEIR FUNCTIONALIZATION BY CONJUGATED POLYMERS

A THESIS
SUBMITTED TO THE DEPARTMENT OF CHEMISTRY AND
THE INSTITUTE OF ENGINEERING AND SCIENCES OF
BILKENT UNIVERSITY
IN PARTIAL FULFILLMENT OF THE REQUIREMENTS
FOR THE DEGREE
OF
MASTER OF SCIENCE

by

BERİL BAYKAL

JANUARY 2011

I certify that I have read this thesis and in my opinion it is fully adequate, in scope and quality, as a thesis of the degree of Master of Science

_____

Assist. Prof. Dr. Erman Bengü (Supervisor)

I certify that I have read this thesis and in my opinion it is fully adequate, in scope and quality, as a thesis of the degree of Master of Science

_____

Prof. Dr. Şefik Süzer

I certify that I have read this thesis and in my opinion it is fully adequate, in scope and quality, as a thesis of the degree of Master of Science

_____

Assist. Prof. Dr. Dönüş Tuncel

I certify that I have read this thesis and in my opinion it is fully adequate, in scope and quality, as a thesis of the degree of Master of Science

_____

Assoc. Prof. Dr. Oğuz Gülseren

I certify that I have read this thesis and in my opinion it is fully adequate, in scope and quality, as a thesis of the degree of Master of Science

_____

Assist. Prof. Dr.Göknur Cambaz Büke

Approved for the Institute of Engineering and Sciences

_____

Prof. Dr. Levent Onural

Director of Institute of Engineering and Sciences

ABSTRACT

SYNTHESIS OF VERTICALLY ALIGNED CNT ARRAYS USING LIQUID BASED PRECURSORS AND THEIR FUNCTIONALIZATION BY CONJUGATED POLYMERS

BERİL BAYKAL

M.S. in Chemistry

Supervisor: Assistant Prof. Dr. Erman BENGÜ

January 2011

In the first part of this work, a new solution based catalyst precursor application method is developed for growing high quality vertically aligned carbon nanotubes arrays (VANTA) through alcohol catalyzed chemical vapor deposition (AC-CVD). For this purpose, various solution based precursor preparation routes are investigated starting from γ-Al_2O_3 / $Fe(NO_3)_3.9H_2O$ mixtures and ranging to catalyst precursors prepared by mixing aqueous aluminium and iron nitrate solutions. Application of these solutions separately layer by layer on Si(100) substrate resulted in high quality dense vertically aligned CNT arrays. By varying the metal nitrate concentration in the precursor solutions, the dependence of the density and quality of CNT arrays on the catalyst layers are investigated. The CNT array quality and density are characterized by dynamic contact angle measurements using water droplets. Higher density CNT arrays resulted in higher contact angle measurements. The chemical and structural characterizations of CNTs are also done by using TEM, SEM, EDX and Raman spectroscopy. Some of the samples are found to be super-

hydrophobic even after 30 minutes of exposure to water. In this effort, application of subsequent layers of aqueous aluminium nitrate and iron nitrate on oxidized Si(100) surfaces are found to be most efficient catalyst layer preparation technique resulting in the highest density of CNT arrays.

In the second part of this work, functionalization of the synthesized CNT arrays is done for the purpose of achieving good dispersibility of CNTs in aqueous media. To this end, a new approach is used to ensure stability of the CNT-water solution. In this approach, conjugated polymer nanoparticles (CPNs) are successfully used to disperse CNTs through non-covalent functionalization of the sidewalls of CNTs. The attachment of CPNs to CNTs is characterized by SEM, EDX and TEM. Moreover, interactions are investigated by UV-VIS, and Raman spectroscopy. The interaction mechanism of polymer chains with side-walls of CNTs are further scrutinized by follow-up experiments where two different conjugated polymers with brominated-alkyl and bare alkyl groups in THF media are mixed with SWCNTs (commercial), MWCNTs and an-MWCNTs (synthesized in the first part of this study). The results of this investigation suggested a limited number of docking configurations of the polymers with the CNT side-walls. Also, it is found that the defect density of the CNT side-walls play an important role in the nature of the interaction.

Overall, in this work a cheap and effective route for application of catalyst is developed for the synthesis of dense, super-hydrophobic CNT arrays using AC-CVD. Then, well-dispersion of these CNTs is successfully achieved using CPNs. Finally, the nature of the interaction between conjugate polymers and CNTs sidewalls are investigated using experimental techniques.

Keywords: Vertically aligned CNTs, AC-CVD, functionalization, conjugated polymer nanoparticles.

ÖZET

SIVI BAZLI PREKÜRSÖRLER KULLANILARAK YÜZEYE DİK KARBON NANOTÜP SENTEZİ VE KONJUGE POLİMERLER İLE İŞLEVSELLEŞTİRMESİ

BERİL BAYKAL

Kimya Bölümü Yüksek Lisans Tezi
Tez Yöneticisi: Yard. Doç. Dr. Erman Bengü
Ocak 2011

Bu çalışmanın ilk bölümünde, yüksek kaliteli yüzeye dik karbon nanotüp sentezi yeni bir yöntem olan solusyon bazlı katalizör prekürsörlerle alkol ile catalize edilmiş kimyasal buhar çöktürme metodu kullanılarak gerçektirilmiştir. Bu amaçla, solusyon bazlı farklı yöntemler geliştirilmesi γ - $Fe(NO_3)_3.9H_2O$ karışımlarından başlayarak katalizör prekürsörlerinin alüminyum ve demir nitrat su bazlı solüsyonlarının karışımlarının hazırlanmasını kapsar. Bu solusyonların ayrı bir şekilde kat kat Si(100) alt taşı üzerine uygulanması, yüksek kaliteli ve yoğunluğu fazla yüzeye dik karbon nanotüp senteziyle sonuçlanmıştır. Metal nitrat prekürsör solüsyonlarının konsantrasyonunu değiştirerek, yüzeye dik karbon nanotüplerin yoğunluğunun ve kalitesinin katalizör katmanlarına bağlılığı araştırılmış, su damlasıyla kontak açısı ölçme yöntemiyle karakterizasyonu yapılmıştır. Yoğunluğu daha fazla olan yüzeye dik karbon nanotüplerin yüksek kontak açısı değerleri verdigi belirlenmiştir. Ayrıca karakterizasyonda Geçişli Elektron Mikroskopu (TEM), Taramalı Elektron Mikroskobu (SEM), Elektron Enerji Dağılım X-ışını (EDX) ve Raman spektroskopisi kullanılmıştır. Bazı numunerlerin super-hidrofobik oldukları

hatta yarım saat sonra bile suya karşı bu özelliklerini korudukları saptanmıştır. Bunların sonucunda, en fazla yoğunlukta yüzeye dik karbon nanotüpü eldesi için en etkili katalizör katmanı hazırlama tekniği alüminyum nitrat ve demir nitrat sulu solusyonlarının ardarda katmanlar halinde oxidize edilmiş Si(100) yüzeylerine uygulanması olduğu sonucuna varılmıştır.

Bu çalışmanın ikinci bölümünde, sentezlenen karbon nanotüplerin su ortamında iyi dispersiyonun sağlanması amacıyla işlevselleştirme uygulanmıştır. Bunun sonucunda, karbon nanotüplerin kalıcı dispersiyonu için yeni bir yöntem geliştirilmiştir. Bu yaklaşımda, karbon nanotüp duvarlarını, kovalent olmayan işlevselleştirilme yöntemi ile konjuge polimer nanotanecikleri (Conjugated Polymer Nano Particles, CPNs) kullanılarak suda karbon nanotüplerin iyi dispersiyonu sağlamıştır. Karbon nanotüplere takılmış konjuge polimerin karakterizasyonu SEM, EDX, TEM, UV-VIS, Floresan mikroskopi ve Raman kullanılarak yapılmıştır. Polimer zincirlerinin karbon nanotüp duvarıyla etkileşimini daha iyi anlamak için iki farklı tür konjuge polimer, tek duvarlı karbon nanotüp (Single Walled Carbon Nanotube, SWCNT, satın alınarak), çok duvarlı karbon nanotüp (Multi Walled Carbon Nanotube, MWCNT, ilk bölümde belirtildiği gibi sentezlenerek) ve tavlanmış çok katlı karbon nanotüp (Annealed Multi Walled Carbon Nanotube, an-MWCNT, ilk bölümdeki sentezlenen karbon nanotüplerin tavlanmasıyla) ile THF ortamında karıştırılmıştır. Sonuçlara göre, karbon nanotüp duvarlarıyla polimerlerin kısıtlı sayıda konfigürasyonda etkileşim halinde bulunduğu önerilmektedir. Ayrıca, karbon nanotüp duvarlarındaki defekt oranının etkileşimlerin doğasında önemli bir rol oynadığı görülmüştür.

Genel olarak, yoğunluğu fazla ve super-hidrofobik yüzeye dik karbon nanotüp sentezi için bu çalışmada ucuz ve etkili bir katalizör uygulaması alkol ile catalize edilmiş kimyasal buhar çöktürme kullanılarak geliştirilmiştir. Sonrasında, karbon nanotüplerin iyi dispersiyonuna konjuge polimer nanoparçacıklar kullanarak ulaşılmıştır. Son olarak, karbon nanotüpler ile konjuge polimerlerin etkileşimi deneysel yöntemlerle incelenmiştir.

Anahtar kelimeler: Yüzeye dik karbon nanotüp, alkol katalize kimyasal buhar çöktürme, işlevselleştirme, konjuge polimer nano parçacıkları.

Dedicated to my beloved family and Burak

ACKNOWLEDGEMENT

I would like to extend my gratitude to;

Asst. Prof. Dr. Erman Bengü for his supervision throughout my studies and for his enthusiasm for new ideas.

Asst. Prof. Dr. Dönüş Tuncel for her encouragement and support during my studies with the functionalization of carbon nanotubes.

Assoc. Prof. Dr. Oğuz Gülseren for fruitful discussions regarding interaction of carbon nanotubes with polymers and computational approach.

My group members Gökçe Küçükayan, Mustafa Fatih Genişel for their continuous help and understanding.

Senior project students Cansu Dal and Gizem Er and Master student Vüsala İbrahimova for their worthy contribution to this thesis.

Seda Şentürk and Safacan Kölemen for their precious friendship.

Burak Yeşilırmak and my family: Bengi, Birsen and Talat Baykal, Bedia and Ayşe Kurtar for their everlasting love and support.

ABBREVIATONS

AC-CVD - alcohol catalyzed chemical vapor deposition

AFM - atomic force microscopy

CA - contact angle

CNT(s) - carbon nanotube(s)

CP - conjugated polymer

CPN - conjugated polymer nanoparticle

CVD - chemical vapor deposition

EDX - energy-dispersive X-ray spectroscopy

DLS - dynamic light scattering

HRTEM – high resolution transmission electron microscope

FTIR - fourier transform infrared spectroscopy

MWCNT – multi walled carbon nanotube

RBM - radial breathing mode

SEM - scanning electron microscope

SWCNT - single walled carbon nanotube

TEM - transmission electron microscope

UV-VIS - ultra-violet visible

VANTA - vertically aligned carbon nanotube arrays

XPS - X-ray photoelectron spectroscopy

TABLE OF CONTENTS

LIST OF TABLES

LIST OF FIGURES

1 GENERAL INTRODUCTION

1.1 Introduction

While there is still some debate about the discovery of multi walled carbon nanotubes (MWCNTs) [1], it is largely accepted that the single walled carbon nanotubes (SWCNTs) were discovered in 1993 [2,3]. Since the discovery of carbon nanotubes, a member of carbon allotrope family, there has been an ever increasing attention regarding CNTs and their applications. Their nano-sized well-ordered structure, unique mechanical and electrical properties make them good candidates to be used in many different fields of science and technology. It is claimed that CNTs may have much more impact on the technology than the silicon revolution [4]. With their extraordinary features, CNTs are now being tested for manufacturing advanced flat panel displays [5], new carbon fibers [6], more efficient gas detectors [7], brighter x-ray sources [8] and etc.

There are numerous publications and patents on CNTs and CNT based applications, however many unsolved challenges remain. The main issue is about the large scale production of CNTs with low cost. On the other hand, desired orientation and selective growth of CNTs is being worked on. There are many approaches for the growth mechanism of CNTs but there isn't any well-accepted one for large-scale production, yet [9,10].

There are several CNT synthesis techniques but the most suitable one for continuous manufacturing is chemical vapor deposition (CVD) technique. Others are generally more expensive and can only grow powder samples. CVD is an easier technique to grow CNTs on various substrates [11]. In addition to ease of growth, carbon precursor selection covers wide range of possibilities such as; methane, ethylene, benzene, carbon monoxide or ethanol. The process includes decomposition of hydrocarbons at temperatures above 500^{o}C over a catalyst covered substrate. As catalyst, transition metals such as Fe, Ni and Co are the most used ones. For high quality CNT growth, suitable substrate selection and efficient catalyst patterning is

important. By catalyst engineering, vertically aligned carbon nanotubes arrays (VANTA) are synthesized with uniform length and distribution of CNTs on flat surfaces. Catalyst deposition can be made by two ways as e-beam deposition or application of solution based catalyst salts on substrate. First one requires expensive vacuum systems for the preparation of catalyst layer on the substrate. Also the application through vacuum is a, time consuming procedure. On the other hand, solution based precursors are simply applied on substrate and left for drying. This method is not expensive and requires much less time. The films can be modified for super-hydrophobic and self-cleaned surfaces or used as adhesives by mimicking the nature as lotus leaf [12,13] and gecko feet [14].

Another problem about CNTs is their low dispersion/solubility in any solvent. Many routes are followed to overcome this problem by dispersion and suspension under specified experimental procedures. These steps include chemical modification and functionalization. Well dispersed carbon nanotubes can open a way to be used in solution based systems. In literature, limited dispersion of CNTs is achieved by using organic solvents [15]. Some of these are cancerogenic, and also for biological applications dispersion of CNTs should be achieved in aqueous systems.

In this study, AC-CVD method is used for the growth of VANTA films. Ethanol used as carbon source. For high quality VANTA growth, a step by step optimization methodology has been followed. Firstly, γ-alumina - $Fe(NO_3)_3.9H_2O$ mixtures are used then aluminium nitrate solutions are added to catalyst design instead of powdered γ-alumina. By further improvement, a solution based sandwich method is developed and found to be most efficient catalyst layer preparation route to get high quality VANTA films. Sandwich method includes application of aqueous solutions of $Fe(NO_3)_3.9H_2O$ and $Al(NO_3)_3.9H_2O$ layer by layer for efficient catalyst design. Also, layer concentrations are varied to achieve best combination at catalyst preparation to improve CNT film quality. The resulting densely and homogenously distributed CNT films are found to be super-hydrophobic for 30 minutes without any chemical modification. It is the first time that a VANTA sample can keep super-hydrophobic character at dynamic contact angle measurements.

The dispersibility of tubes in aqueous media is achieved by functionalization of the synthesized CNTs. To get good dispersion of tubes, a new approach is used; mixture of conjugated polymer nanoparticles (CPNs) and CNTs. By non-covalent interaction of the sidewalls of CNTs by CPNs, CNT dispersion achieved up to 5:1 ratio CNT:CPN. Investigation of interaction mechanism of polymer chains and CNTs are also detected by using two different conjugated polymer types PF and PFB-B with SWCNTs, MWCNTs and an-MWCNTs. According to results there can be different wrapping mechanisms through interaction with different types of CNTs.

1.2 Objectives

The purpose of this study is to develop an effective and simple methodology to synthesize dense and high quality vertically aligned CNT films. This includes preparation of substrate and design of catalyst for achieving a homogenous dispersion of CNTs on substrate after synthesis by AC-CVD method. We started with first trying a γ-alumina - $Fe(NO_3)_3.9H_2O$ mixtures (powder-dispersion) improvement of catalyst preparation techniques are investigated. Then, a simple solution based sandwich method is investigated by our group which includes layer by layer application of aqueous solutions of $Fe(NO_3)_3.9H_2O$ and $Al(NO_3)_3.9H_2O$. By varying catalyst preparation parameters, dense and high quality CNT films are observed. To best of our knowledge it is the first time that a VANTA sample can keep super-hydrophobic character at dynamic contact angle measurements up to 30 minutes of water droplet explosure. Also, by varying applied catalyst and base layer concentrations, CNT density in the array can be adjusted to the hydrophobicity of the CNT film.

Another aspect of this study is to achieve successful dispersion of synthesized CNTs in aqueous media by functionalization of CNT side-walls. This is achieved via using a new approach that is the first time used conjugated polymer nanoparticles (CPNs) with CNTs. Moreover, the interactions of polymer chains and CNT side-walls are investigated by conjugated polymer – CNT mixtures.

1.3 Organization of the thesis

In Chapter 2, a detailed literature review of the related to CNTs, synthesis techniques, functionalization, vertically aligned carbon nanotubes and growth parameters will be covered. Also, details of hydrophobic-behavior of CNTs will be explained. Chapter 3 includes experimental procedures that are used during CNT synthesis and functionalization will be covered. Results of the experiments are provided in Chapter 4. Finally, Chapter 5 will cover conclusions of synthesis of vertically aligned CNT arrays and functionalization of CNTs. Future work section is also provided in Chapter 6.

2 LITERATURE REVIEW

2.1 Carbon nanotubes

In nature, carbon can be found in forms that significantly differ from each other in structural, chemical and physical properties. Also, the bonding properties show changes according to different allotropes. In diamond, the state of the orbitals of carbon atoms are sp^3 hybridized, forming four bonds within the lattice. This rigid and stable configuration of carbon bonds is behind the hardest material that is known. On the other hand, graphite having sp^2 hybridized graphene sheets has strong bonding in the plane, weak van der Waals bonding between planes. Another form allotrope of carbon, fullerenes is discovered in 1985 by Kroto, O'Brien, Curl and Smalley [16]. They won the Nobel Prize for chemistry in 1996. Ball-like structures, called buckyballs are another stable form of the carbon matrix by having sp^2 hybridized bonds. Carbon nanotube is an allotrope of carbon that can be considered as a rolled up graphene sheet into tubular form. The organization of the carbon atoms with different bonding angles enable the structural changes from graphite to carbon nanotubes with decreasing total energy to form stable compounds.

Carbon nanotubes can be called SWCNT or MWCNT according to the number of sidewalls. In Figure 1, differences between graphene sheet, buckball, SWCNT and MWCNT can be seen. Carbon nanotubes first got introduced to popular culture by Iijima *et al*, in 1991 [17]. High resolution TEM images of MWCNTs and graphitic planes are represented with adjacent wall spacing of ~0.34 nm. This landmark report could also be considered as the start of nanotechnology and first step into the nano-world. Nevertheless, this is not the first paper with images of CNTs but it is the first announcement with the 'nanotube' nomenclature and providing high resolution images showing details of the sidewall structure. Two years later, Iijima and Ichihashi [3] and Bethune *et al*.[2] synthesized SWCNTs. Indeed, there are some earlier reports showing lower resolution TEM images of CNTs such one published in the Journal of Physical Chemistry of the former USSR by Radushkevich and Lukyanovich [18] in 1952, as shown in Figure 2. During 50's and 60's, it was not

possible to get high resolution images but the structure of the tubes can be seen in the images provided. The diameter of CNTs is nearly 50 nm that corresponds to a MWCNT.

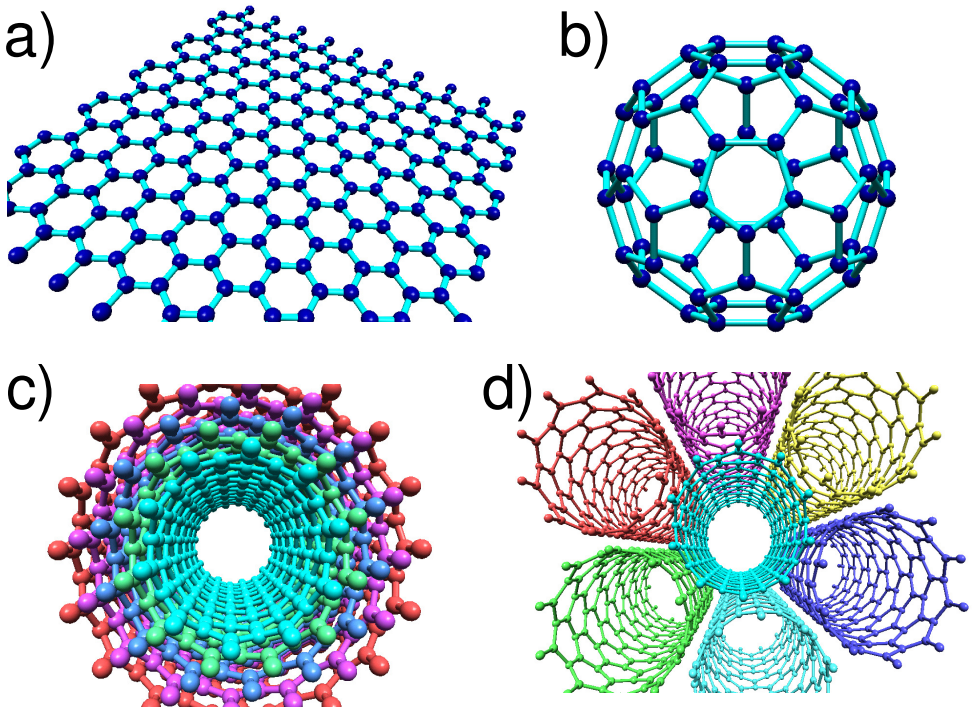

Figure 1. a) Graphene sheet, **b)** C60, **c)** multi-walled carbon nanotubes (MWCNT), **d)** single-walled carbon nanotubes (SWCNTs).

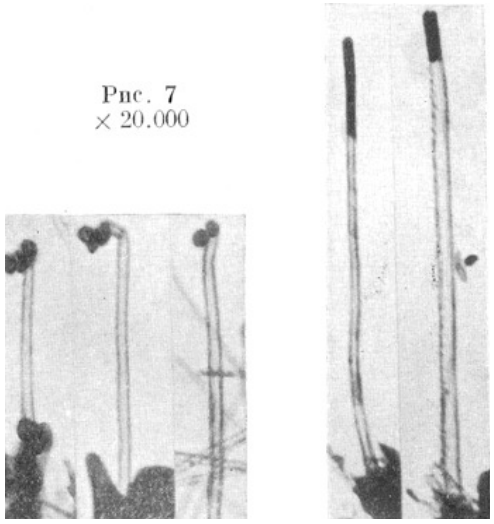

Figure 2. TEM image of the first known evidence found in the literature for carbon nanotubes. [18]

For SWCNTs the wrapping scheme of the graphene sheet results with changes in their properties. The different twist angles of graphene sheet determine the chirality of single-walled carbon nanotubes, which defines the electronic properties as well. The helicity is defined C_h in Eq.1 as;

$$C_h = n\,\mathrm{a} + m\,\mathrm{b} \tag{1}$$

where a and b are primitive vectors and n and m are integers [19]. In Figure 3 tube axis, wrapping plane and resulted armchair, zigzag and chiral tubes with respect to changing of φ and θ angles within lattice are shown. SWCNTs according to their geometry can be separated in three groups [20];

1) zigzag tubes, (n,0) or (0,m);

2) armchair tubes, (n,n);

3) chiral tubes, (n≠m).

Chirality determines whether a SWCNT is metallic or semiconductor. For the equation (n-m) = 3k (k is the greatest common divisor) SWCNT will have metallic character. All other m,n combinations resulted in semiconducting tubes.

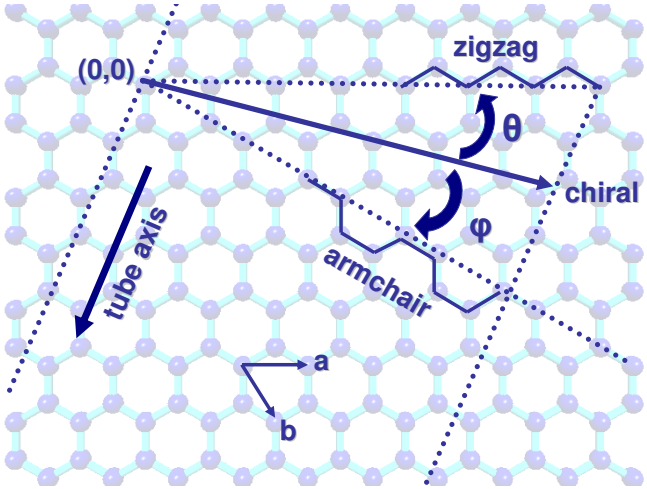

Figure 3. Graphene sheet wrappings correspond to the chirality of single walled carbon nanotubes according to rolling up angle to tube axis with the lattice vectors a, b and angles φ and θ.

Chiralities of SWCNTs can be identified through analysis of Raman spectrum. There are unique signatures of special Raman signals called radial breathing modes (RBM) of the CNTs [21]. For MWCNTs, they are all metallic and chirality of individual layers can not be distinguished.

Carbon nanotubes attract much attention because of their uncommon properties than any other material [22]. Their low density with combination of elastic properties makes CNTs interesting to work with. Moreover, the hard structure of CNT, being strong against deformation with electrical and thermal properties found so many researchers from different disciplines. By being excellent electron emitters, they are chemically stable but also can be functionalized.

2.2 Synthesis techniques for carbon nanotubes

The synthesis of carbon nanotubes can be achieved through different methods such as arc-discharge, laser ablation, CVD and pyrolysis [23]. Other techniques for synthesis of carbon nanotubes can be found also. Here, the three most common techniques will be discussed.

Firstly, the arc-discharge method is the first technique for the synthesis of carbon nanotubes. The arc-discharge method is used for multi-walled carbon nanotube synthesis [17]. Also in 1992 Ebbesen and Ajayan succeed the synthesis of MWCNTs up to a gram [24]. In 1993, Bethune *et al*., were also able to synthesize l SWCNTs in grams [2]. This technique is generally used under He atmosphere at low pressures, based on the vaporization of the carbon by passing arc current between two graphite electrodes. In Figure 4, the schematic representation of reaction chamber is given. While the arc current passes from anode to cathode, the anode graphite source is heated to temperatures where carbon starts evaporating, then carbon from the anode deposits on the cathode side by the formation of single walled and multi-walled carbon nanotubes. Also catalyst particle addition inside graphite source is possible for increasing the growth yield. However, this technique has the major disadvantage of not being selective of the size of the CNTs synthesized.

Furthermore, CNTs synthesized using this method has to be purified due to significant amorphous carbon inclusion.

Secondly, the laser ablation method is tried for carbon nanotubes synthesis by Smalley in 1995 with relatively good results; 1-10g high quality SWCNTs were produced [25]. This method includes irradiation of graphite target by a laser beam and vaporization of carbon molecules from the graphite target. The vaporized carbon particles adsorbed on the relatively colder target surface or on the walls of the system. Again a low pressure and inert atmosphere conditions are used similar to arc-discharge technique. In Figure 5, details of laser ablation method are schematically described. The technique has the advantage of allowing the synthesis of diameter controlled nanotubes. Unfortunately, laser systems are expensive which make this method less favourable for CNT growth. Both techniques of arc-discharge and laser ablation can be used for growing only powdered or bundled CNTs hence, it is not possible to have control over CNT synthesis on desired substrates with a specified orientation.

Finally, CVD technique has become the most commonly used method for carbon nanotubes synthesis [26–28]. The decomposition of a carbonaceous gas in a furnace with hot walls or a chamber and triggers the formation of CNTs on a variety of substrates with catalyst islands, such as iron and nickel. Temperature of the furnace or the substrate during the synthesis can be in a wide range 500-1000^{o}C which enhances the decomposition of the carbonaceous gas. Schematic drawing of the system can be seen in Figure 6. Catalyst introduction to reaction chamber can differ; in some cases catalyst particles are injected with the carrier gas or they can be directly deposited on a substrate. Decomposition of the carbon source can be achieved by thermal ways or with the help of plasma environment. Plasma generation is generally achieved with radio frequencies (RF) [29,30], direct current (DC) [31,32] or microwaves (MW) [33].

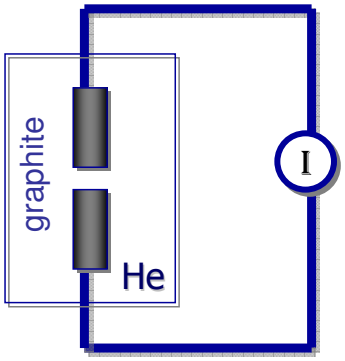

Figure 4. Schematic representation of the arc-discharge method. An arc current passes from anode to cathode causing the formation carbon nanotubes.

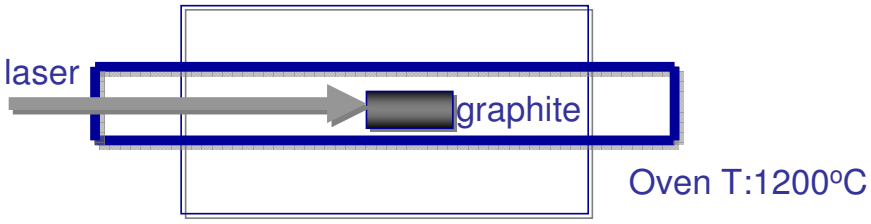

Figure 5. Schematic representation of the laser ablation method.

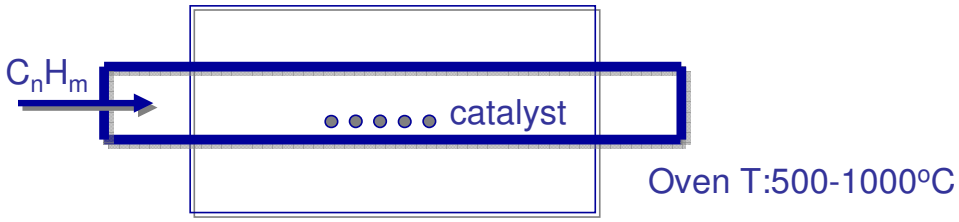

Figure 6. Schematic representation of the chemical vapor deposition method.

One of the key points in CVD growth is the catalyst size. Moreover, the catalyst size is related with radius of the synthesized nanotubes. The reduction step during CVD technique helps suppress the catalyst size, which also sometimes decreases the catalyst size. During the reduction step hydrogen gas or ammonia gas is introduced to the chamber.

CVD is the most commonly used technique for large scale synthesis of nanotubes. Fortunately, it is cheaper than other techniques mentioned above and allows for control over the desired production parameters. The vertical alignment of the carbon nanotubes are reached by this technique.

2.3 Functionalization of carbon nanotubes

There are numerous inter-disciplinary studies on CNTs investigating the functionalization of tubes for various applications. Unfortunately, new routes should be followed for implementation of large amounts of CNTs for efficient applications. Low solubility of CNTs in solvents is one of the problems towards wide-range usage. Studies dealing with the chemistry of tubes can be divided into two groups; side-wall functionalization and endohedral filling. In this study, side-wall functionalization via polymers and polymer nanoparticles, as new concepts, will be studied. Interaction of CNTs with polymer nanoparticles is also analyzed. The CNT synthesis is done by using sandwich method and polymer nanoparticles are synthesized at Bilkent University, Department of Chemistry by Asist.Prof.Dr. Dönüş Tuncel's group. Details and results of the work will be explained in Chapter 4.2.

The side-wall (exohedral) functionalization generally aims to increase the CNT solubility by enhancing hydrophilic behavior of the outmost tube side walls [34]. Interactions of graphitic sidewalls with other molecules can be roughly considered as reaction of graphite surface with the specified molecule. The sp^2 hybridized carbon atoms on the surface can go under many reactions [21,35]. Common point of these reactions is the breaking of the double bonds. Nevertheless, there are other functionalization types for carbon nanotube sidewalls. These are through van der Waals interactions and Π-Π stacking. These interactions do not have a direct role on the carbon nanotube sidewall framework but have effects on the solubility and electronic properties of the tubes [36-41]. These results are promising for further applications of them with composites, or usage in sensor technology.

There are several approaches for dispersion of CNTs, but recently usage of conjugated polymers as dispersants is gaining attention. By this method, electrical and mechanical properties of CNTs will not be affected. Furthermore, enhanced electrical and optical properties can be generated by conjugated polymers (CPs) [37, 42-47]. By changing the type of CP used as dispersant agent, the CP/CNT composites can become well dispersed in organic solvents even in water. As the CPs are not very effective on dispersing CNTs in water, new approaches will be considered as big improvements for widespread usage of CNTs in fields such as biomedical applications.

The interaction between polymer and CNTs is being worked on. There are some studies suggesting the helical wrapping of polymers around CNTs, and also in some others non-helical adsorption by alignment of the polymer chain to maximize Π-Π stacking is suggested. This is dependent on the flexibility of polymer backbone. To better understand the mechanism between polymer units and CNT side-walls, some limited computational studies are undertaken [48-52].

To enhance dispersibility of CNTs in water and in organic solvents, we studied interactions of polymer-CNTs with conjugated polymer nanoparticles (CPNs) [53] and CPs in aqueous or THF media. To find out different trends of interaction, MWCNTs, SWCNTs and an-MWCNTs are used. For CPNs poly[9, 9-bis-(6'-bromohexylfluoren-2, 7-diyl)-co-(benzen-1, 4-diyl)] (PFB-B) polymer is used. In THF media PFB-B and another fluorene-based CP, namely poly (9,9-dihexylfluorenyl-2,7-diyl) (PF) is chosen.

2.4 Vertically aligned carbon nanotube arrays

The main issue related with the synthesis of CNTs is to control over the properties and alignments of them. Ajayan *et al.*, developed a way to produce aligned arrays of CNTs by using a polymer resin which is already mixed with carbon nanotubes in 1994 [54]. The orientation of carbon nanotubes in the composite is not in the same direction and influenced easily by the thickness of the slices. On the

other hand, Heer *et al*, examined a suspension of CNTs that are transferred on ceramic filter and then transferred to the plastic surface in 1995 [55]. As a result, some of the tubes were sticking vertically but the control over homogeneity could not be reached. In 1996, Li *et al.*, synthesized vertically aligned CNT arrays first , with the help of mesoporous silica embedded iron nanoparticles in CVD system [56]. In Figure 7, an image of aligned CNTs by this method is shown. Spacing between the tubes are about 100 nm and the tube lengths are up to 50 micrometers.

After the vertical alignment of the tubes reached, researchers continued patterning the surfaces with vertically aligned CNT films. Dresselhaus *et al.*, synthesized blocks of CNT towers that are separated with fixed distances from each other, in 2001 [57]. In Figure 8, synthesized vertically aligned CNT film can be seen. The growth is achieved with porous silica substrate and iron nanoparticle patterning.

The concern about increasing the carbon nanotube forest length caused the development of the super-growth technique. In 2004 Iijima *et al.*, found that the addition of some water vapor to the reaction chamber resulted in the increase of the CNT length. Moreover, synthesized CNTs are found to be ultra pure >99.9% by this way [58]. Super-growth carbon nanotubes forest can be seen in Figure 9.

The vertical alignment is an indication of high yield growth from the densely packed catalyst particles. It is assumed that a single tube grows from an active catalyst particle, and interaction of neighbouring tubes leads to vertical growth. This growth approach involves catalyst patterning and rational design of the substrate to enhance catalyst-substrate interactions and control the catalyst particle size.

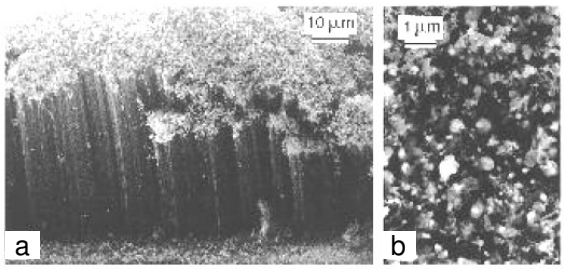

Figure 7. **a)** Low magnification SEM image of the aligned carbon naotube arrays from the side view of the film. **b)** Tip structure of the aligned tubes with the top view of the film. [56]

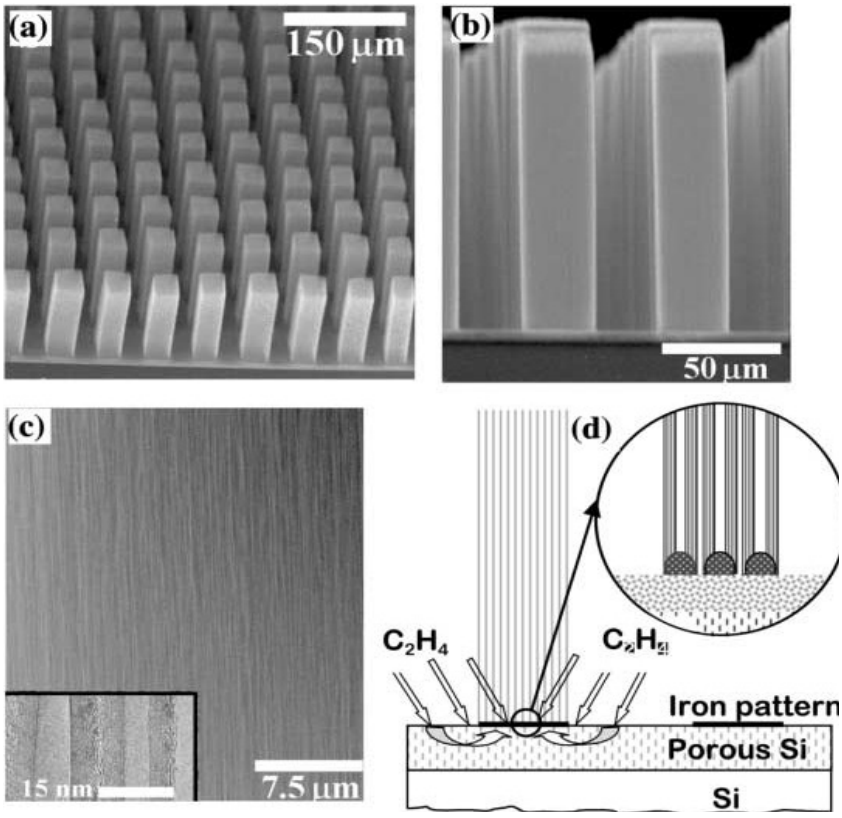

Figure 8. **a)** SEM image of tower structures consisted of aligned nanotubes. **b)** SEM image showing aligned nanotubes from side view. **c)** High resolution SEM image. Inset: TEM image showing multi-walled carbon nanotubes. **d)** Schematic representation of the possible growth process. [57]

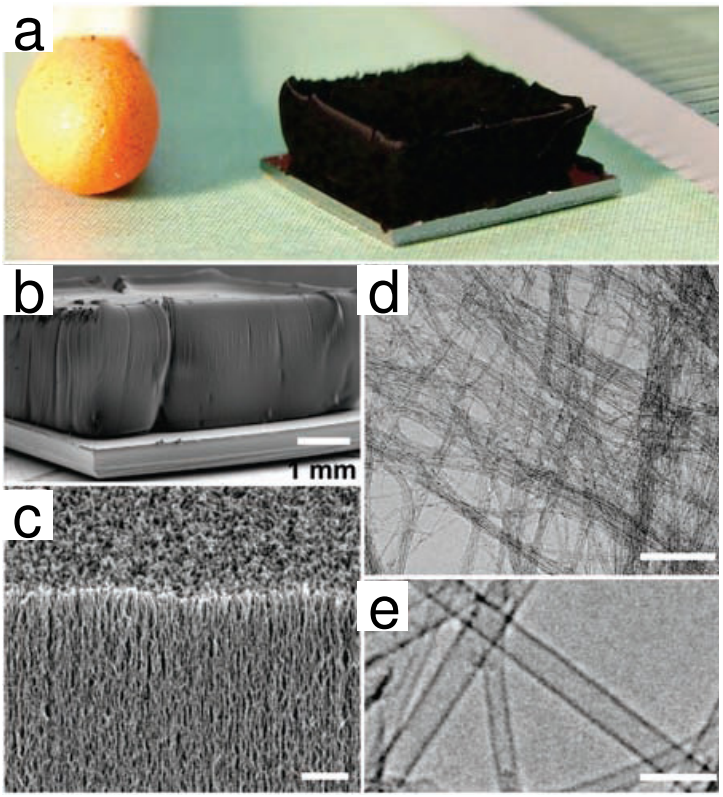

Figure 9. **a)** Single-walled carbon nanotubes forest synthesized by water-assisted chemical vapor deposition technique. Height: 2.5mm **b)** SEM image of the forest. **c)** SEM image of the same SWCNTs. Scale bar: 1µm **d)** TEM image of the nanotubes. Scale bar: 100 nm **e)** High resolution TEM image of the SWCNTs. Scale bar: 5 nm. [58]

2.4.1 Growth mechanism

The control over the growth of carbon nanotubes is still not very well understood. Because the exact mechanism of the growth steps have not been distinguished yet.. Indeed, understanding the growth mechanisms for different techniques is hard. Critical parameters change one method to another as there are many of them; reaction temperature, catalyst type, carbon precursor, reaction atmosphere and so on. Another problem for understanding the growth mechanism is about *ex situ* analysis that includes investigation of the end product. In recent years,

with the usage of *in situ* techniques more evidence from the reactions were obtained in real-time.

The growth mechanism suggested by Saito *et al.* includes three main stages [59]. First, generation of the catalyst particles at high temperatures is achieved. This can be achieved by deposition of nanoparticles via condensation of metal vapors, decomposition of organometallic compounds or reduction of pre-catalyst synthesized film. Secondly, a carbon source is injected to the high temperature system which then decomposes into smaller carbon compounds. Finally, these carbonaceous species gets adsorbed on surface of substrate and/or dissolves into the liquid metal phase of the catalyst. Eventually, supersaturation of the catalyst particle is achieved which is the starting point of CNT growth. As a result, the precipitation of carbon atoms around the catalyst particles forms CNTs.

The binary phase diagrams can give an explanation about VLS mechanism. The binary Fe-C phase diagram shows the melting point of iron at eutectic point in the bulk is 1175^{o}C. The size of the iron particle plays a great role on the eutectic point of Fe-C system. Harutyunyan *et al*., showed that the melting temperature of Fe catalyst particles decrease with the size [60]. The experimental results of Kim *et al*., indicate the rate limiting step should be carbon diffusion in metal catalyst, hence it is reported that for different metal catalyst usages the growth rate of CNTs change [61].

Dissolution of carbon in the active metal particles is explained by Sinnott *et al*.; the carbon precipitation on the catalyst particle follows the concentration gradient where the low and high local carbon concentration cause the movement of the carbon precipitate to the low carbon concentrated region [62].

With the real time imaging of *in situ* carbon nanofiber growth by Helveg *et al*., new ideas are suggested about the growth mechanism [63]. At low temperatures, VLS mechanism did not seem to be responsible for growth. Helveg *et al.,* showed that the catalyst was crystalline during the growth.. According to these results, this new mechanism is called vapor-solid mechanism. The continued debate can be

collected under two growth approaches; root and tip growth. In Figure 10, root growth and tip growth mechanisms are schematically indicated.

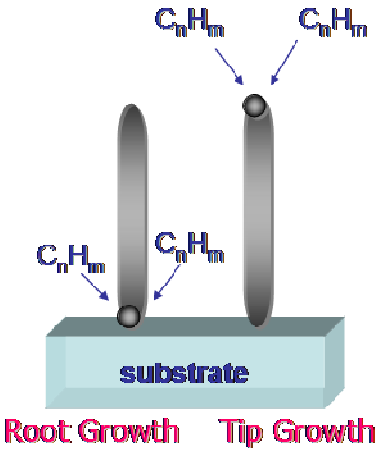

Figure 10. Representation of the root and tip growth approaches for vertically aligned carbon nanotubes arrays.

In root growth mechanism, the catalyst particle has a large interaction with the substrate surface, during the synthesis catalyst remains on the substrate. Many researchers affirmed root growth model for the growth of vertically aligned CNTs. In the root growth of vertically aligned CNTs, the resistance to the growth rate is observed. The reason of this resistance is related with the decrease at feedstock of carbon source to active catalyst particles. As feedstock gas cannot reach the catalyst, growth rate decreases. Another rate limiting step is catalyst deactivation.

In tip growth mechanism, dissolved carbon on catalyst particles precipitate to form CNTs by lifting catalyst up from substrate. If the interaction between catalyst particle and substrate is low, catalyst can easily leave substrate. CNT growth takes place at backwards of the catalyst. To sum up, if the substrate - catalyst interaction is insufficient, the CNT growth mechanism will be tip growth. However, if there is high interaction between substrate and catalyst, synthesis favours the root growth.

For vertically aligned CNT growth mechanism, there are many determinants affecting the growth dynamics. First of all, catalyst patterning is the key factor to get vertical alignment of growing tubes. Distance between neighbouring catalyst nanoparticle on substrate, should be in a critical range for VANTA growth.

Deviations at the distances between catalysts during calcination and reduction conditions, will determine whether synthesized film is vertically aligned or not. High quality VANTA growth is possible when well isolated catalyst patterns are used. By eliminating catalyst mobility at high temperatures, isolation of them can be achieved. As the CNTs synthesis take place, each CNT will be in the interaction with neighbouring tubes. As the distance between neighbouring tubes is less than critical distance, van der Waals forces between tubes kept all of the CNTs aligned. Other than catalyst design, the kinetics during the synthesis is also crucial. Olag *et al*., suggest, lack of carbon penetration to root of the CNTs after a critical length of the film has reached prevents further growth [64]. However, carbon species are effective on initiating CNT growth at the top side of VANTA film. This causes a density difference at top and down side of synthesized vertically aligned CNT arrays.

There are many different approaches to understand the real mechanism behind VANTA growth. But a common growth mechanism has not been accepted, yet. The reasons are; many factors playing role on the growth mechanism can not be generalized for all the CNT synthesis techniques, the *ex situ* analysis of CNT growth. As the *in situ* analytical techniques give rise to high resolution data analysis, the logic behind the vertically aligned CNT array growth can be resolved in near future.

2.4.1.1 Substrate selection and preparation

To improve possible applications of CNTs, suitable substrates and templates are examined to be advantageous for electronics or other applications. Firstly, CNT growth is examined on silica (SiO_2) or silicon (Si) surfaces. Generally the substrates studied are Si(100) wafers having an oxide layer at the top nearly 100nm. In some cases, patterns of Si/SiO_2 surfaces are performed by lithographic techniques. Ajayan *et al.*, indicated the selective growth of CNTs on SiO_2 and Si surfaces. The metal-organic ferrocene catalyst entered the system with a carrier gas into the CVD set-up, resulted with VANTA growth at the SiO_2 sides. Hence, the reaction of metal particles with Si surfaces formed $FeSi_2$ and Fe_2SiO_4 compounds, CNT formation is suppressed [65].

The usage of metal substrates is studied by Ng *et al.*. through catalyst deposition on Si wafers. The deposited iron/nickel (Fe/Ni) and Ni catalysts on aluminium (Al) under layers indicate increase at the yield of VANTA synthesis [66]. According to a new study of Talapatra *et al*., the direct growth of aligned CNT arrays is performed on metal alloy, Inconel, with a vapor phase floating catalyst CVD system [67]. Also Parthangal *et al*., used a wet method for catalyst deposition on different substrates as; Si, Au, Ag, Cu, Al, Pt, W, TiN, NiCr, steel. In these set of experiments, CNTs on Cu substrate are non-uniform and random. Although, Pt surface is resulted with no CNT growth, the other substrates worked well for vertically aligned CNT array growth [68].

To grow vertically aligned CNT arrays effectively, introduction of an aluminium or aluminium oxide layer with metal catalyst significantly enhances the quality and yield of synthesized VANTA. Due to the reaction conditions, aluminium oxide acts as a barrier to reduce agglomeration of catalyst particles. There are three main routes towards carbon nanotube synthesis: preparation of catalyst film on the suitable substrate and formation of active nanoparticles from the catalyst film; achieving the desired catalyst size and dispersion on the film to initiate carbon nanotube nucleation; and the growth of carbon nanotubes to generate the CNT film on the substrate. The surface morphology and the catalyst dispersion have great affect on CNT growth.

2.4.1.2 Catalyst application

The importance of the catalyst design in CVD technique is essential for the synthesis quality. Many researches have been done for achieving the most effective catalyst amount, type and combination with a suitable catalyst support. To better understand the catalyst behavior corresponding to different catalyst design techniques, the field of catalyst film generation will be summarized in two sub-sections as; physical vapor deposition such as e-beam deposition or magnetic sputtering of the catalyst and solution based catalyst deposition on the substrate.

2.4.1.2.a Physical vapor deposition of catalysts on the substrate

Control over catalyst particle size is the main issue for synthesizing VANTA [69]. Physical vapor deposition enables thin catalyst film deposition on flat substrates. By this way homogenous and nanometer sized film deposition is done on many substrate in high vacuum systems that are most suitable for VANTA growth [58, 70 - 72]. Also, by controlling catalyst layer thickness CNT side wall adjustment can be done [72]. The deposition systems are expensive vacuum systems. Also deposition of catalyst steps brings several treatments before introducing of substrate into CVD chamber. On flat surfaces, it is advantageous deposition of catalyst by e-beam deposition or sputtering but for non-planar surfaces it isn't preferred [73]. Moreover, for the large scale synthesis of VANTA films, this way of catalyst deposition can not be integrated into industrial synthesis systems.

2.4.1.2.b Solution based catalyst preparation

Solution based catalyst preparation methods are used via application of the catalyst salt mixture on the substrate by spin coat [74], dip coating [75] or drop-wise addition [68]. In general, the salt of the catalyst dissolved in a solvent that will volatile as leaving a homogenous distribution of the catalyst particle on the substrate. With dip coating technique, the solution collects at some regions of substrate according to inhomogeneous drying pattern. Also with spin coating, same problems can be seen. By drop-wise addition, not a homogenous film but according to drying pattern patched form VANTA growth is observed [68].

2.4.1.3 Carbon source

Many different carbon compounds can be suitable candidates for being carbon source of CVD technique during CNT synthesis. Methane CVD is first used by Dai *et al*., for the synthesis of high yield SWCNTs [76]. Recently, a new method for CNT growth is introduced by Maruyama *et al.*, which is the alcohol catalyzed CVD (AC-CVD) that significantly reduces the amorphous carbon [77]. By the usage

of methanol and ethanol as a carbon source, with TEM and SEM imaging no evidence for amorphous carbon is detected. The principle behind the AC-CVD is decomposition of the alcohol molecules at reaction temperatures to form -OH radicals. These radicals plays important role on the removal of amorphous carbon and other carbonaceous side products generated during VANTA synthesis.

In limited number of reports, the selective synthesis of CNTs with respect to different carbon sources is mentioned. Catalytic activity is dependent on the type of the carbon source as it is reported by Kimura *et al*.. They observed Co metal catalyst is active with methanol but inactive with methane [78]. For the achievement of a satisfied conclusion regarding the selectivity of catalyst particles, further studies must be done.

2.5 Hydrophobic behavior of carbon nanotubes

Surface engineering on the CNTs has gained great interest in the wide range application areas such as; biomedical applications [79,80], biosensors [81,82], composites [83,84], catalyst supports [85] and scaffolds for cell seeding [86]. Wetting and hydrophobic properties of CNTs make them useful in wet application systems. Unfortunately, the insolubility of carbon nanotubes in many solvents limits their possible applications. There are plenty of ways to modify the CNTs from superhydrophobic to hydrophilic or vice verse such as;, oxygen plasma etching [87], microwave and acid treatments [88] and introducing new compounds on CNTs.

The wettability of the surface is generally observed by contact angle measurements and is controlled by its chemical composition (related to the surface energy) and geometrical structure (related to the surface roughness). To characterize wettability of a solid surface two criteria can be used; the static contact angle (CA) of a liquid droplet in thermal equilibrium on a horizontal surface and the dynamic sliding angle (SA) as inclination angle at which a water droplet rolls of the surface. In the literature general usage of the wettability definition corresponds to static CA measurements.

The static CA measurements can define two criteria against examined surface; hydrophilicity or hydrophobicity. The CA of a hydrophobic surface is higher than 90^o whereas super-hydrophobicity limit of a surface is CA > 150^o [89]. The indications of hydrophobicity are; high contact angle, poor adhesiveness, poor wettability and low solid surface free energy. A hydrophilic surface having low CA values less than 90^o, are having the properties; good adhesiveness, good wettability and high surface free energy. Super-hydrophilicity limit is considered as CA under 5^o [89]. In Figure 11, the hydrophobic and hydrophilic surfaces and their different CA results are indicated.

The factors playing role on the wetting behavior of a surface can be analyzed with three components; liquid-solid interface, liquid-vapor interface and vapor-solid interface. These three components are described on water droplet staying on a surface at equilibrium conditions in Figure 12. Young's equation is given in Eq.(2) and CA indicated as α , solid-vapor interface vector as $\gamma_{S,V}$, solid-liquid interface vector as $\gamma_{S,L}$, liquid-vapor interface vector as $\gamma_{L,V}$, ;

$$\cos \alpha = (\gamma_{S,V} - \gamma_{S,L}) / \gamma_{L,V} \quad (2)$$

The roughness of the surface is an important factor towards hydrophobicity. The CA of a solid substrate can be changed with a proper design of the surface structure due to increase roughness. This evidence indicates the hydrophobicity does not rely on only chemistry of the surface but also with physical structure. In the literature, two possible explanations can be found according to hydrophobic states, Wenzel [90] and Cassie [91] states. In Figure 13, both of the states are schematically represented. For the Wenzel approach, the roughness cause increase at surface area of the substrate, hence make the substrate more hydrophobic. But there is another possibility; in the holes between rough asperities some air can be trapped. The water droplet then stays at the tips of the asperities and the air trapped inside them. This approach is called Cassie state.

The Wenzel state accepts the apparent contact angle α^* as a function of surface roughness with respect to Young's contact angle α. Surface roughness factor

defined as r which is a number greater than 1. The Eq.(3) indicates the relation between α^* and α ;

$$\cos \alpha^* = r \cos\alpha \quad (3)$$

In Eq.(3), the surface roughness is the enhancement factor of wetting of a surface. As r value is always greater than 1, wetting increases in hydrophilicity for $\alpha < 90^o$ apparent contact angle gets smaller $\alpha^* < \alpha$. Vice versa, the hydrophobic character rises as the surface roughness increases ($\alpha > 90^o$, $\alpha^* > \alpha$).

The Cassie state is accepted for heterogeneous surface wetting where Wenzel state can not further explains the behavior of water droplet. Interestingly, Bico *et al*., indicates if a water droplet's apparent CA is in correlation with Cassie's theory, after physically pressing of droplet it became in agreement with Wenzel theory. CA changed from 170^o to 130^o in their work after pressing step [92].

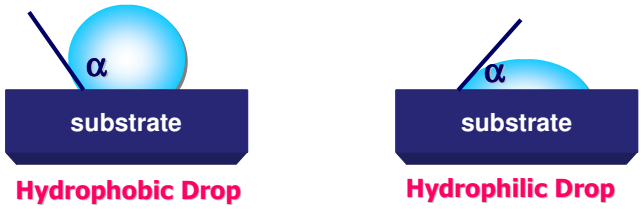

Figure 11. Properties of hydrophobicity versus hydrophilicity. Hydrophobic drop > 90^{o}, hydrophilic drop < 90^{o}.

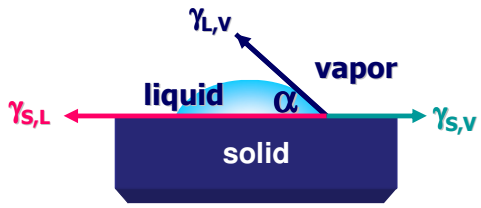

Figure 12. Three vector components of water droplet-substrate surface.

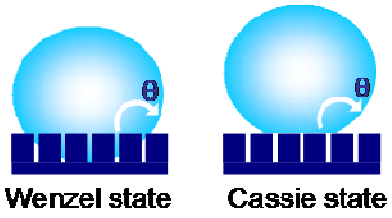

Figure 13. Wenzel state: the liquid drop is in interaction with all of the surface area of the substrate (Filling all the holes). Cassie state: the liquid drop is in interaction with the tips of the asperities. (Leaving air trapped in the holes)

The vertically aligned carbon nanotube surface consists of nano-sized diameter tip of each CNT. This creates a rough surface. CNT film roughness can be varied by changing the distribution of CNTs on substrate or by chemical modification.

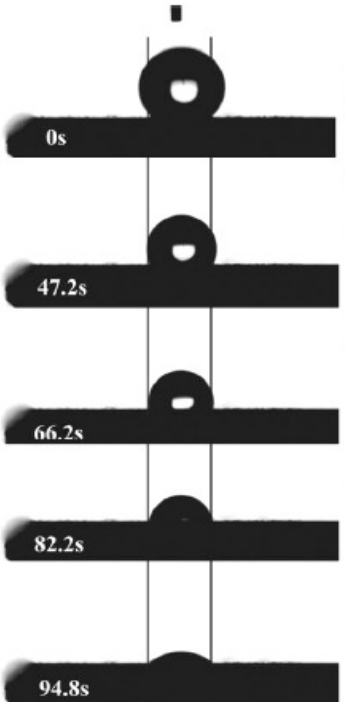

Figure 14. Dynamic CA measurements, recorded by CCD camera. The time of the pictures captured after the initial contact of water droplet with surface is; 0s, 47.2s, 66.2s, 82.2s and 94.8s. As the water droplet penetrates into CNT film, the contact area does not change [93].

In the study of Huan Liu, Jin Zhai and Lei Jiang, unmodified 19μm in length VANTA samples are super-hydrophobic at 0^{th} second. The dynamic CA measurements on VANTA sample can be seen in Figure 14. CA against water droplet is recorded by CDD in 0s, 47.2s, 66.2s, 82.2s and 94.8s after the interaction of water droplet with surface. In a short time, at 80 seconds, hydrophobicity diminishes immediately [93]. They also indicate the contact area of water droplet does not change during the process, in Figure 14. There are competing processes during CA measurements; the surface roughness versus capillary effect between tubes. But the other important issue is air trapped between pillars and hydrophilic CNT side-walls are also affecting the apparent CA.

3 EXPERIMENTAL PROCEDURE

3.1 Experimental set-up

The AC-CVD apparatus used in this work is a combination of several sub-systems. These components can be seen in Figure 15, and actual photographs are given in Figure 16. These components can be listed as a high temperature furnace (Proterm, PTF 15 / 75 / 450), 3 inch quartz tube, home built magnetic sample holder arm, load lock system, a baratron (MKS, Type 626 Pressure Transducer), mass flow controllers (MFC, MKS 1179 type) for argon, hydrogen and nitrogen separately, ethanol bubbler, a home built liquid N_2 cold trap and a vacuum pump (Varian DS 3002).

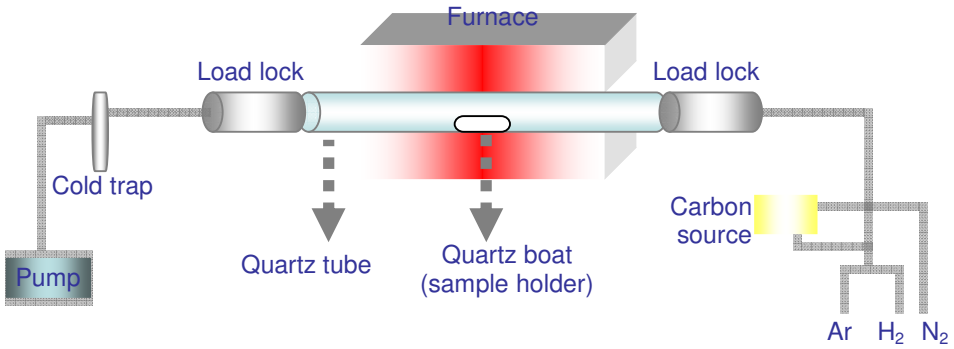

Figure 15. Schematic representation of the components corresponding chemical vapor deposition CVD system in order; pump, cold trap, load lock, quartz tube, high temperature furnace, carbon source and gas mass flow controllers (MFCs).

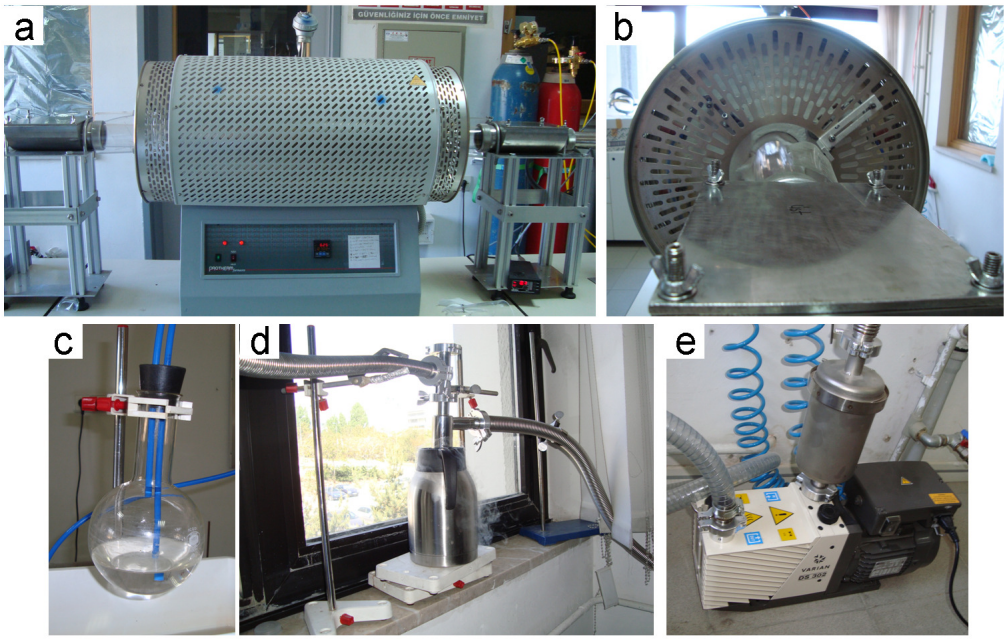

Figure 16. Photographs of the components corresponding CVD system **a)** quartz tube - high temperature furnace and load-lock systems, baratron, at the background argon and hydrogen gas tubes, **b)** load-lock and side view of furnace, **c)** bubbler and outlet system for the carbon source, **d)** cold trap mechanism, **e)** vacuum pump.

The baratron is positioned before load lock for the pressure control in the system. A pre-made mixture of argon and hydrogen gasses is passed through the carbon solution. Carbon source can be chosen as any carbon solvent that is volatile and has a high vapor pressure. In this study, absolute ethanol (99% purity) is used as the carbon source at room temperature 150ml. Cold trap unit is essential and practical for usages to increase lifetime of vacuum pump. By the help of liquid nitrogen container, impurities and already reacted ethanol are collected easily at the cold trap. The cold trap unit is designed by us. Detailed scheme of cold trap design can be seen in section - Appendix A. For achieving desired temperatures, correct heat zone is found at the middle of the furnace as nearly 30 cm wide heat zone. The sample holder is designed to reach and stay at the middle part of the furnace during the reduction and reaction steps.

3.2 Experimental procedure

This study includes main part of VANTA synthesis and functionalization parts. The parameters for optimized VANTA synthesis will be explained firstly. Functionalization part includes polymer-CNT interaction, polymer nanoparticle - CNT interaction and effect on solubility.

3.2.1 Carbon nanotube synthesis

Carbon nanotubes synthesis has several steps to achieve controlled CNT films. The substrate preparation from silicon wafers Si(100) and the results of surface modifications and improved catalyst distribution will be explained in detail at results and discussion part. The catalyst preparation and application on oxidized Si(100) substrate, developed efficient route for VANTA synthesis will be covered.

3.2.1.1 Oxidation of Si (100) surface

Silicon dioxide formation is performed at 900^{o}C for 30 minutes at high temperature furnace in air atmosphere. The thickness of the oxide layer after treatment is nearly 20nm and the formation conformed by Elipsometry and FT-IR Si-O signal around 1100cm^{-1}. The oxidized Si(100) surfaces than undergo cleaning steps to achieve suitable surface properties for desired catalyst patterning. The CNT growth is done by solution based precursors, wetting of the surface plays a great role during catalyst film deposition. To enhance wetting properties of the substrate, appropriate cleaning mechanism should be found. For this reason, comparison of three different solutions is done to achieve most hydrophilic surface properties. The FT-IR spectrum of the cleaned substrates by using acetone, ethanol and 1:1 H_2O_2:H_2O solutions separately for 30 minutes with sonicator. The Si-O signal can be seen in Figure 17 for all of the samples. The background of the signal for all of the data is bare silicon wafer.

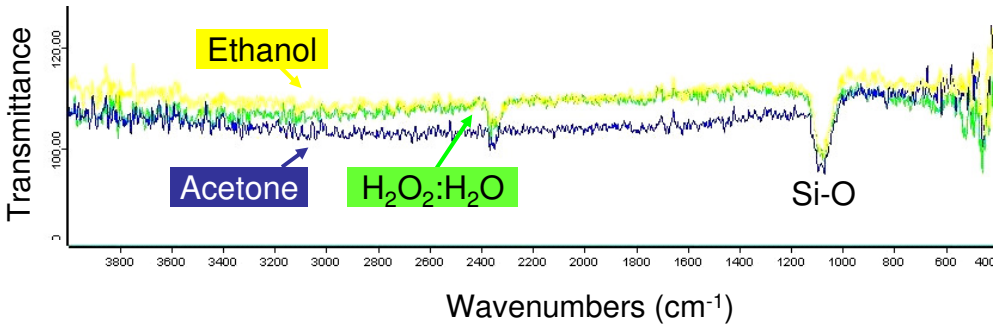

Figure 17. FTIR spectrum of SiO_2 films after cleaning treatment with acetone, ethanol and 1:1 H_2O_2:H_2O separately. Background of the signal is bare silicon wafer. Yellow signal corresponds to ethanol treated sample; blue is acetone and green is hydrogen peroxide-water treated sample.

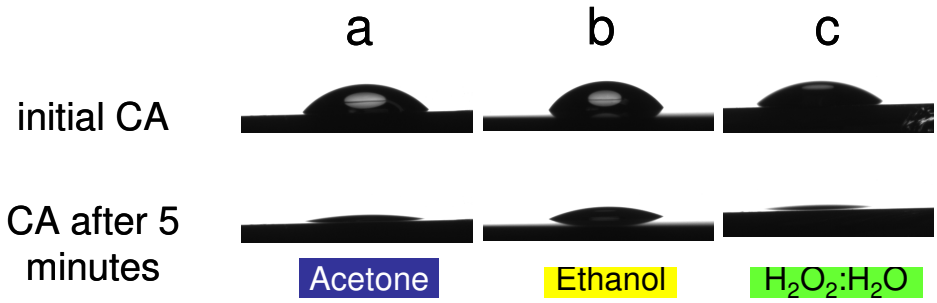

Figure 18. Dynamic contact angle measurements against 8µl distilled water on the surfaces **a)** acetone treated SiO_2, **b)** ethanol, **c)** 1:1 H_2O_2:H_2O treated SiO_2. Photographs of the initial contact angle (CA) and CA after 5 minutes captured with CCD camera.

Solutions of acetone, ethanol and hydrogen peroxide are used for cleaning step of the substrates in order to achieve best wettability against same amount of water. Wettability of the surfaces is detected by dynamic CA measurements. The results can be seen from Figure 18. Initial contact angles of acetone, ethanol and hydrogen peroxide solutions are 42.6 °, 56.6 °, 40.4° respectively. After 5 minutes CA of the samples' are 10.8 °, 24 °, 4 ° respectively. The dynamic CA measurements indicate the wetting of the surface is enhanced with peroxide treated sample. After these findings, all of the oxidized Si(100) samples are cleaned by using 1:1 H_2O_2:H_2O solution for 30 minutes at sonicator before catalyst film deposition.

3.2.1.2 Catalyst solution preparation and application to Si(100) surface

Precursors for metal catalysts are prepared by using the dissolution of metal nitrates. Metal nitrates are used for catalyst deposition on oxidized silicon substrate. First the required amount of metal nitrate powder is mixed with 10 ml of double distilled water and let to stir in a closed vial for 12 hours at room temperature. We found that this allows for the homogenous dissolution and complex formation to achieve a uniform distribution of metal nitrate on the oxide surface. Following the preparation of nitrate solution, it is either spin coated or applied to the oxidized Si (100) surface using a micropipette and left for drying at room temperature.

After the catalyst deposition is done, samples are introduced into AC-CVD chamber. Furnace at 625^{o}C, is taken under vacuum after all the connections of the vacuum line are closed. Nitrogen gas is passed for 5 minutes at 2.0 mTorr for cleaning of the chamber. System is again vacuumed to prevent any residuals from nitrogen gas. Then mixture of 5:1 Ar:H_2 gases are prepared, introduced into chamber to fix the pressure to 3.8 mTorr. Samples are placed at the heat zone by flowing argon-hydrogen gas mixture for reduction step. At the bubbler, ethanol is measured as 150ml and the water environment around bubbler is set to 25^{o}C for eliminating daily or seasonal temperature fluctuations. Temperature fluctuations in the air are directly related to the vapor pressure of ethanol. The reduction step finishes after 15 minutes. Mixture of 5:1 Ar:H_2 is bubbled through ethanol solution and let get into the system. By this step reaction starts and ends after 30 minutes. The chamber is cleaned again by nitrogen gas flow, opened to atmosphere.

3.2.2 Polymer – carbon nanotube mixture preparation

Two different polymer types are used to investigate the carbon nanotube-polymer interactions; one is a brominated end grouped polymer (PFB-B) and the other is a non-brominated polymer (PF) with alkyl groups. Also, different types of carbon nanotubes, e.g. SWCNTs, MWCNTs and an-MWCNTs are utilized to further analyze the interaction. Detailed preparation steps are provided in the following sections.

3.2.2.1 Preparation of carbon nanotubes for functionalization

SWCNTs are purchased from Sigma Aldrich. Multi-walled carbon nanotube synthesis is done according to sandwich method. For annealing step, already synthesized MWCNTs are taken under argon atmosphere at 625^{o}C for 30 minutes without any oxygen residues entering to the system. During the annealing process, pressure kept at 12 Torr.

3.2.2.2 Polymer preparation

Two different polymer types used are: brominated polymer (poly[{9,9–Bis(6-bromo-hexyl)} fluorene-co-p-xylene]) and non-brominated polymer with akly groups (poly[(9,9-dihexyl-9H-fluorene)-co-(9,9-dihexyl-9H-fluorene)]).

For the investigation of effect of Br end grouped polymer on the solubility of CNTs and polymer interactions, PFB-B and PF polymers are used. In Figure 19, schematic representation of the PFB-B and PF monomers can be seen. Polymer synthesis has been done at Bilkent University, Department of Chemistry by Asist. Prof. Dr. Dönüş Tuncel's group.

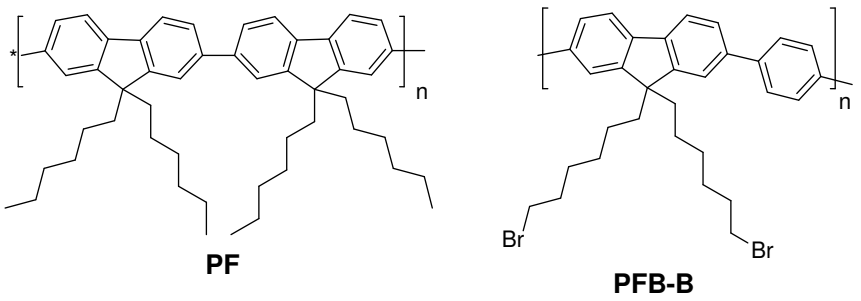

Figure 19. Schematic representation of PF (poly[(9,9-dihexyl-9H-fluorene)-co-(9,9-dihexyl-9H-fluorene)]) and PFB-B Poly[9,9-bis-(6'-bromohexylfluoren-2,7-diyl)-*alt co*-(benzen-1,4-diyl)].

3.2.3 Mixing of Polymers-Carbon Nanotubes

Six separate vials with PFB-B and PF solutions have been prepared by dissolving 0.005mg of the polymers in 10 ml of THF. Equal amounts of CNTs are then introduced to these solutions and homogenization is ensured by sonication of the polymer-CNT mixtures for 60 min. Polymer-CNT combinations are named starting from Set-1 to Set-6 in Table 1.

Table.1 Mixtures of the PFB-B and PF with SWCNT, MWCNT and an-MWCNT.

	PFB-B	**PF**
SWCNT	Set 1	Set 4
MWCNT	Set 2	Set 5
an-MWCNT	Set 3	Set 6

3.2.4 Conjugated polymer nanoparticle preparation

CPNs are prepared in two different sizes. For the preparation of stock polymer solution, 10 mg polymer is dissolved in 10 ml THF and stirred overnight. The solution is made up to volume of 100 ml by adding THF. The solution is filtered through 0.45 µm syringe filter.

3.2.4.1 CPNs with average sizes of 70 nm

4 ml of this stock solution is injected rapidly into 40 ml of water while stirring using sonicator. The dispersion of nanoparticles is sonicated further for 20 min and stirred additionally another 30 min using magnetic stirrer. THF is removed under reduced pressure; the resulting nanoparticle dispersion is filtered through 0.45 um syringe filter. Concentration of polymer: 0.1×10^{-1} mg ml^{-1}.

3.2.4.2 CPNs with average sizes of 40 nm

Procedure is the same but here 2 ml of polymer stock solution is injected into 100 ml of water to prepare CPNs. Concentration of polymer: 0.2 $x10^{-2}$ mg ml^{-1}.

The sizes of the nanoparticles are determined by dynamic light scattering (DLS) and by scanning electron microscope (SEM) and transmission electron microscope (TEM).

3.2.4.3 Interaction of CPN and CNTs

The VANTA samples with silicon substrate are placed inside vials with 10 ml of CPN solutions. These VANTA samples are sonicated in these nanoparticle-water mixtures for 60 minutes at room temperature. With sonication CNTs are removed from the surface of silicon wafer and dispersed in solution by getting interaction with CPNs. Figure 20 is the representation of introducing of VANTA samples into the CPN solution and after sonication CPN attached to CNTs are illustrated.

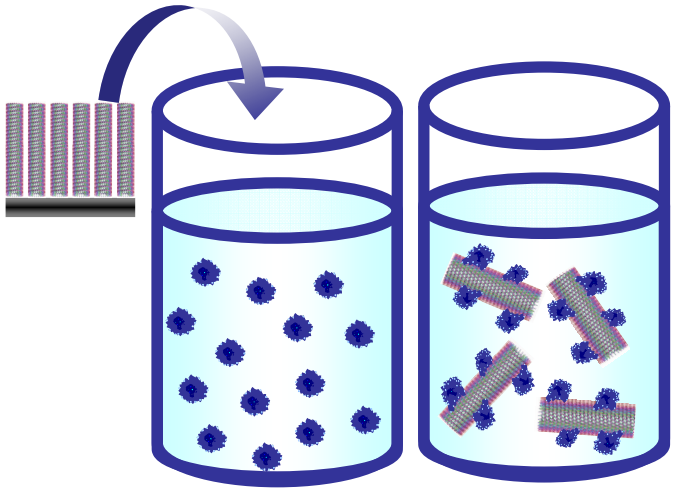

Figure 20. Schematic representation of addition of VANTA film into the CPN solution.

3.3 Characterization techniques

A Carl-Zeiss EVO 40 XVP scanning electron microscope (SEM) is used to investigate the morphology of synthesized CNT films and their interaction between CNTs and polymers. CNTs and CNTs-polymer mixtures are ultrasonically mixed for 30 minutes in ethanol solution then applied on a Cu grid for TEM investigations. A JEOL 2100F transmission electron microscope (TEM) working at 200kV is used for TEM analysis with a JEOL EDX attachment. The Raman spectra of the samples are acquired using a HORIBA Jobin Yvon LabRam HR 800 instrument with a 532.1 nm Nd:YAG laser. The laser power is kept constant for all of the samples as 20 mW to overcome heating effects or formation of defects on samples. The incident light source is dispersed by a 600 grooves/mm holographic grating focused on the sample by using a 100X objective. The confocal hole and the slit entrance are set at 1100 μm and 200 μm, respectively. For each sample, three Raman spectra are recorded. After baseline correction of these 3 spectra is done, mean data is calculated for each sample. Fluorescence spectra are recorded on The Cary Eclipse fluorescence spectrophotometer. UV-Vis spectra of the samples are recorded on a Thermo Scientific Evolution 300/600 UV-Visible spectrometer. Quarzt quvettes are used during the record and the base line correction is made for each of the samples at room temperature. Contact angle measurements are done by OCA 15 EC by DataPhysics which is video-based optical contact angle measuring instrument. By single direct dosing system standard dosing of 8μm is applied for all samples. For the CA fitting Laplace-Young fitting is done on the photographs of water droplets by software. The XPS analysis are done by Thermo XPS instrument as K-Alpha - Monochromated high-performance XPS spectrometer. During the analysis, a pass energy of 25 eV is used, and step size is set at 0.005 eV. Dynamic Light Scattering (DLS) measurements are done by Zeta Sizer equipment for achieving size distribution of conjugated polymer nanoparticles (CPNs). FTIR measurements are carried out with Bruker, bare Si(100) wafer is used as baseline. For the detection of oxide layer formed on Si(100) substrate, Ellipsometer J.A.Woolam, V-VASE is used.

4 RESULTS AND DISCUSSION

4.1 Vertically aligned carbon nanotube synthesis

In this study, vertically aligned CNT array synthesis is achieved starting from scratch with solution based catalyst usage. First of all, motivation to this study is to produce CNTs without e-beam deposition or thermal deposition techniques which are expensive and done under high vacuum systems. Solution based catalyst preparation will be simple to prepare and easy to apply on any substrate.

Carbon nanotube synthesis is firstly achieved by using γ-alumina – iron nitrate mixture. Porous structure of γ-alumina is used for dispersing catalyst nanoparticles. Aluminium nitrate – iron nitrate solution is then used to achieve homogeneous CNT film on the substrate. Sandwich method is developed for growing vertically aligned CNT arrays. In this section, steps towards synthesizing high quality, well ordered and homogenous VANTA film will be explained.

4.1.2 Catalyst preparation and application

4.1.2.1 γ-alumina – Iron nitrate mixture

As a first approach to CNT synthesis, γ-alumina is tried for catalyst design with the combination of iron nitrate as catalyst solution. Porous structure of γ-alumina is chosen to enhance iron particle dispersion. As the calcination, reduction and reaction steps are performed at about 600^{o}C, γ-alumina has advantageous property by having stable pore size and structure up to 800^{o}C. During reduction step, iron nitrate reduces to active iron nanoparticles but γ-alumina is resistive among reduction. The nitrate decomposition reaction of iron nitrate during calcination step can be seen from Eq.(4). The reduction step at 625^{o}C in 5:1 Ar:H_2 atmosphere initiates reducing of iron oxide particles to active iron catalyst particles. Reduction equation of iron oxide species to active iron nanoparticles can be seen in Eq.(5).

Another suggested mechanism for iron oxide reduction in the alumina environment can be seen in Eq.(6).

$$4Fe(NO_3)_3.9H_2O_{(s)} \rightarrow 2Fe_2O_{3(s)} + 12NO_{2(g)} + 3O_{2(g)} + 36H_2O(g) \quad (4)$$

$$3\ Fe_2O_3 + H_2 \rightarrow 2\ Fe_30_4 + H_20 \quad (5)$$
$$Fe_30_4 + 4\ H_2 \rightarrow 3\ Fe + 4\ H_20$$

$$3\ Fe_2O_3 + 2\ Al_2O_3 \rightarrow 2\ FeAl_20_4 \quad \text{(fast)} \quad (6)$$
$$FeAl_20_4 \rightarrow Fe + Al_2O_3 + H_2O \quad \text{(slow)}$$

The mixture of γ-alumina – iron nitrate is the impregnation of iron nanoparticles at the pores of γ-alumina structure in aqueous media. The pores will be barriers preventing agglomeration of the iron nanoparticles during calcination, reduction and reaction steps at high temperatures. The mixture is prepared with addition of mass ratios of 8:2, 6:4, 4:6, 2:8 γ-alumina:Fe_2O_3 by γ-alumina powder (ACS reagent, ≥ 98%, Sigma Aldrich) and iron nitrate ($Fe(NO_3)_3.9H_2O$, ACS reagent, ≥ 98%, Sigma Aldrich) powders mixing in aqueous media of 20ml and let stirring in a closed vial for 12 hours. This way enhances the complex formation and homogenous dissolving. Afterwards, the iron nitrate – γ-alumina solution is spin coated on already cleaned silicon dioxide substrate. The calcination step is performed at 600^oC under Ar flow. During this step iron nitrate transforms to iron oxide. After samples are loaded to the AC-CVD system, the reduction step starts to get active iron nanoparticles under argon and hydrogen flow. Following step is introducing carbon source to initiate CNT growth.

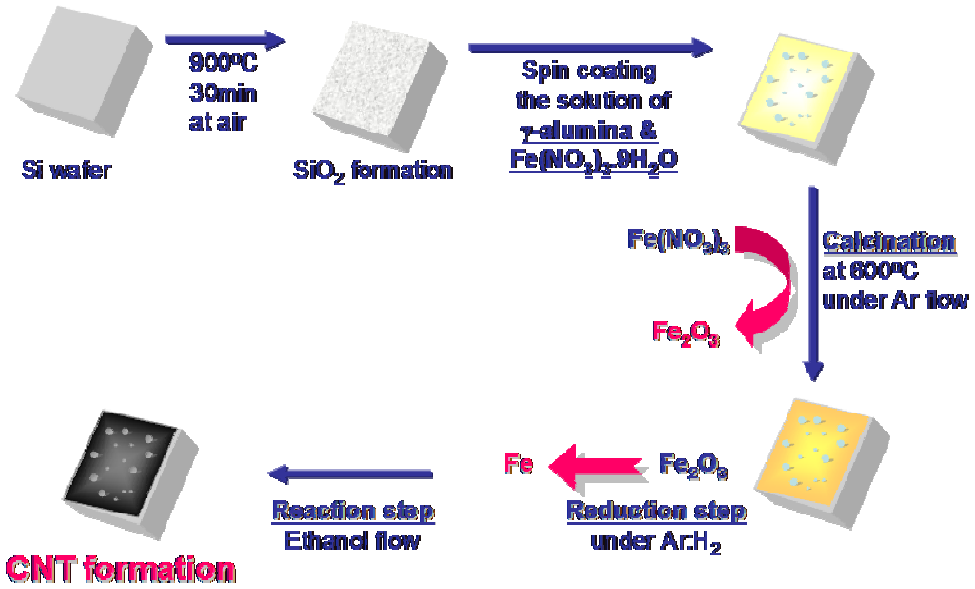

Figure 21. Schematic representation of the sample preparation by γ-alumina and iron nitrate mixture. The steps of catalyst preparation, calcination, reduction and reaction.

Experimental steps;

1) Oxidizing Si(100) surface at 900^{o}C for 30 minutes

2) Clean Si(100) surface by 1:1 H_2O_2:H_2O solution at sonicator for 30 minutes at room temperature

3) Spin coat 1ml γ-alumina - iron nitrate solution at 4000 rpm for 45 sec, and dry at room temperature

4) Calcination at 600^{o}C for 2 hours at Ar atmosphere

5) Loading sample to ACCVD system

The effect of iron nitrate concentration on impregnated γ-alumina solutions are examined by the weight percentage combinations of γ-alumina:Fe_2O_3 8:2 , 6:4 , 4:6, 2:8. Under EDX measurements representative images from iron and aluminium distribution of corresponding samples can be seen in Figure 21. The images represents γ-alumina:Fe_2O_3 clusters after calcination step which is just before introducing of the samples into AC-CVD.

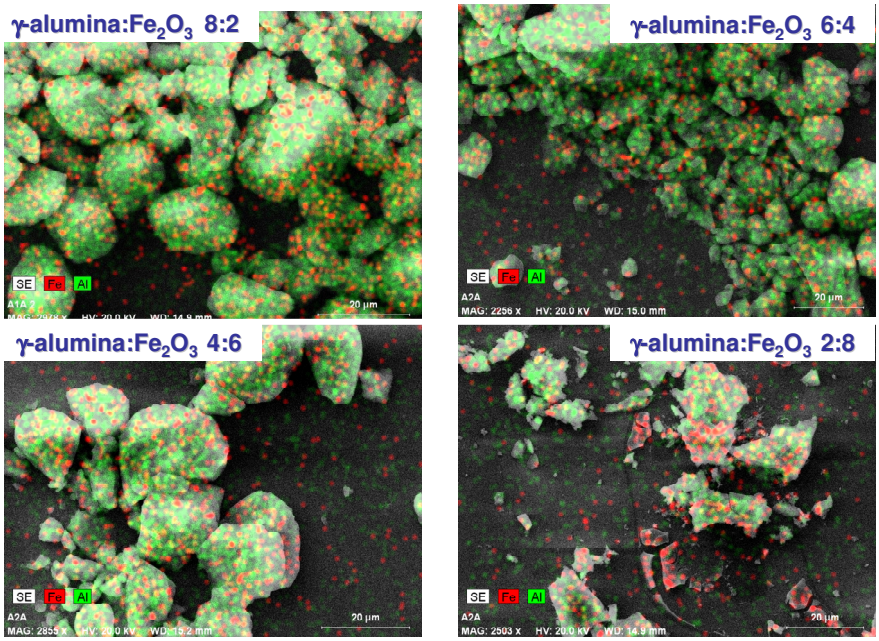

Figure 22. EDX image of different weight percentage concentrations of γ-alumina - iron nitrate solutions applied on silicon dioxide substrate.

As the iron concentration increase inhomogeneous distribution of iron particles on γ-alumina clusters can be seen by the red colour indication from Figure 22. The iron signal indicates agglomerated features at higher concentrations of iron nitrate added samples. After the samples are treated with reduction and reaction steps the resulting samples are coloured black and the CNT formation is detected by SEM imaging. The CNTs synthesized using 8:2 γ-alumina:Fe_2O_3 sample image at the left side as a general view and at the right side detailed image can be seen in Figure 23-a. In 8:2 γ-alumina:Fe_2O_3 sample, there formed a fine layer of CNT film on oxidized Si(100) substrate. Nevertheless, the structures of γ-alumina clusters agglomerate at some regions on substrate and resulted with inhomogeneous distribution. All of substrate surface is covered by CNTs after reaction, also the clusters. By increasing iron content in prepared catalyst solution, CNT covered γ-alumina particles start to stand up from substrate. The distribution of synthesized CNTs have less coverage on the surface with respect to CNT film synthesized by 8:2 γ-alumina:Fe_2O_3 mixture. In Figure 23-b, the detailed image of 6:4 γ-alumina:Fe_2O_3 after synthesis can be seen. Some of the particles are able to stand on top of the grown CNTs on every side of the γ-alumina clusters. The samples that have much more iron concentration in

preparation step become ball like shape covered by CNTs all around after synthesis. These experiments indicate the effect of iron to alumina ratio on synthesized CNT film. Moreover, the distribution of CNTs on substrate is affected whether they are on the substrate or lifting up from the substrate.

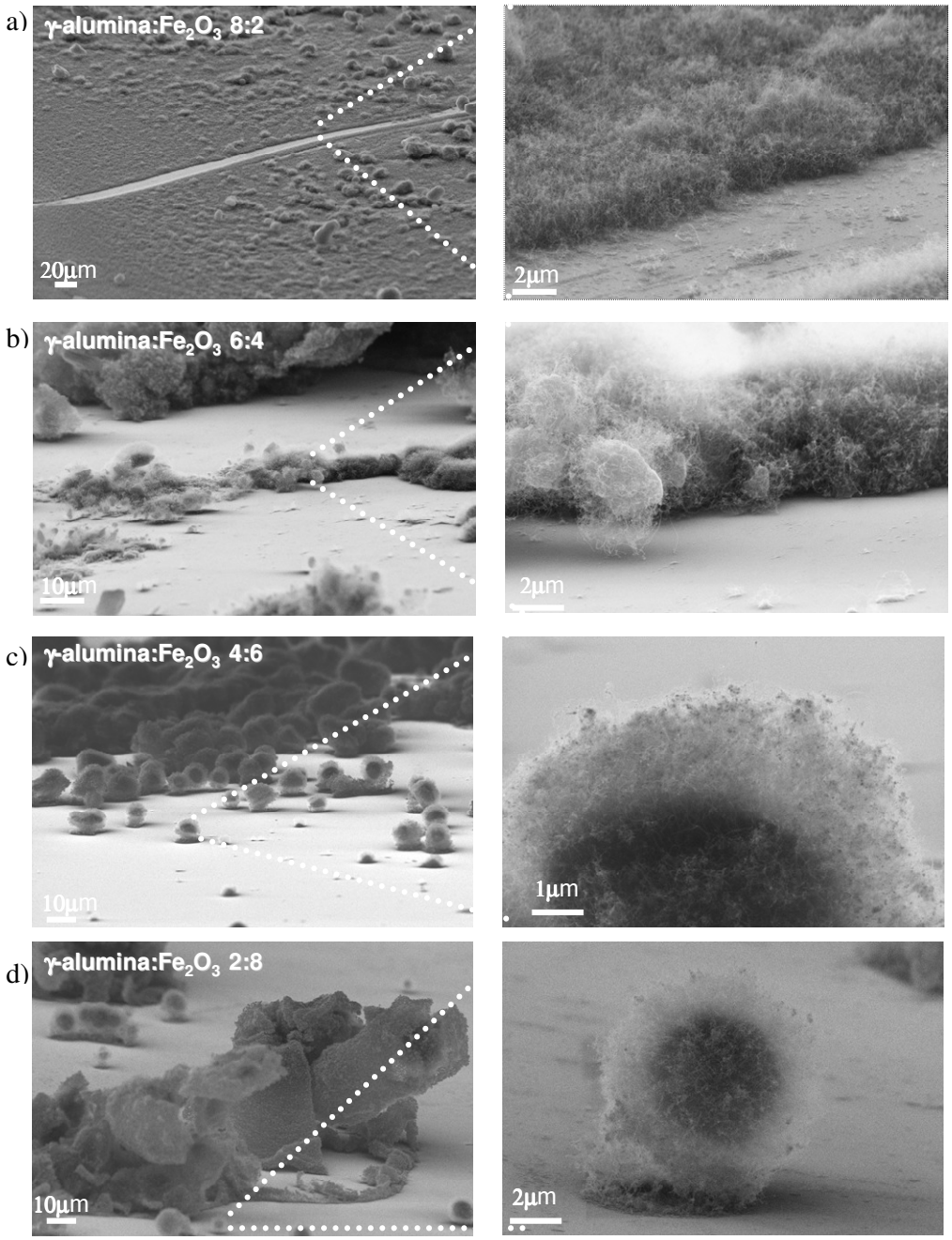

Figure 23. SEM images of different loadings of γ-alumina - iron nitrate solution applied on silicon dioxide substrate. Left images are general views of the samples and the right sides are higher magnification SEM images of indicated zone of the

general image by dotted white arrows. The loadings of γ-alumina:Fe_2O_3 from top to down are as follows; **a)** 8:2, **b)** 6:4, **c)** 4:6 and **d)** 2:8.

4.1.2.1.a Iron nitrate solution

The investigation of the importance of γ-alumina at CNT synthesis mechanism, iron nitrate ($Fe(NO_3)_3.9H_2O$, ACS reagent, ≥ 98%, Sigma Aldrich) solution is prepared without γ-alumina content for application as catalyst layer. Same experimental steps with γ-alumina – iron nitrate treated samples are followed to make the comparison accurately. After samples are loaded to AC-CVD system, the reduction step starts to get active iron nanoparticles under hydrogen – argon flow. Following step is introducing carbon source to initiate CNT growth. Flow diagram of the procedure can be seen in Figure 24.

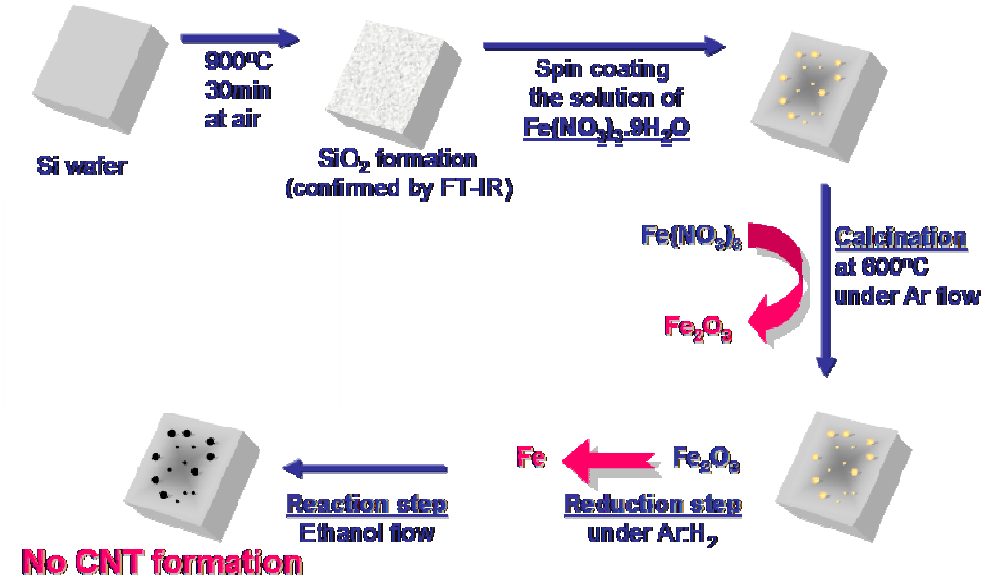

Figure 24. Schematic representation of the sample preparation procedure with iron nitrate solution. The steps of catalyst preparation with spin coating, calcination, reduction and reaction.

Experimental steps;

1) Oxidizing Si(100) surface at 900^{o}C for 30 minutes

2) Clean Si(100) surface by 1:1 H_2O_2:H_2O solution at sonicator for 30 minutes at room temperature

3) Spin coat 1ml iron nitrate solution at 4000 rpm for 45 sec, and dry at room temperature

4) Calcination at 600^{o}C for 2 hours at Ar atmosphere

5) Loading sample to ACCVD system

After the aqueous solution of iron nitrate application on already cleaned silicon dioxide substrate, treatments of calcination, reduction and reaction steps are performed. The calcination step is removal of nitrate groups from the iron nitrate structure, replacing oxides. The agglomerated iron clusters can be seen from the Figure 25.

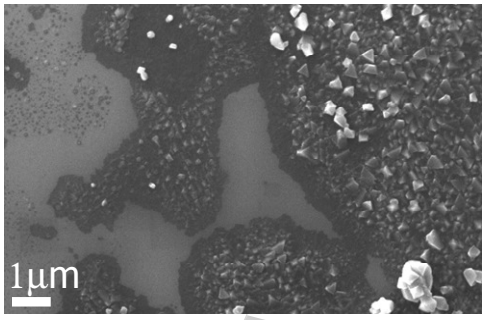

Figure 25. SEM image of iron nitrate solution applied catalyst oxide layer on silicon dioxide background after reaction step.

At the temperatures above 400^{o}C, catalyst particles have tendency to get into clusters, became mobile on substrate to decrease surface energy. In that case, the iron nanoparticles agglomerate to crystallize and decrease surface energy by formation of clusters. Above critical catalyst size, CNT synthesis do not initiate as the surface energy is getting lower as the cluster size increase. With this regard, usage of iron nitrate solution without a diffusion barrier to achieve a homogenous catalyst layer film is not a successful method for growing CNTs. As a result, substantial structure of porous γ-alumina is found to be essential for CNT growth acting as a diffusion barrier at reaction temperatures.

4.1.2.2 Aluminium nitrate – Iron nitrate mixture

Inhomogeneous distribution of the γ-alumina agglomerates prevents formation of a high quality, homogenous CNT film synthesis. To overcome this problem, aluminium is introduced to the mixture as solution based by dissolving aluminium nitrate ($Al(NO_3)_3.9H_2O$, ACS reagent, ≥ 98%, Sigma Aldrich) in aqueous media. Aluminium nitrates are oxidized in reaction chamber to produce alumina matrix. Iron nitrate ($Fe(NO_3)_3.9H_2O$, ACS reagent, ≥ 98%, Sigma Aldrich) is used as dissolving catalyst salt in aqueous media. The flow diagram of experimental steps can be seen from Figure 26. The mixture of aluminium nitrate and iron nitrate is prepared in aqueous media in closed vial by stirring 12 hours. The oxidation step is removed to limit the catalyst agglomeration as the both alumina and iron particles are in solution as ions. Mixture is then applied on cleaned silicon dioxide surface with a micropipette and let to dry at room temperature. According to drying pattern of the mixture drop some part of the samples contain more material causing an inhomogeneous film formation.

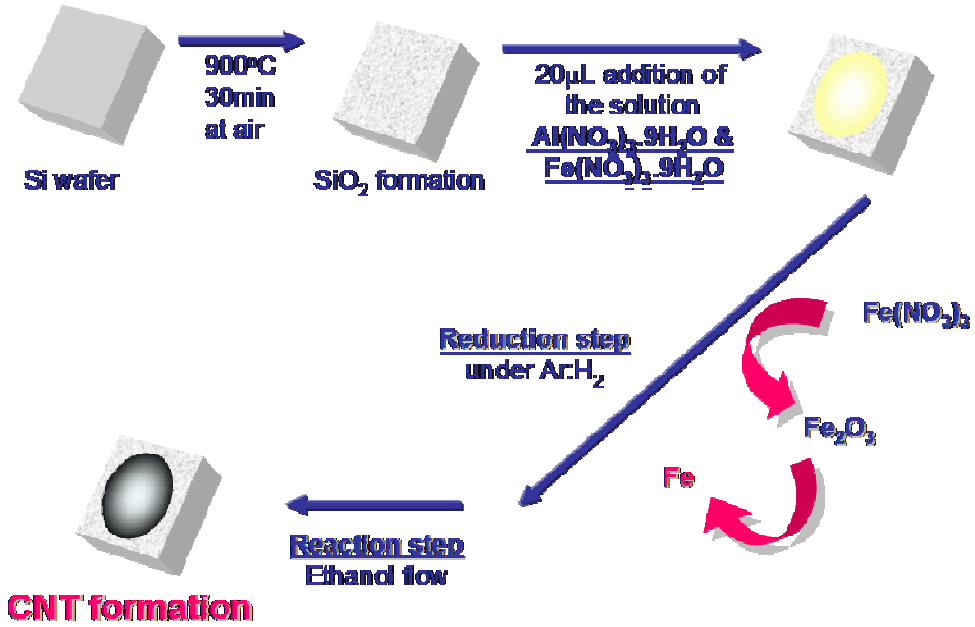

Figure 26. Schematic representation of the sample preparation by aluminium nitrate and iron nitrate mixture. The steps of catalyst preparation with introducing mixture on silicon dioxide substrate, reduction and reaction steps.

Experimental steps;

1) Oxidizing Si(100) surface at 900^{o}C for 30 minutes

2) Clean Si(100) surface by 1:1 H_2O_2:H_2O solution at sonicator for 30 minutes at room temperature

3) 60µl of the solution applied on oxidized Si(100) substrate by micropipette

4) Applied solution left for drying at room temperature

5) Loading sample to ACCVD system

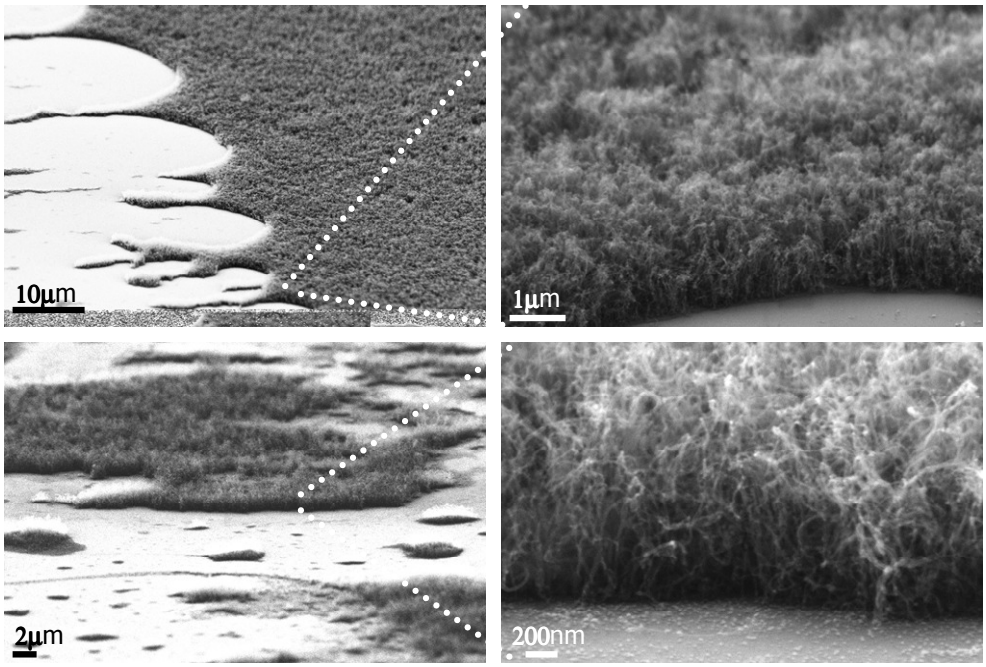

Figure 27. SEM images of aluminium nitrate - iron nitrate mixture applied sample after reaction step. Left side – images as a general view, right side – high magnification images of indicated zones.

Uncontrolled pattern of drying mechanism of aluminium nitrate - iron nitrate mixture on silicon dioxide substrate, leads vacancy sides. In Figure 27, SEM images of synthesized CNT film is shown as semi-vertical and dense at the places that the film is homogenously grown. This step is an improvement for catalyst modification as the two compounds are found at the same phase in aqueous media and during application step to the substrate. Addition of aluminium with solution based methods enables homogenous size distribution of iron catalyst particles in alumina matrix. The alumina matrix will act as a diffusion barrier at synthesis temperatures

preventing iron agglomeration. It is known that Fe and Al nitrates thermally decompose to Fe_2O_3 and Al_2O_3 above 250^oC [94]. During reduction step firstly iron and aluminium oxides are formed. Afterwards, in reduction step at 625^oC with gas ratio Ar:H_2 5:1 aluminium oxide is stable but iron oxide reduces to active iron nanoparticles at this hydrogen concentration. The stable structure of alumina matrix at these conditions provides iron nanoparticle size not to exceed critical catalyst size for CNT growth. To sum up, semi-vertical CNT growth achieved, but the homogenous film distribution can not be investigated by this method. At some regions dense CNT film synthesis is observed. By this method, the route towards solution based precursor usage is encouraged.

4.1.2.3 Sandwich method

Sandwich method is a novel method that is used for the first time in this study. Motivation to work is achieved by the method used as aluminium nitrate-iron nitrate mixture. It shows dense and semi-vertical CNT growth at some regions. To overcome inhomogeneous drying pattern, layer by layer addition of the aluminium nitrate solution as base layer, then catalyst layer iron nitrate solution addition and finally, aluminium nitrate solution addition as top layer is studied. In a study of Yanli Zhao, Dexiu Huang and Yahachi Saito, similar sandwich method is prepared by e-beam deposition of Al/Co/Al catalyst layers for vertically aligned CNT growth [95]. The route towards VANTA growth is adapted to solution based methods as an easier way for preparation of catalyst film. We introduce this approach to solution based catalyst preparation technique as sandwich method by using aqueous aluminium and iron nitrate solutions. The reason of layer by layer addition of aluminium nitrate and iron nitrate solutions is to trap iron catalyst at the alumina matrix during reduction and reaction temperatures to limit mobility of iron nanoparticles.

Vertically aligned MWCNT production is achieved using sandwich method by AC-CVD system. Therefore, a uniform distribution in height and diameter of CNTs has been achieved. Synthesis process starts with the growth of a 20 nm thick oxide layer of silicon on a Si(100) substrate. Secondly, oxidized Si(100) wafers are cleaned ultrasonically in peroxide-water mixture for 30 minutes. For solution based

catalyst preparation, 5 mM iron nitrate ($Fe(NO_3)_3.9H_2O$, ACS reagent, ≥ 98%, Sigma Aldrich) and 5 mM aluminium nitrate ($Al(NO_3)_3.9H_2O$ ACS reagent, ≥ 98%, Sigma Aldrich) are used. The aqueous solutions of aluminium nitrate and iron nitrate is stirred for 12 hours at room temperature in a sealed container. By application of 20µm by micropipette of the aluminium nitrate and iron nitrate solutions in an alternating fashion aluminium nitrate / iron nitrate / aluminium nitrate on oxidized silica substrates. After first layer aluminium nitrate solution is dried on substrate forming a thin film at room temperature, second layer iron nitrate solution is applied and let for drying. Finally, top aluminium nitrate is applied. Si wafer with the dried catalyst film is then loaded to an atmosphere controlled, vacuum capable quartz tube-furnace. The first step in the tube furnace is the reduction step, where oxides of the catalysts are reduced at 625ºC under a flowing (150 sccm) $Ar:H_2$ (5:1 ratio) gas mixture while the pressure of the system is kept at 12 Torr for 15 min. Mass flow controllers are used to ensure the correct gas ratio and constant gas flow rate. Following the reduction step, ethanol vapor is introduced to the tube furnace through a second gas line for the CNT synthesis. Flow diagram of the experimental procedure can be seen in Figure 28.

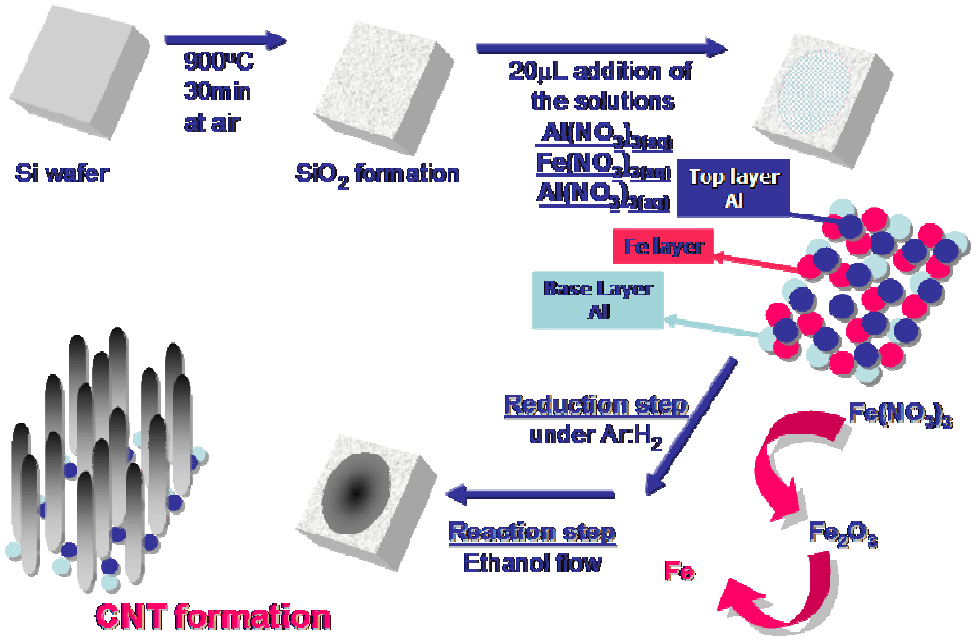

Figure 28. Schematic representation of the sample preparation by sandwich method via addition layer by layer of aluminium nitrate and iron nitrate solutions.

Experimental steps;

1) Oxidizing Si(100) surface at 900^{o}C for 30 minutes

2) Clean Si(100) surface by 1:1 H_2O_2:H_2O solution at sonicator for 30 minutes at room temperature

3) 20µl of 5mM aluminium nitrate solution as base layer is applied on oxidized Si(100) substrate by micropipette left for drying at room temperature

4) 20µl of 5mM iron nitrate solution as catalyst layer is applied on dried aluminium nitrate film by micropipette left for drying at room temperature

5) 20µl of 5mM aluminium nitrate solution as top layer is applied dried aluminium nitrate / iron nitrate catalyst film by micropipette left for drying at room temperature

6) Loading sample to ACCVD system

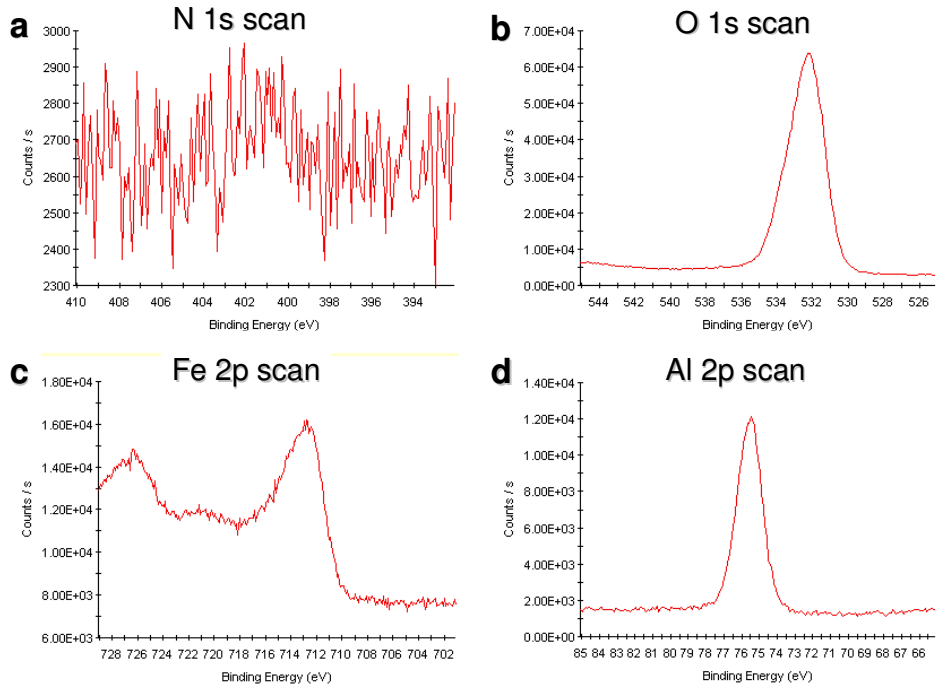

Figure 29. XPS analysis of sandwich sample after reduction step. Detailed analysis of **a)** nitrogen 1s scan, **b)** oxygen 1s scan, **c)** iron 2p scan and **d)** aluminium 2p scan.

The XPS analysis of the sandwich catalyst film is done after reduction step to detect nitrogen presence. After reduction treatment for 15 minutes at 625^{o}C, sample is taken under vacuum for XPS analysis. Unfortunately, some oxide form at the catalyst particles as the XPS analysis are *ex-situ*. In Figure 29, detailed scans of N 1s,

O 1s, Fe 2p and Al 2p are done. After reduction no nitrogen signal is observed whereas Al, Fe and O remain at the catalyst film as expected.

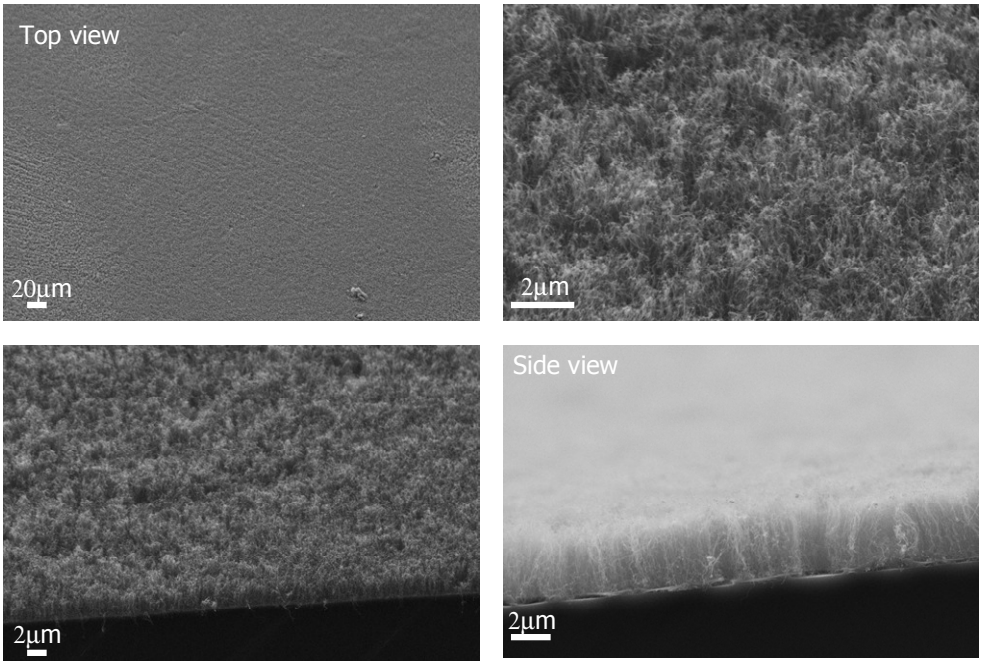

Figure 30. SEM images of the sample synthesized by layer by layer method addition of aluminium nitrate / iron nitrate / aluminium nitrate solutions. Top views and side views of sample.

Figure 31. TEM images of CNTs from VANTA sample.

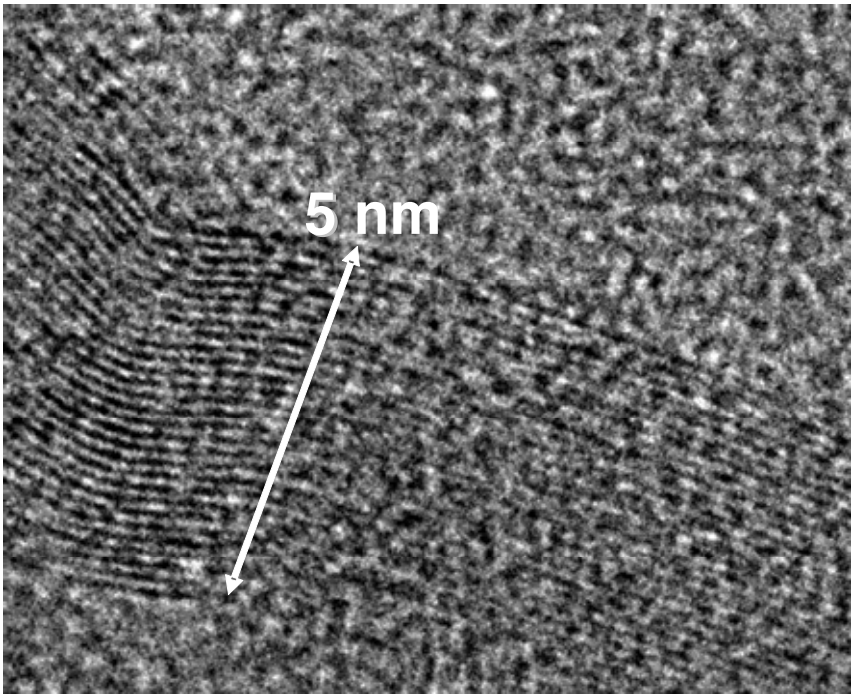

Figure 32. Detailed TEM image of a CNT from VANTA samples. Graphitic planes at side-walls (nearly 30 graphitic planes).

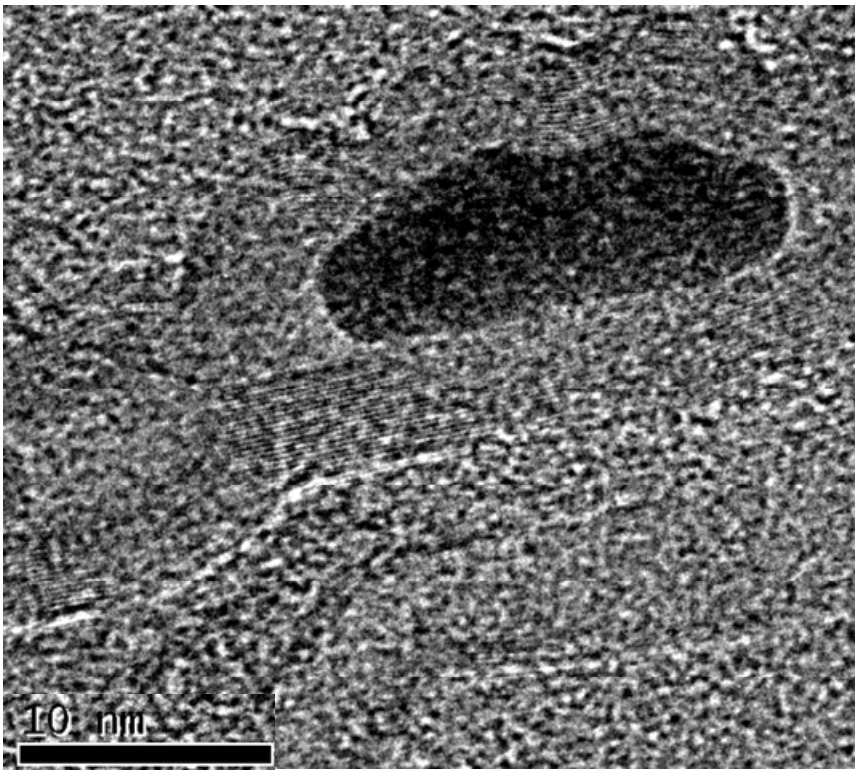

Figure 33. Detailed TEM image of a CNT from VANTA samples. Graphitic planes at side-walls.

The vertically aligned CNT array that is synthesized via sandwich method can be seen in Figure 30. SEM images show general and side views of the CNT arrays. Height of the film is nearly 2.5µm, it is dense and vertical to the substrate. Also, the general view of the sample indicates the homogenous film formation. TEM images in Figure 31, are MWCNTs get into bundles on TEM grid. Also, catalyst particles can be seen inside the nanotubes. Iron particles are elongated inside tube hole at the middle of CNT during synthesis by capillary force, in Figure 31 and Figure 33. Detailed TEM image indicates graphitic planes of the CNT side walls in Figure 32. One side wall is 5 nm having nearly 30 graphitic planes corresponds to walls. As a result inner distance between each graphitic layer is found to be ~0.18 nm. By sandwich method CNT growth with uniform distribution on substrate and well vertical alignment is succeeded. As mentioned, this method is applied first time for catalyst film deposition on Si(100) substrate via solution based precursors to synthesize dense, vertically aligned CNT arrays.

4.1.3 Effect of applied layer concentration on CNT array

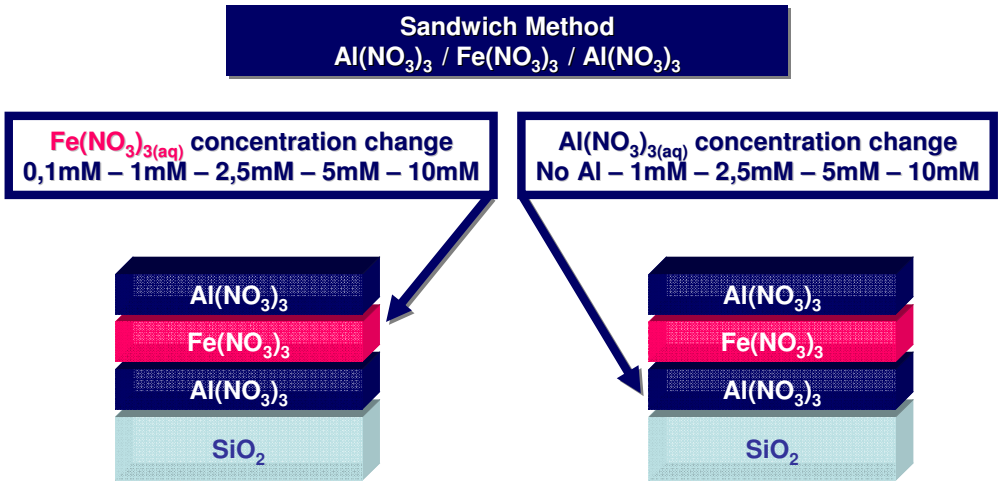

Figure 34. Schematic representation of two routes to determine effect of concentration variation on catalyst layer and base aluminium layer.

To better understand the role of catalyst and base layers at sandwich method, concentration variation of them separately is studied. Schematic representation of concentration variation experiments of sandwich method can be seen in Figure 34.

The applied volumes of the solutions, reduction and reaction conditions are kept same for all samples. After synthesis, the analysis of the samples is done by SEM imaging, Raman spectroscopy and dynamic CA measurements. Effect of the concentration variation on CNT arrays will be discussed by comparing the parameters; film quality, density and the dynamic hydrophobicity.

The effect of the catalyst layer concentration on the synthesized VANTA film is examined by changing applied catalyst layer concentrations as the top and base layer aluminium concentrations are kept constant at 5mM, the catalyst layer concentrations are; 0.1mM, 1mM, 2.5mM, 5mM and 10mM.

The effect of the base layer aluminium concentration on the synthesized VANTA film is observed by changing the concentration as; no aluminium layer, 1mM, 2.5mM, 5mM, 10mM aluminium nitrate solution.

4.1.3.1 Effect of catalyst layer density on CNT film

Investigation of catalyst concentration variation on film synthesis is done by varied catalyst layer concentration application between two aluminium nitrate layers. The catalyst molarity variation of the prepared iron nitrates as follows; 10mM, 5mM, 2.5mM, 1mM, 0.1mM. Base and top layer aluminium nitrate concentration kept constant at 5mM. In Figure 35, catalyst concentration varied samples after synthesis can be seen from top and side views. The sample prepared by 10mM catalyst layer is dense, homogenous and individual CNTs can be differentiated and they are vertically aligned. Hence, 5mM catalyst layer applied sample is much denser. This can be explained by the catalyst size effect. As the catalyst size increases the synthesized CNT gets wider in diameter. By twice as iron concentration it is possible that the iron clusters are wider in diameter than found in 5mM applied catalyst layered sample. Film height is 2.5µm nearly same for two sample. As the concentration decreases to 2.5mM, vertical alignment of CNT array is diminished and the height of the film decreases to almost 1µm. As the catalyst concentration decreases, their orientation in alumina matrix leads changes. Increase at the distance between neighbouring catalysts particles resulted with non vertical alignment of each tube during synthesis

as the van der Waals interactions between tubes disappears. They loose self alignment, folded on one another as they are flexible. This trend is more obvious in 1mM catalyst layer applied sample; the CNT density drastically decreases and CNTs are rare, height is in the range of 700nm-500nm. Catalyst layer concentration of 0.1mM treated sample showed no CNT formation at all. There formed a thick alumina layer.

The catalyst layer concentration varied samples are also characterized by CA measurement device. Dynamic CA studies are done on samples by same amount of double distilled water 8µm, at room temperature for 30 minutes. In every 5 minutes CA values of corresponding sample recorded and water droplet on sample surface captured by CCD camera. Changed surface property shifts against varied catalyst layer concentration can be seen in Figure 36. The graph in Figure 36 (CA versus time) and Figure 37 (minutes versus concentration of the base layer), is summarized data of measured samples in every 5 minutes.

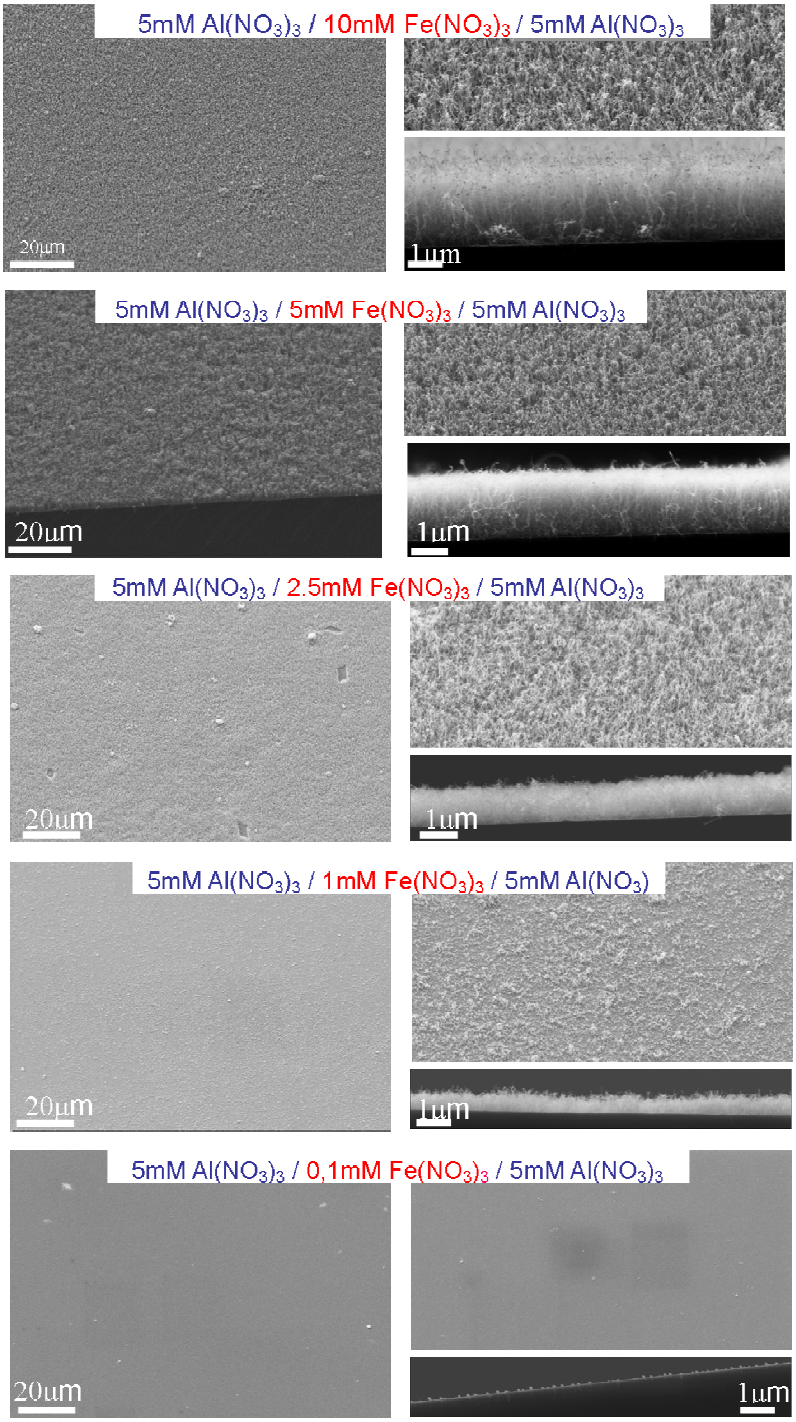

Figure 35. Schematic representation of the experimental sets; Left side - general view of iron nitrate concentration varied samples prepared by sandwich method. Right side - high magnification SEM images and side view of corresponding samples.

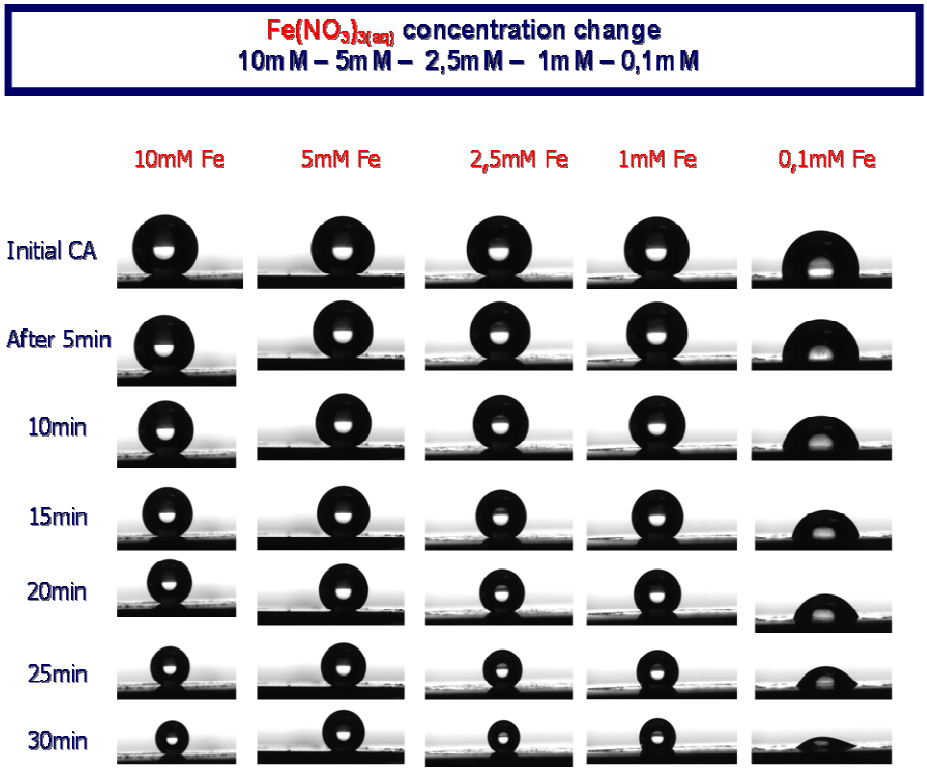

Figure 36. Dynamic CA measurements are done by same volume of double distilled water 8µm on catalyst layer concentration varied samples. The CA measurements are done in every 5 minutes.

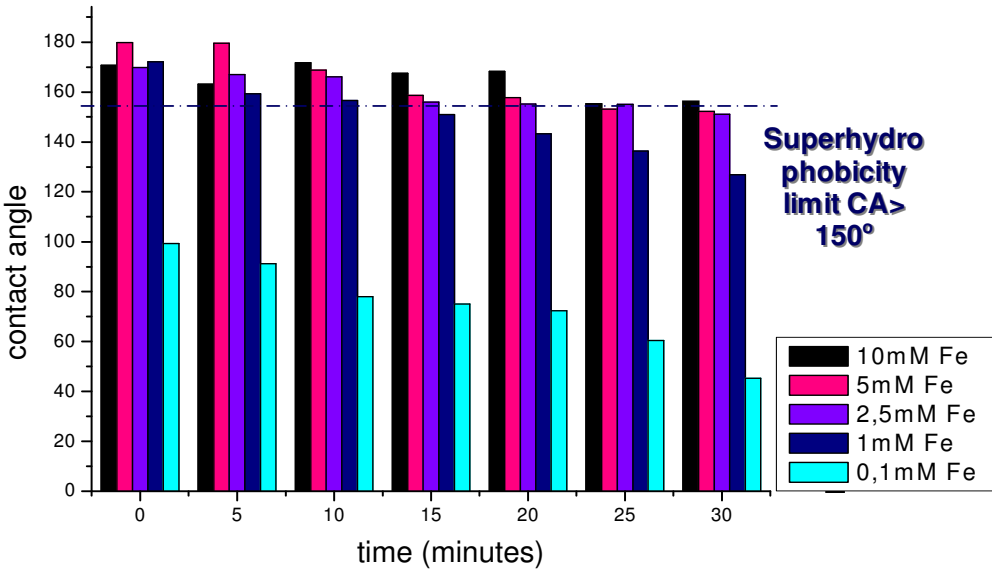

Figure 37. Dynamic CA measurements on varied catalyst layer concentration samples. CA values in angles versus 30 minutes. Indication of super-hydrophobicity limit > 150°C.

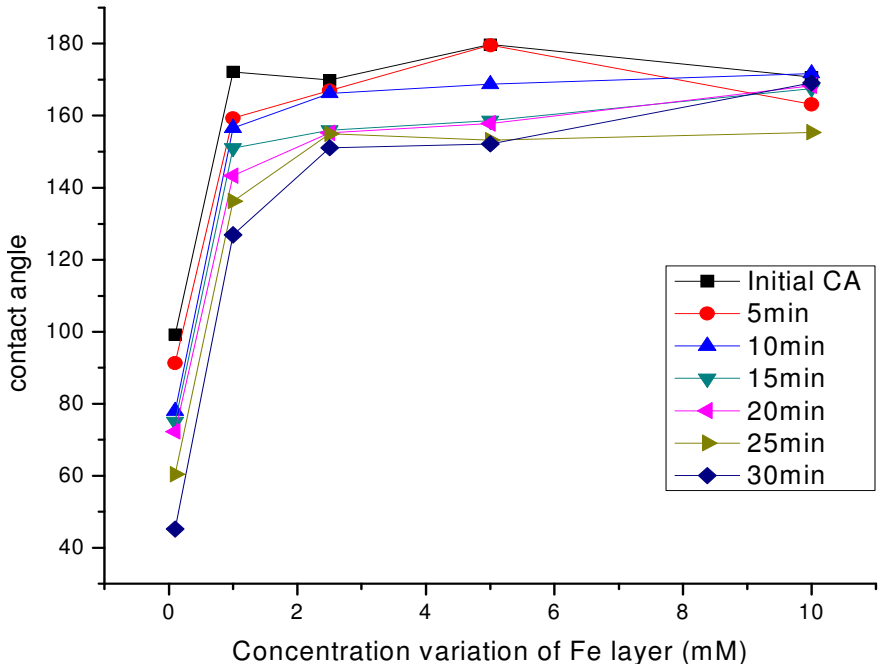

Figure 38. Dynamic CA measurements onto VANTA samples that are synthesized with varied catalyst layer concentration. CA versus concentration variation of applied catalyst layer.

The measurements of dynamic CA corresponding catalyst layer concentration varied samples indicate the well ordered CNT arrays demonstrate super-hydrophobic character even after 20 minutes, in Figure 37 and Figure 38. Without any surface modification, stable super-hydrophobic character at CNT arrays is first time indicated in this study. Maximum CA angle is achieved by 5mM $Fe(NO_3)_{3(aq)}$ at initial CA measurements, other 3 samples (10mM, 2.5mM and 1mM) are also super-hydrophobic. At the end of 30 minutes 10 mM catalyst layer applied sample is the closest one to super-hydrophobicity limit. Also 10mM, 5mM and 2.2mM catalyst layer applied samples have close CA values at 30^{th} minute measurement. After 10th minute 1mM catalyst layer applied sample fall behind the super-hydrophobic zone. Trend at sample (0.1mM catalyst layer) that even no CNT growth observed is different than other four samples, initial CA is 100^{o} decrease to 40^{o} after 30 minutes.

In the literature, it is claimed that without chemical modification CNT arrays are hydrophobic at initial CA but water droplet quickly penetrates into CNT array resulted as hydrophilic [96]. There are many reports showing CNT arrays are collapsed and lost their alignment, forming polygons after contact with water droplet [93, 97, 98]. Nevertheless, CNT arrays synthesized by sandwich method reached stable super-hydrophobicity without any chemical modification. According to our knowledge, this is the first time that stable super-hydrophobicity of CNT arrays is indicated without any chemical modification.

Raman analysis of the catalyst layer concentration varied samples is done by 532 nm green laser. From each sample, three different spectra are collected via x100 lens. For every sample, base line corrections and peak fitting analysis are done with mean spectrum of three spectra. In Figure 39, Raman spectra of 5 samples can be seen. The details of first order Raman peaks can be seen. The origins for the first-order Raman bands of CNTs at spectra have been covered in detail in recent works [99,100].

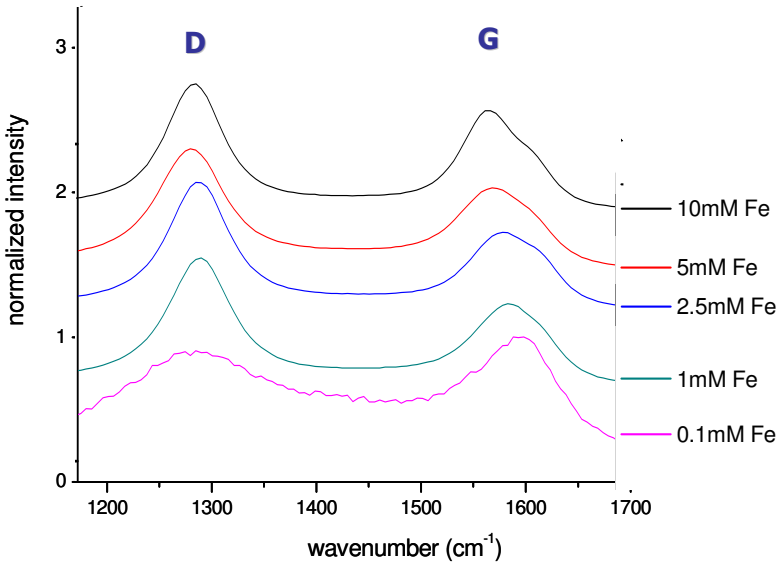

Figure 39. Raman analysis of the catalyst layer concentration varied samples. Intensities are normalized.

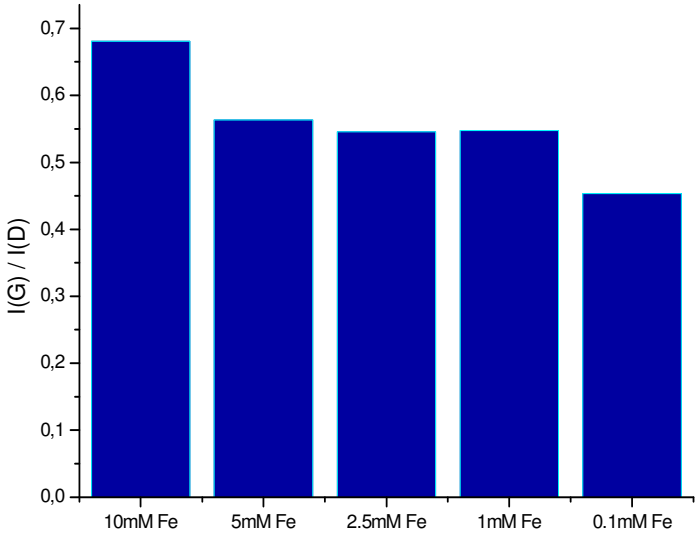

Figure 40. I(G) / I(D) results of the corresponding Raman analysis of the catalyst layer concentration varied samples.

The defectiveness of CNTs can be compared one sample to another by the intensity ratio of the G band versus the D band, I(G)/I(D). The defect density at the hexagonal carbon network of CNTs resulted with the formation of D band [101 – 103]. Intensities are normalized and peak fitting of D and G peaks are done by Gauss*Lorentz method in PeakFit v14.12 programmer. Area under each peak is then

inserted in I(G) / I(D) ratio to get information about defectiveness of CNTs as the intensity of D band is directly related with the defect density in hexagonal carbon network. In Figure 40, highest I(G)/I(D) ratio is achieved from 10mM iron nitrate added sample. For the samples having catalyst layer concentration 5mM, 2.5mM and 1mM, I(G)/I(D) values are nearly same by having a decrease after 5mM catalyst layered one. The lowest value of I(G)/I(D) is corresponds to 0.1mM iron nitrate added one that have no CNT growth at all. It may refer to amorphous carbon collected on the top of the alumina layer during reaction step. Also the Raman signal is not strong, in Figure 39.

4.1.3.2 Effect of base layer density on CNT film

The effect of base layer aluminium application on vertically aligned CNT arrays is detected by variation at concentration of aluminium nitrate solution. Concentration variation is as follows; 10mM, 5mM, 2.5mM, 1mM and no Al layer. Catalyst and top layer concentrations kept constant as 5mM. Synthesized samples from top view and side view can be seen in Figure 41. Applied aluminium nitrate concentration of 10mM, resulted with inhomogeneous CNT film formation. The reason is related with high amounts of alumina formation during reduction step. This thick alumina layer prevents CNT formation as the all iron nanoparticles can not be activated as being embedded through alumina matrix. This indication is important because of showing the critical concentration combination of aluminium nitrate to iron nitrate ratio for high quality VANTA growth. As the base layer aluminium nitrate concentration decreases, the film density is affected but the vertical alignment is not diminished. SEM images of the samples can be seen in Figure 41, as general view at the left side and detailed and side image at the right side.

Dynamic contact angle measurements are done on base layer concentration varied CNT samples against 8µl of double distilled water for 30 minutes at room temperature. In every 5 minutes CA of the samples are captured by CCD camera. Initial CA of the samples is higher than 150^{o} that refers to super-hydrophobic surface characteristics for 5mM, 2.5mM, 1mM and no Al layered samples. Even after 30 minutes 5mM and 2.5mM base layer applied CNT samples are super-hydrophobic. In

Figure 42, dynamic CA measurements against 30 minutes can be seen for five samples. The CA values of corresponding samples are graphitized in Figure 43 (CA versus minutes) and Figure 44 (minutes versus concentration of the base layer).

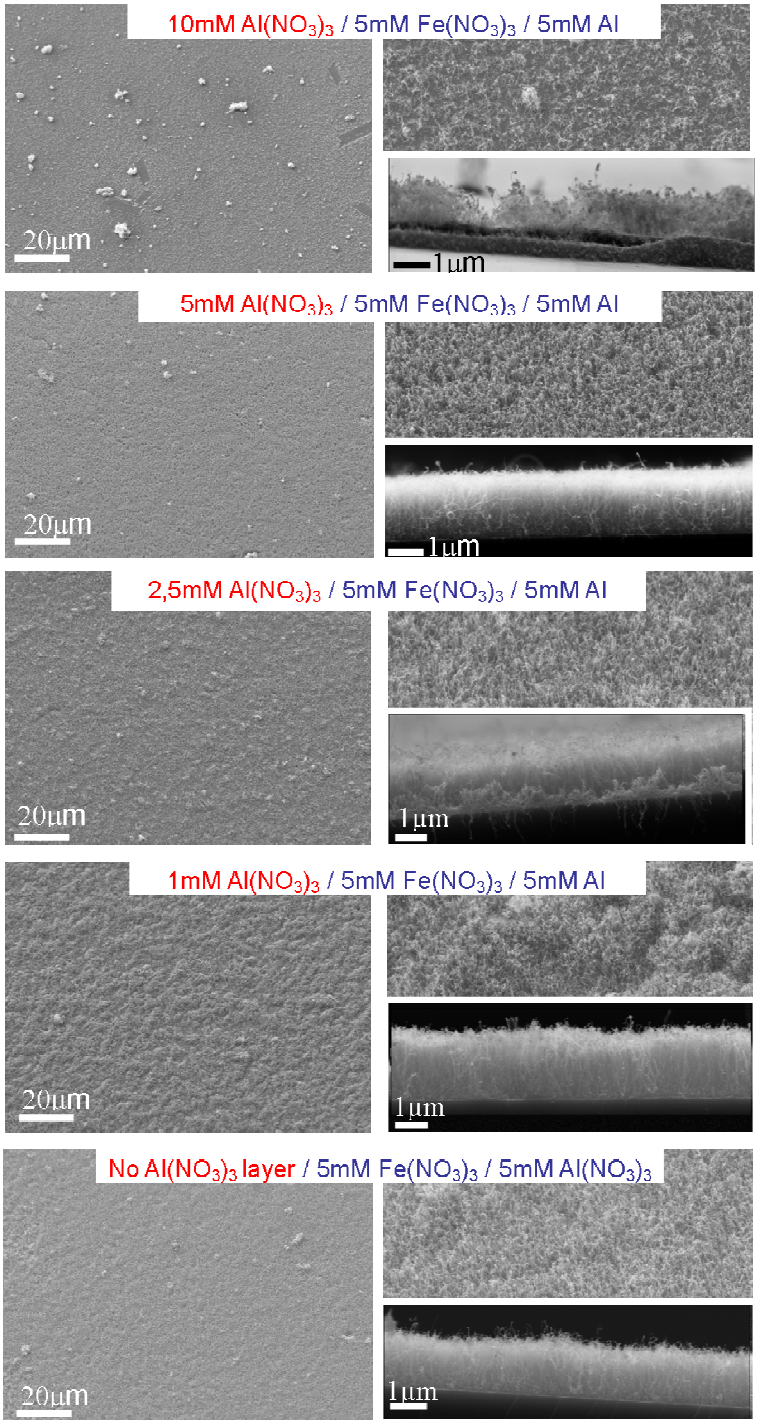

Figure 41. Schematic representation of the experimental sets; Left side - general view of base layer aluminium nitrate concentration variation at the applied layers of sandwich method. Right side - high magnification SEM images and side view of corresponding samples.

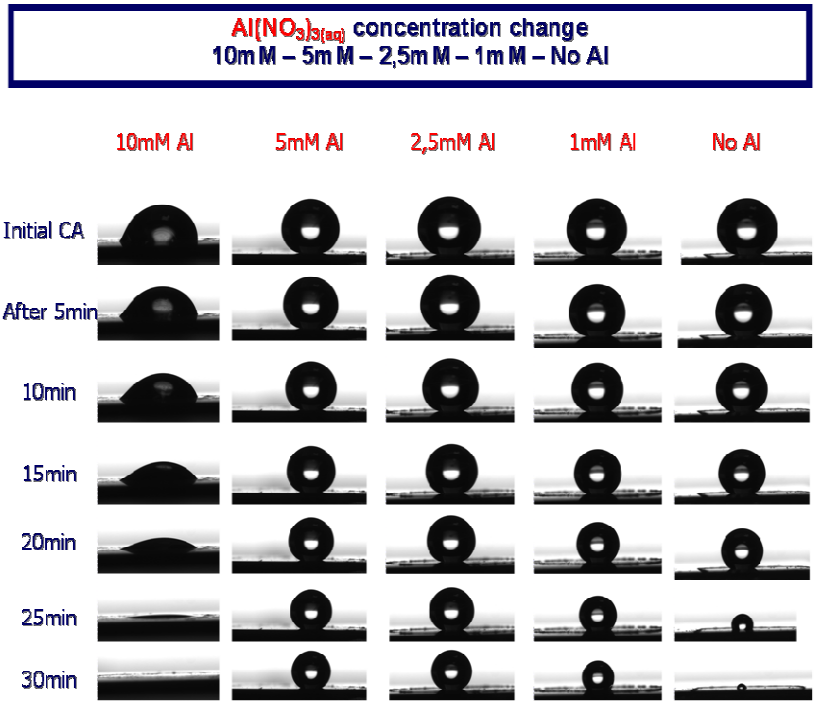

Figure 42. Contact angle measurements onto VANTA samples that are synthesized with varied catalyst layer and aluminium base layer concentration separately. CA measurements are done with 8µm distilled water and the change at CA is captured by camera at every 5 minutes.

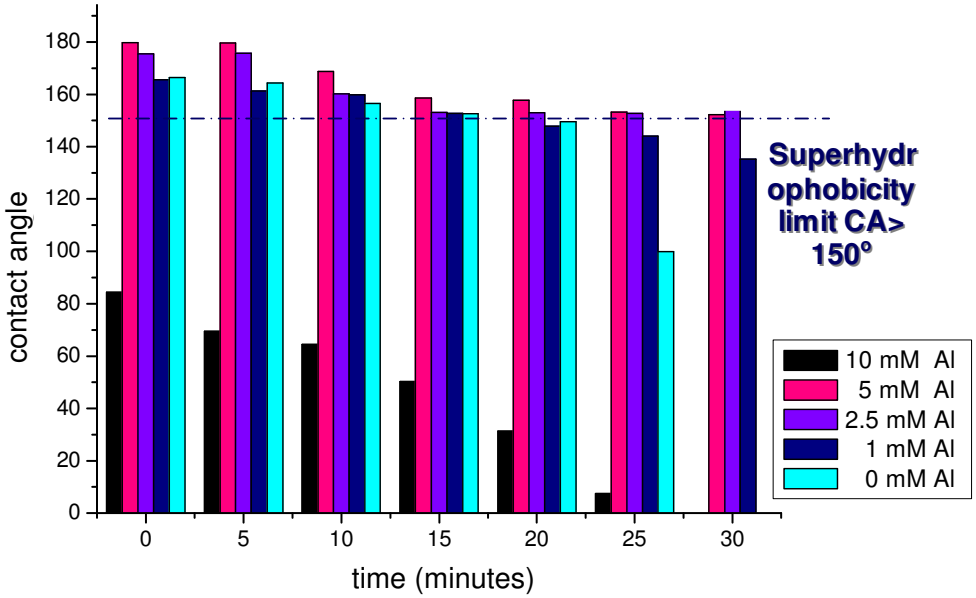

Figure 43. Dynamic CA measurements on varied base layer concentration samples. CA values in angles versus 30 minutes. Indication of superhydrophobicity limit > 150°C.

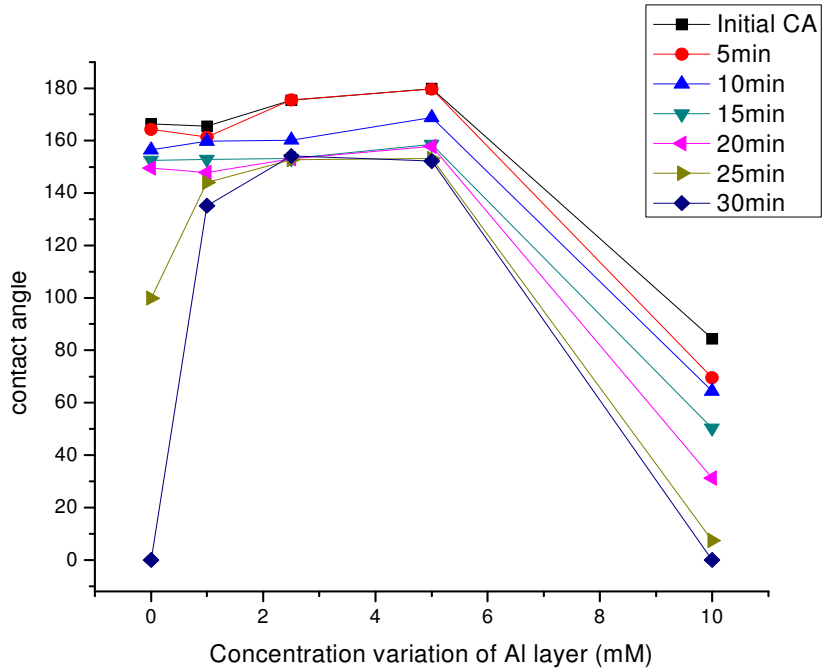

Figure 44. Dynamic contact angle measurements onto VANTA samples that are synthesized with varied base aluminium layer concentration.

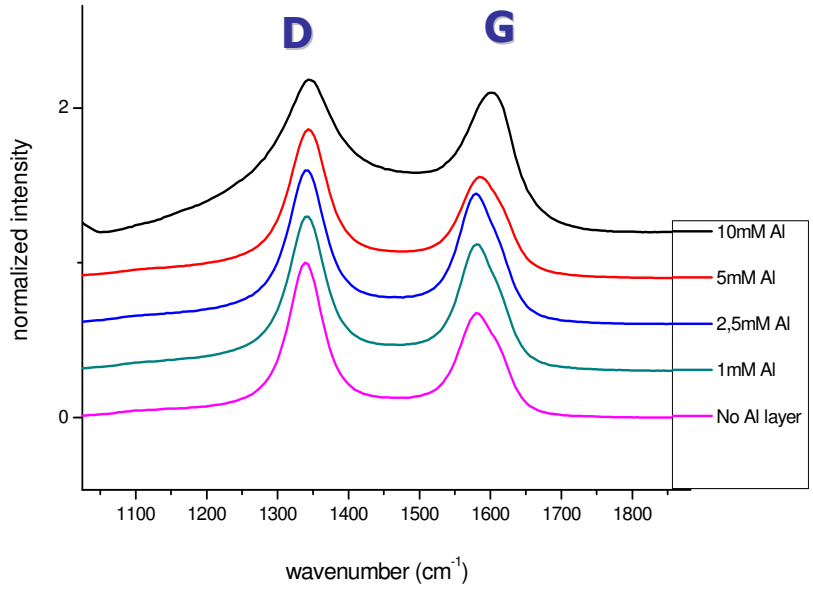

Figure 45. Raman analysis of the base layer aluminium nitrate concentration varied samples. Intensities are normalized.

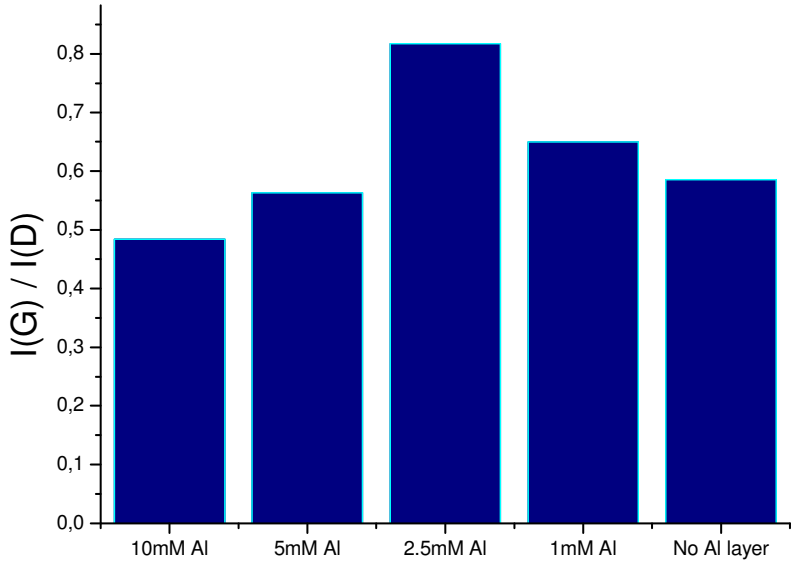

Figure 46. I(G) / I(D) results of the corresponding Raman analysis of the base layer aluminium nitrate concentration varied samples.

Raman spectrum of each sample can be seen in Figure 45. Raman analysis indicates the I(G) / I(D) ratio is maximum for 2.5mM base Al layer applied sample,

in Figure 46. This result is important for showing the critical Al layer and Fe layer concentration combinations for high quality CNT film growth. The Raman analysis is also coherent with CA measurements of corresponding samples. Even after 30 minutes of CA measurement 2.5mM base Al layer applied sample is above the super-hydrophobicity limit.

The efficient combinations of Al to Fe ratio enables well aligned and super-hydrophobic VANTA films. With no Al layered sample, it is also well aligned and show super-hydrophobic surface characteristics until 15^{th} minute of CA measurement. After 15^{th} minute water encapsulated inside CNT forest may reach oxidized silicon substrate and spread on it over the roots of CNTs. 5mM and 2.5mM Al layer applied CNT films are remained super-hydrophobic after 30 minutes of water interaction. If the SEM images of each sample are compared, they are dense and nearly 2µm in length. The sample with 10mM base layered Al, is having inhomogeneous and rare CNT growth. This surface can not be considered as hydrophobic under same conditions with other Al layer varied samples. The film density and homogeneity is found to be determinant on super-hydrophobicity of the growth vertically aligned CNT arrays.

To sum up, the synthesis of vertically aligned CNT arrays are achieved by finding an optimum catalyst design as sandwich technique. Dense and homogenous film synthesis is achieved by layer by layer addition of aluminium nitrate / iron nitrate / aluminium nitrate 5mM / 5mM / 5mM. Moreover, stable super-hydrophobicity is achieved first time by this technique without any chemical modification of the VANTA. In Figure 47, summary of the improvement at catalyst design is given. All of the requirements are achieved by sandwich method.

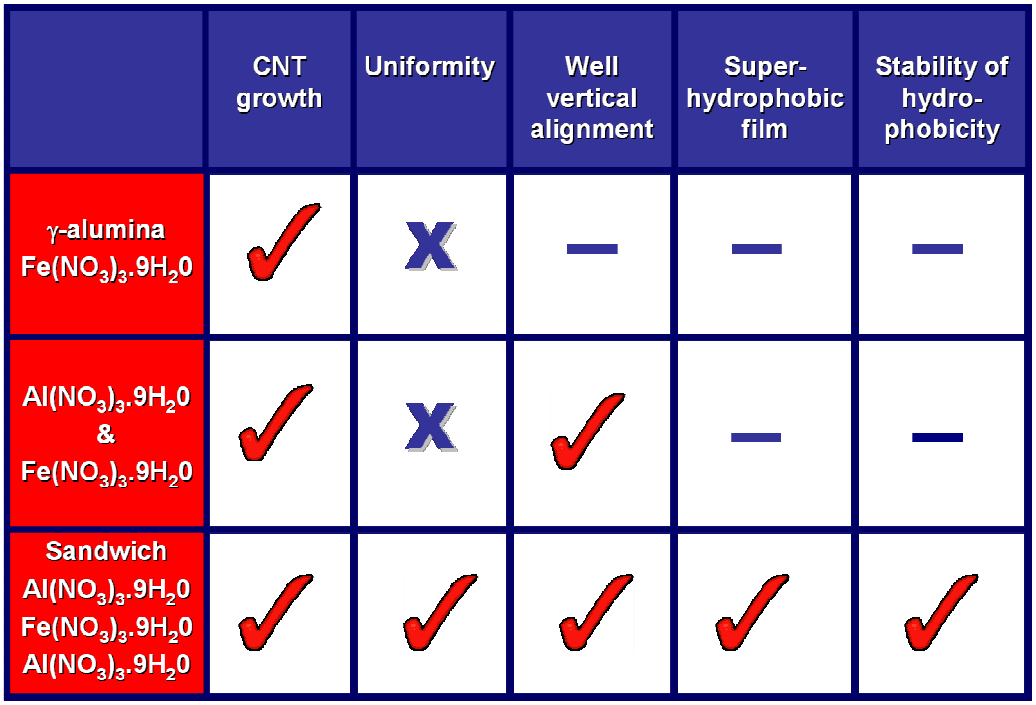

Figure 47. Indication of the effectiveness of three different catalyst preparation techniques on the parameters CNT growth, uniformity, well vertical alignment, super-hydrophobic film and stability of hydrophobicity.

The effect of varied catalyst and base layer alumina concentration is studied. Synthesized CNT film characterization is done via Raman and CA analysis. For catalyst layer concentration varied samples, 10mM, 5mM and 2.5mM iron nitrate catalyst layer applied samples are dense and show homogenous vertically aligned CNT synthesis. Furthermore, they keep super-hydrophobic character even after 20 minutes exposure to water droplet. The highest I(G)/I(D) ratio is found to be achieved 10mM catalyst layered vertically aligned CNT arrays, suggests less defectiveness in graphitic network of CNT side-walls. For base layer concentration variation, the highest film quality is achieved by 2.5mM aluminium nitrate added sample according to Raman and CA analysis. These results refer a critical concentration adjustment for the synthesis of high quality VANTA film by sandwich method. According to layer combinations of sandwich method as aluminium nitrate / iron nitrate) / aluminium nitrate, catalyst layer concentration changed sample with the combination of 5mM / 10 mM / 5 mM and base layer concentration varied sample 5

mM / 5 mM / 2.5 mM indicates the total applied Fe:Al concentration ratios are 10:10 and 5:7.5 (1:1 and 2:3), respectively.

4.2 Functionalization of carbon nanotubes

4.2.1 Effective dispersion of carbon nanotubes with CPNs

The conjugated polymer nanoparticles (CPNs) are prepared in two different size distributions using the re-precipitation method which involves solubilizing of the polymer in a good solvent (e.g.THF) and injecting the polymer-THF solution in a poor solvent (e.g. water) during rapid stirring of the dispersion via ultrasonication. Injecting step is important to achieve CPNs which are in a narrow size distribution nearly same size. For this, injection of the polymer-THF solution is done by a 0.45µm sized filter fitted at the end of the syringe during the transfer of polymer-THF solution to poor solvent. The removal of the good solvent is done by rotary system. By the evaporation of the good solvent, nearly spherical nanoparticles are obtained that are water soluble. The size distribution of the nanoparticles (CPNs) can be arranged due to changing added polymer concentration and the volume of the poor solvent. The average sizes of the nanoparticles are determined first by DLS as ~70 nm and ~40 nm average sizes as shown in Figure 48.

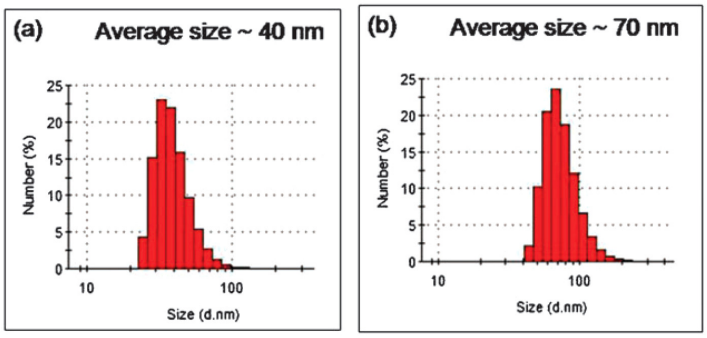

Figure 48. Histograms for 40 nm **a)** and 70 nm **b)** CPNs measured by DLS.

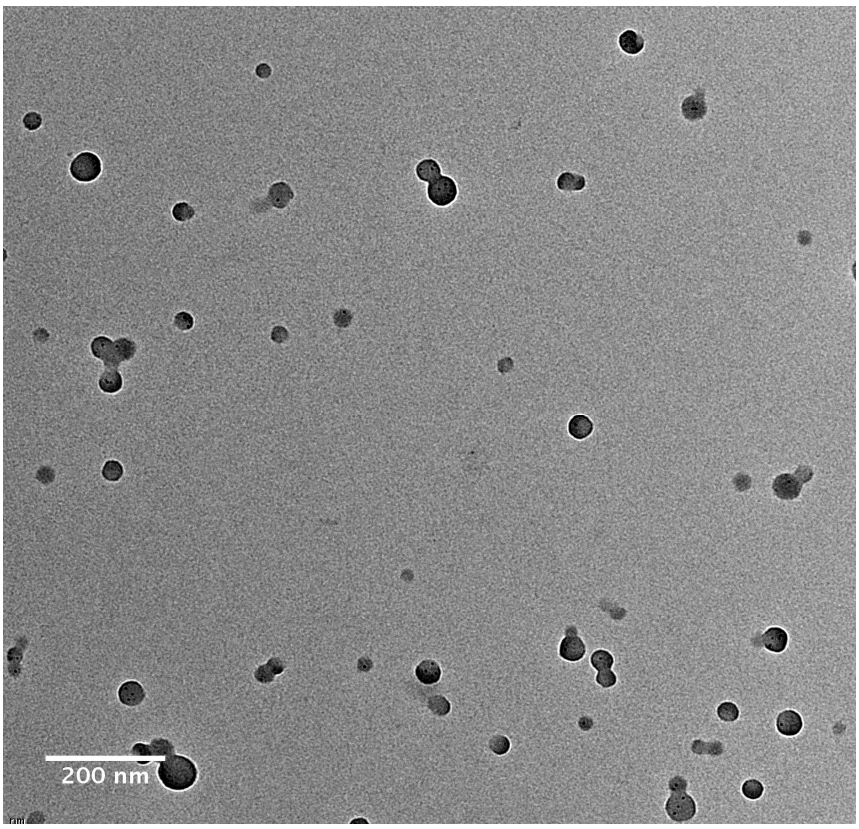

Figure 49. A TEM image showing CPNs of average size 40 nm

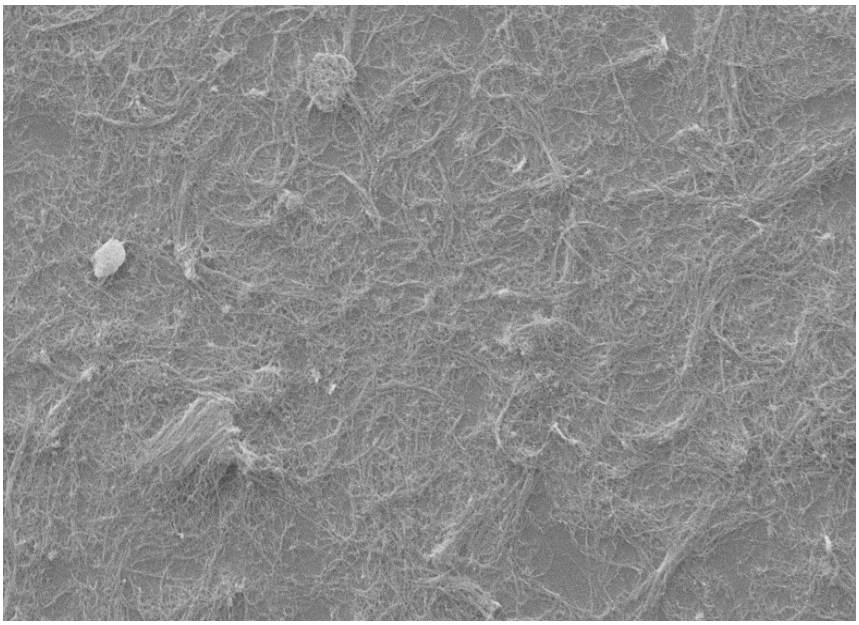

Figure 50. SEM images of bundled CNT clusters dispersed in water dried on Si wafer.

Conjugated polymer nanoparticles are prepared in two different sizes. Firstly, 10 mg polymer of PFB-B is dissolved in 10 ml THF and stirred overnight at room temperature. To decrease interaction between polymer strains, volume of the solution is increased to 100 ml by adding access THF. Then, solution is injected by filtering through 0.45 um syringe filter to be used as stock solution for CPN preparation.

The size distribution of CPNs are detected by dynamic light scattering (DLS) in Figure 48 and transmission electron microscope (TEM). In Figure 49, TEM images of CPNs of average size 40 nm are shown.

4.2.1.1 Interaction of CPNs and carbon nanotubes

Our calculations and measurements resulted that there is approximately ~ 6 x 10^{-2} mg of CNT on 1x1 cm^2 Si substrates. Detailed information can be seen in Appendix B. These substrates with vertical CNT arrays are placed inside vials with several different sized nanoparticles solutions ranging from 0.2mg/ml to 0.002mg/ml. These VANTA samples are sonicated in these nanoparticle-water mixtures for 60 minutes at room temperature. As a control sample another CNT array is also dispersed in water. As shown in Figure 51-a, upon introduction of CNTs the colour of the CPN–water dispersion in the vial turns greyish indicating good dispersion. Good dispersion can be achieved with a minimum mass ratio of 0.2 for CPN to CNT demonstrating that CPN is a remarkably efficient dispersant for CNTs in water. SEM image of the bundled CNT clusters dispersed in water can be observed in Figure 49.

4.2.1.2 The maximum concentration of carbon nanotubes with CPNs

Many of VANTA samples are synthesized (around 2 mg nearly 30cm^2) to decide maximum concentration of CNTs in CPNs. These samples are placed into 100 ml of CPN water dispersion (0.2 mg, 40nm-sized CPN) containing beaker and as a

control experiment the same amount of VANTA sample is placed into a 100 ml of aqueous media. Both mixtures are sonicated for an hour and same procedures are followed by keeping the temperature of the sonicator at room temperature. After sonication step, most of the CNTs in CPNs are well dispersed. On the other hand, CNTs in aqueous media are started precipitation just after removal from sonication bath. To separate if there are any un-dispersed bundled CNTs from the CNTs/CPNs mixture, filtration step is added. As the whole solution transferred from filtrate, filter is found clear without any remaining from the CNTs/CPNs mixture. The filtrated mixture is then evaporated under reduced pressure to volume of 5ml. The mixture is stable after concentrated conditions without any precipitate observation. After these findings, highest CNT to CPN concentration of stable dispersions is ~0.25 mg mL^{-1} by 0.2:1 polymer to CNT mass ratio. Although some precipitation can occur after 12 h, dispersions can be easily redissolved by 1-2 minutes sonication. In Figure 51-a maximum amount of CNTs in 40 nm sized CPNs after sonication can be seen. Under UV radiation in Figure 51-c this solution shows intense blue colour. The control sample with the same amount of CNTs in water only can be seen as Figure 51-b and under UV as Figure 51-d.

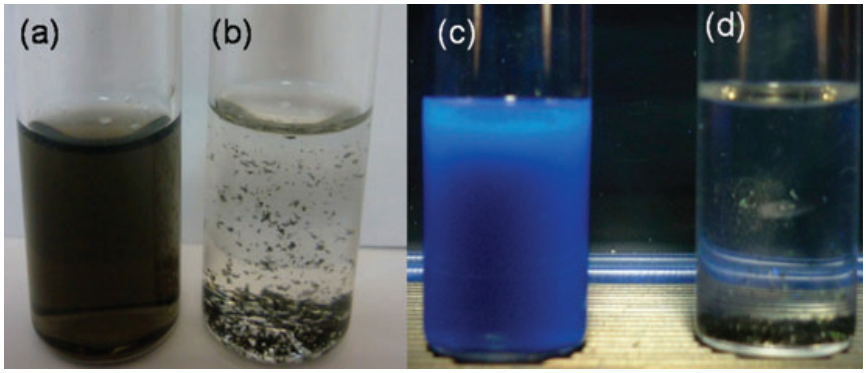

Figure 51. (a, c) Images of CPN (40 nm-sized)–CNT with 0.2 : 1 CPN to CNT mass ratio and **(b, d)** CNT–water dispersion, **(a, b)** under ambient and **(c, d)** UV-light irradiation.

The average size of CPNs is found to be effective on the well dispersibility of CNTs. This is investigated by UV-Vis and fluorescence spectroscopy. 40 nm average sized CPNs are better dispersants with respect to 70 nm average sized CPNs. The interaction between CPNs and CNTs is first investigated by. Effect of different

sized CPNs on interaction with CNTs can be seen in Figure 51-c. The UV-Vis spectra of 40 and 70 nm-sized CPNs in the presence and absence of CNTs in water is shown. Absorption spectra do not indicate a significant change suggesting that the electronic structure of the nanoparticles is not altered upon complexation with CNTs, Figure 51-(a,b).

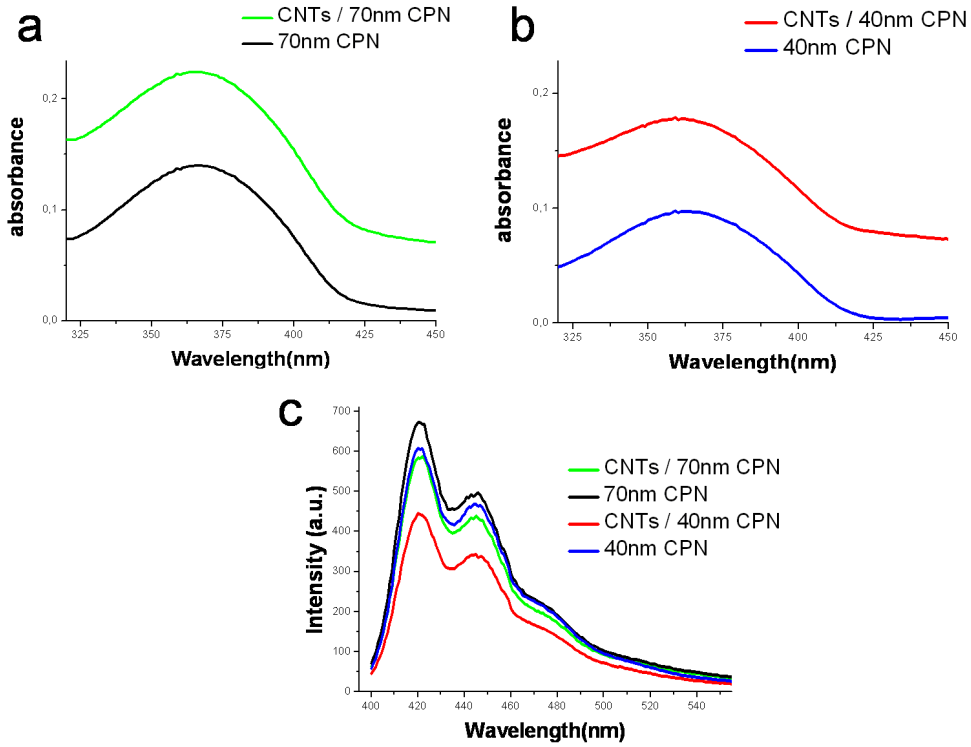

Figure 52. The UV-Vis absorption **(a, b)** and emission spectra, **c)** of 40 and 70 nm-sized CPNs in water and CPN–CNT dispersions.

Aqueous solution of CPNs indicates a strong fluorescence emission at 421 nm, decreasing after dispersing the CNTs from VANTA samples, in Figure 52-(a,b). The quenching at the mixtures of CPNs with CNTs shows differences via using 40 and 70 nm-sized CPN–water dispersions. A higher degree of quenching can be seen in Figure 52-c, with 40 nm sized CPNs - CNTs with respect to 70 nm sized CPNs – CNTs some 25% and 10%, respectively. This behavior can be explained by much more efficient energy transfer of smaller sized CPNs with CNTs. This indicates stronger interaction of CPNs that are 40 nm sized with CNT surface than 70 nm sized CPNs – CNTs interaction.

Interaction between CPNs and CNTs can also be examined by Raman spectroscopy. As a control sample CNTs added in water used to make a better comparison towards CPN-CNT interaction. The Raman spectra of CPN–CNT mixtures and CNTs dispersed in water are given in Figure 53. The first order Raman peaks of CNTs are indicated as D band (1347 cm^{-1}) and G band (1584 cm^{-1}). Additional deconvolution peak of G peak, D' is also indicated as a shoulder in the Raman signal of CNTs in H_2O. The details of first order Raman peaks of the samples are given in Table 2. The CNTs dispersed in water show all of the expected first-order structures [99,100].

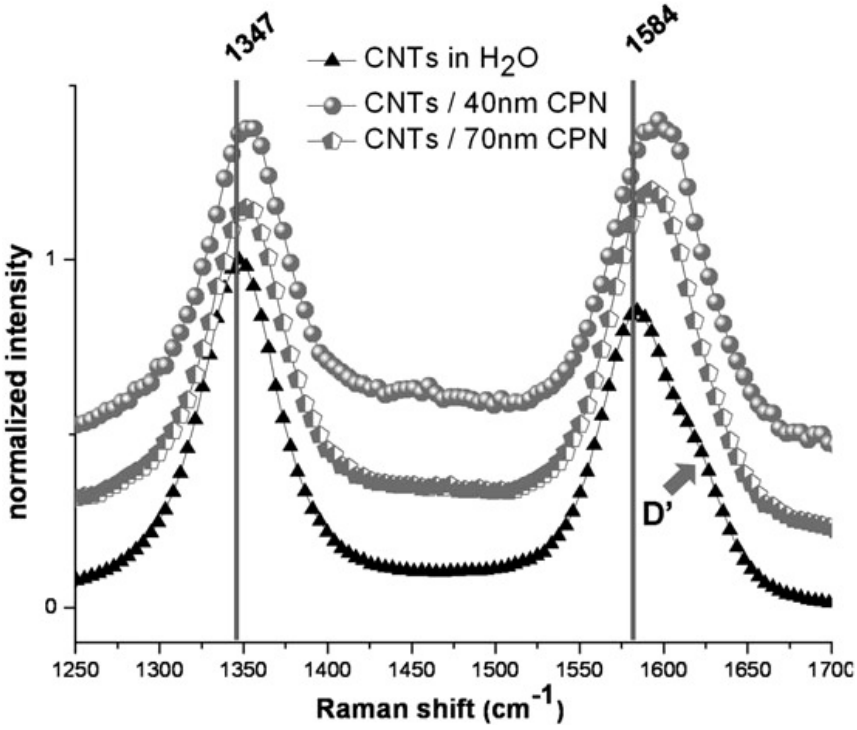

Figure 53. The first-order Raman spectra from pristine CNTs dispersed in water and CPN–water dispersions.

Table 2. Numerical data regarding Raman spectra analysis

	D peak position/cm^{-1}	G peak position/cm^{-1}	Δ(G–D)/cm^{-1}	I_G/I_D
A	1347	1584	237	0.7
B	1352	1593	241	0.8
C	1356	1597	241	1.0

A: Pristine CNT in water; B: CNTs/70 nm CPNs; C: CNTs/40 nm CPNs.

The defect density at the hexagonal carbon network of CNTs resulted with the formation of D band [101, 102]. The I(G)/I(D) ratios of three sample can be seen in Table 2 with the peak positions and (G-D) values. According to our calculations, CPN–CNT mixtures indicate higher I(G)/I(D) ratios than CNTs dispersed in water. An improvement at the defect density can be the reason of this increased value. Same result has been found by Patole *et al.* for the mixture of polystyrene - CNTs refers saturation of dangling bonds in the hexagonal network of CNTs [103]. Decrease at D band intensity and diminished D' band at the Raman signals of CPN–CNT mixtures explains the saturation behavior as described in the literature. Another indication from these results can be the interaction of CPNs with CNTs is responsible of electronic structure changes on CNT surface. On the other hand, there is a small shift at G band to higher frequency as the (G-D) value increases. This result is considered as a proof of interaction of polymer with CNT surface.

The interaction between CPNs and CNTs is also investigated by using electron microscopy techniques, such as SEM and TEM. In Figure 54-a and -b, attached CPNs on CNTs is clearly seen. To make comparison of the de-bundling process of CNTs, one can compare Figure 50 and Figure 54 as first one is only CNTs in water and the other ones are CPN-CNT mixture in water. Images with CPN attached CNTs are obviously de-bundled. Detailed TEM imaging shows the spherical nanoparticles of conjugated polymer replace on the outer wall of CNT. In Figure 54-(c,d) the attachment of CPNs on nanotube surfaces are examined by TEM.

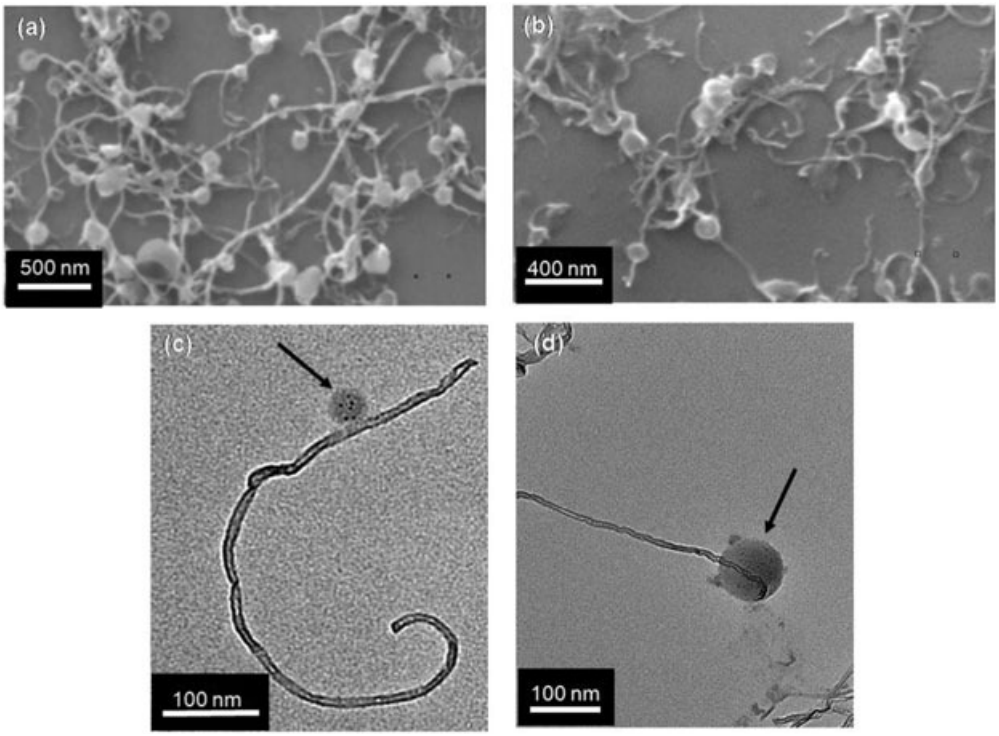

Figure 54. a) 40 nm and **b)** 70 nm CPNs attached to CNTs imaged by SEM; **c)** 40nm CPN-CNT and **d)** 70nm CPN-CNT by TEM.

Brominated structure of the CPNs is detected by EDX analysis. In Figure 55, presence of bromine in nanoparticles attached on CNTs is investigated by EDX data focused on CPN placed on a CNT. Figure 55-a, corresponds to 40 nm sized CPN and -b is 70 nm sized CPN on CNT. As the TEM grid is a copper grid the Cu signals and other metallic signals are originated from the grid.

.

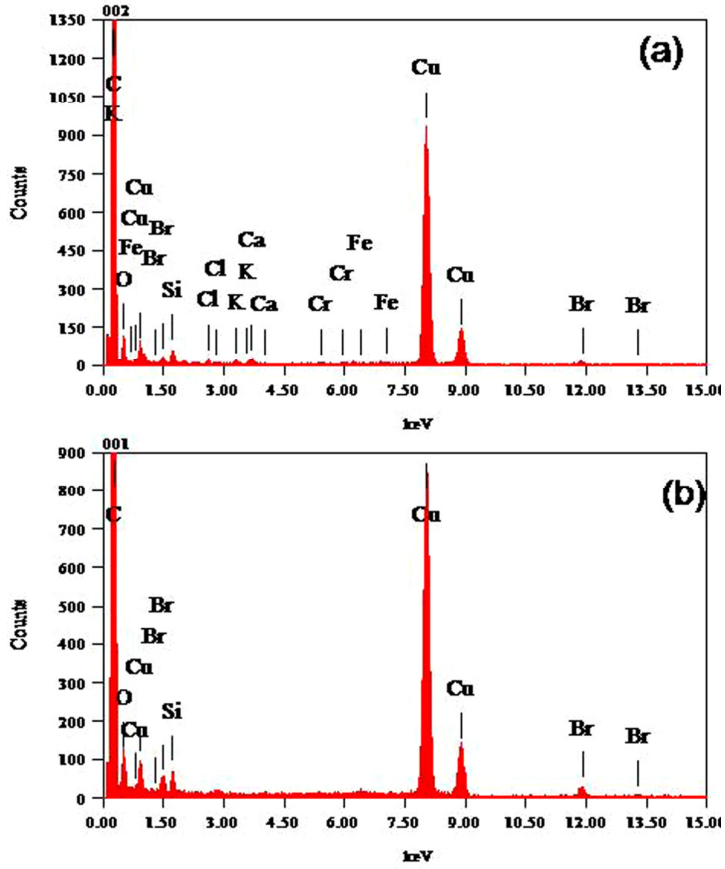

Figure 55. EDX data from **a)** 40 nm and **b)** 70 nm CPNs attached to CNTs.

Finally, the bromine signal originated from CPNs suggest a strong and stable molecular interaction between the CPNs and CNT walls, most likely Π-Π stacking interactions between the polymer aromatic backbones and carbon nanotube side-walls as well as due to the hydrophobic effect. We are continuing our attempts to provide more detail regarding this interaction using techniques such as advanced electron microscopy and first principles density functional theory calculations.[104]

4.2.2 Interaction of carbon nanotubes with CPs

The analysis of polymer-CNT interactions is done with polyfluorene based conjugated polymers (CP). By changing CNT types as MWCNTs, SWCNTs and annealed MWCNTs (an-MWCNTs) and by changing polymer type the interactions are examined. This works are detected by using spectroscopic techniques of UV,

Fluorescent and Raman spectrums. In previous section, CPN-CNT interaction is proved and resulted with well dispersed CNTs in aqueous media. This time, aim is to find out whether the interactions between polymer and CNTs are Π-Π stacking by backbone of the CP with the sidewalls of the CNTs or through the interactions of side chains of CPs with the sidewalls of the CNTs. For instance, two different fluorene-based CPs are used which are poly (9,9-dihexylfluorenyl-2,7-diyl) (PF) and poly[9, 9-bis-(6'-bromohexylfluoren-2, 7-diyl)-co-(benzen-1, 4-diyl)] (PFB-B).

The dispersibility of MWCNTs, an-MWCNTs and SWCNTs in two different polymer media as PF and PFB-B in THF is explored. Figure 19 includes two types of polymer structures as PF and PFB-B. Experimental sets that are done with these two kinds of polymers can be seen in Table 1.

Six sets of experiments are done under same conditions at room temperature by addition of same amount of CNT in each vial and same volume of polymer-THF solution. After 30 minutes of sonication process, the dispersed CNTs in vials form a greyish coloured solution without any clustering formation. In Figure 56, six vials under day light can be seen with indications of S-1 to S-6 representing each corresponding set of experiment. Furthermore, under UV radiation vials turn to intense blue colour, Figure 57. Interestingly, S-1 SWCNTs / PFB-B sample is almost black under day light even under UV light. This is a proof of enhanced interaction of PFB-B type polymer with SWCNTs, polymer loosed all fluorescent property and quenched after interaction. These findings are also coherent with fluorescent spectrum of the samples.

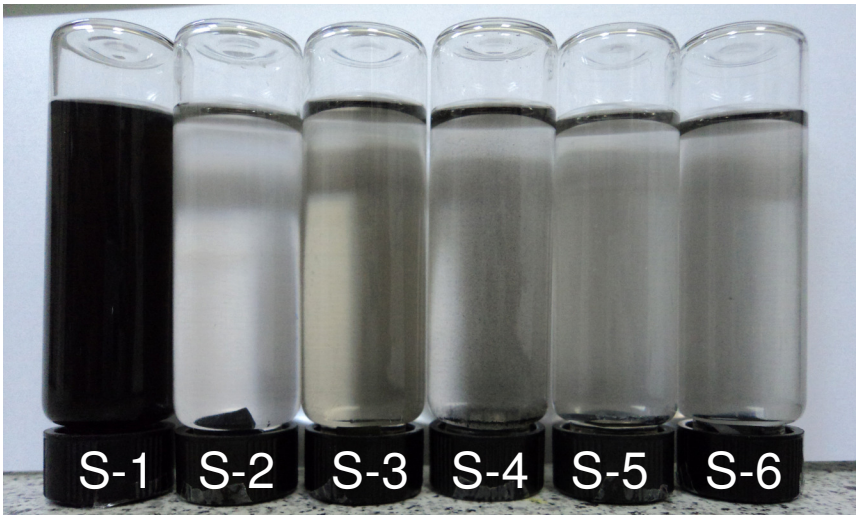

Figure 56. Images of Set-1 to Set-6 indicating as S-1 to S-6 under day light.

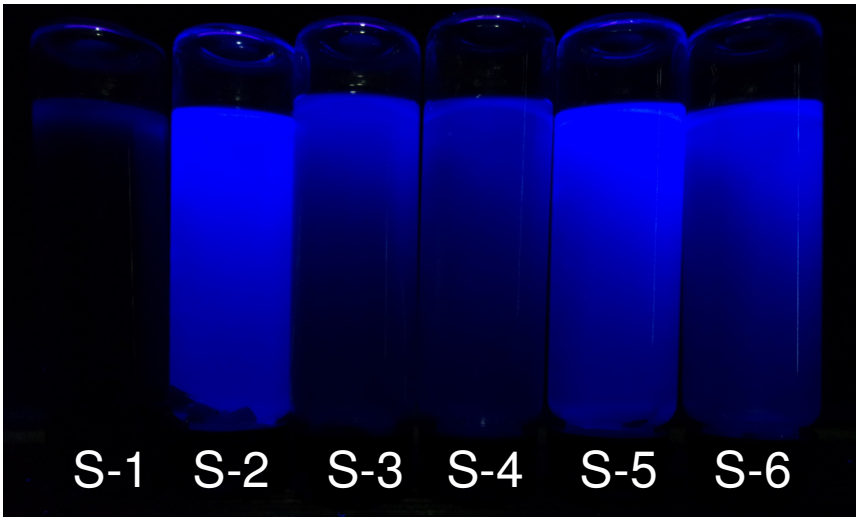

Figure 57. Images of Set-1 to Set-6 indicating as S-1 to S-6 under UV-light (254 nm) irradiation.

4.2.2.1 Flourescence results

The fluorescence data according to each set of experiment is recorded as a comparison to stock solutions of polymer-THF mixtures with same concentration. Separated spectrum of PF and PFB-B polymer with combinations of SWCNT, MWCNT and an-MWCNT is given in Figure 58. For both of the CNT mixtures, there occur decline at the intensities. Instead of using same polymer concentration for

all of the samples, the quenching regimes show different trend at two different polymer types. The quenching efficiency is 67%, 91% and 95% for the solutions of PF/MWCNTs, PF/SWCNTs and PF/an-MWCNTs, respectively. On the other hand fluorescence spectrum of the complexes PFB-B with CNTs are resulted dissimilar regime that the quenching efficiencies are found to be as 78%, 87% and 100% for PFB-B/ an-MWCNTs, PFB-B/MWCNTs and PFB-B/SWCNTs, respectively. These findings regarding such differences at each polymer type can give same clue about the interaction mechanism between CNT surface and polymer type.

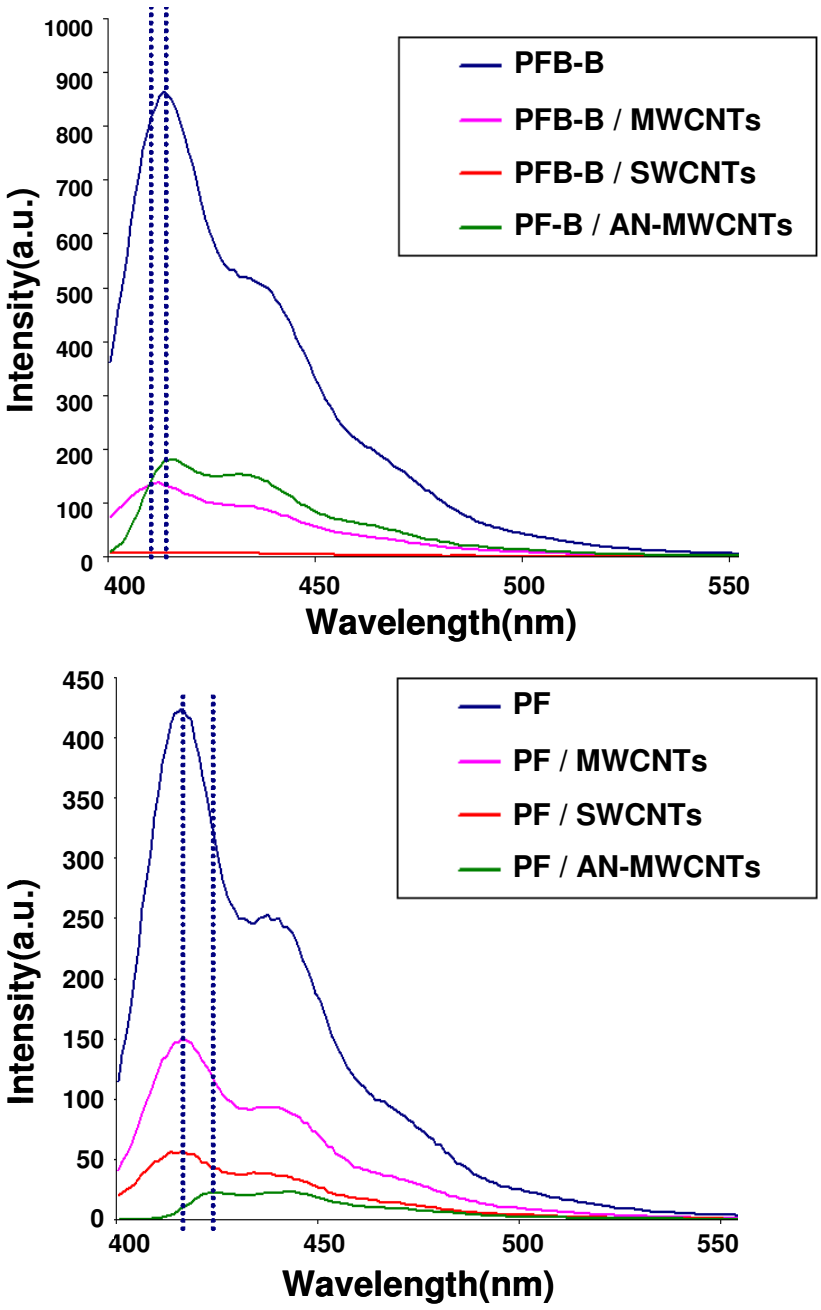

Figure 58. The fluorescence spectra of PF and PFB-B polymers with SWCNT, MWCNT and an-MWCNT.

There are two possible interaction type for conjugated polymers with CNTs; wrapping of polymer chains around the CNTs or Π-Π stacking between the aromatic backbone of the polymer and the hexagonal network at the sidewalls of the CNTs. Two possible interactions can resulted with conformational deviations at polymer chains such as shortening or extended conjugation length of polymer in the media.

The shortening of polymer chain corresponds to wrapping type of interaction and the extended, longer conjugation length is regarding the other type of interaction.

The results of fluorescence spectrum in Figure 58, indicates the total quenching is detected at PFB-B / SWCNTs sample which is also consistent with the photographs of same sample under UV radiation. This result refers the most efficient interaction between polymer-CNT achieved by this sample by total quenching. Some researchers indicate the quenching as photoinduced energy or electron transfer of exited CPs to CNTs [48,49] Adronov and co-workers [105] suggest a dynamic equilibrium can occur between polymer and CNT after desorption of polymers by CNT side walls. For the cases of PF/MWCNTs and PF/SWCNTs mixtures, fluorescent quenching is detected with no shifts in the vibronic bands of 0–0 and 0-1 of PFB at 420 nm and 440 nm, respectively. Nevertheless, fluorescence spectra of PF/an-MWCNT shows ~5 nm red shift at the vibronic peak of 0-0 coupled with quenching. On the other hand, PFB-B/MWCNTs sample indicate blue shift as there occur no shift with the PFB-B/an-MWCNT sample. These findings strengthen the different interaction types can be effective on data achieved from such samples. The conformational changes related with the effective conjugation length of the polymer chains upon binding onto sidewalls of the CNTs are responsible of shifts at the spectrum.

In the case of PFB-B/CNT, the total quenching at the polymer signal is achieved with the sample of PFB-B/SWCNTs. The sample of PFB-B/MWCNTs shows 87% fluorescent quenching and ~5nm blue-shift in the 0-0 vibration peak. A decrease at the average conjugation length of PFB-B can be resulted with such energetic change at the fluorescent spectra. As there seen no shifts with an-MWCNTs case, the defect sides on MWCNT walls are became suitable interaction places for the Br groups at the polymer to be attached, thus cause conformational changes at polymer wrapping structure and effects binding mode of the polymer.

Discrete results at the fluorescence intensities of MWCNTs and An-MWCNTs with PF and PFB-B emphasizes structural changes at CPs are closely related with the nature of the interaction. Most efficient interaction at PF-CNT case is stated by an-MWCNTs with the highest fluorescent quenching efficiency of 95 %

efficiency, red-shift at 0-0 vibronic peak with ~5 nm. This energetically decrease coming from polymer chain signal is probably due extended polymer chains during the interaction with the CNT sidewalls by Π-Π stacking. For the other CNT combinations with PF, SWCNTs are more efficiently interacted with polymer chains with respect to MWCNTs. Due to the non-defective, continuous hexagonal graphitic network of SWCNT side-walls the interaction with PF is improved.

Raman analysis is done under same conditions for all samples at room temperature with 532.1 nm green laser. Each Raman spectra corresponding one sample is mean data of three different spectra taken from one corresponding sample. Figure 59, Figure 60 and Figure 61 shows the result of the Raman analysis separately in the order; PFB-B/CNTs, PF/CNTs and overall six sets of experiments including bare Raman spectrums of SWCNTs, MWCNTs and an-MWCNTs. In order to make a comparison between the polymer – CNT mixtures with the pristine CNTs, SWCNTs, MWCNTs and an-MWCNTs are taken under identical analysis conditions.

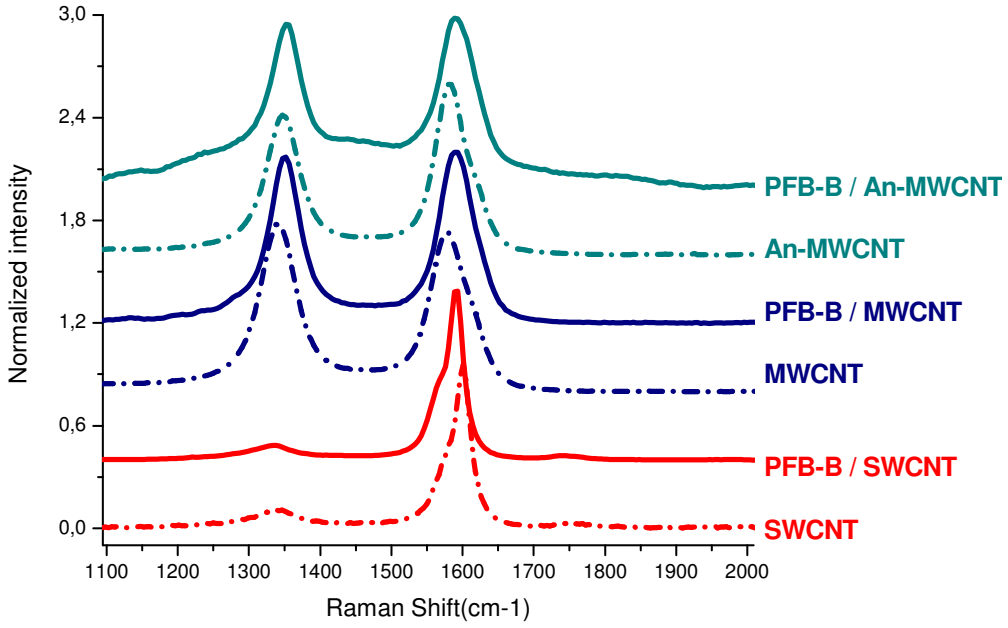

Figure 59. The Raman analysis of the samples Set-1, Set-2, Set-3 interaction with PFB-B and their bare Raman shift results as a reference.

Table 3. The detailed analysis of the Raman data: D and G peak positions of CNTs with and without interaction PFB-B. The G-D represented as Δ to indicate the shifts at different spectrums.

	D (cm-1)	G (cm-1)	Δ(cm-1)
SWCNT	1338.2	1600.9	262.7
PFB-B / SWCNT	1334.3	1592.9	258.6
MWCNT	1343.1	1575.9	232.8
BFB-B / MWCNT	1351.8	1592.9	241.1
An-MWCNT	1347.4	1580.2	232.8
BFB-B / An-MWCNT	1351.8	1588.7	236.9

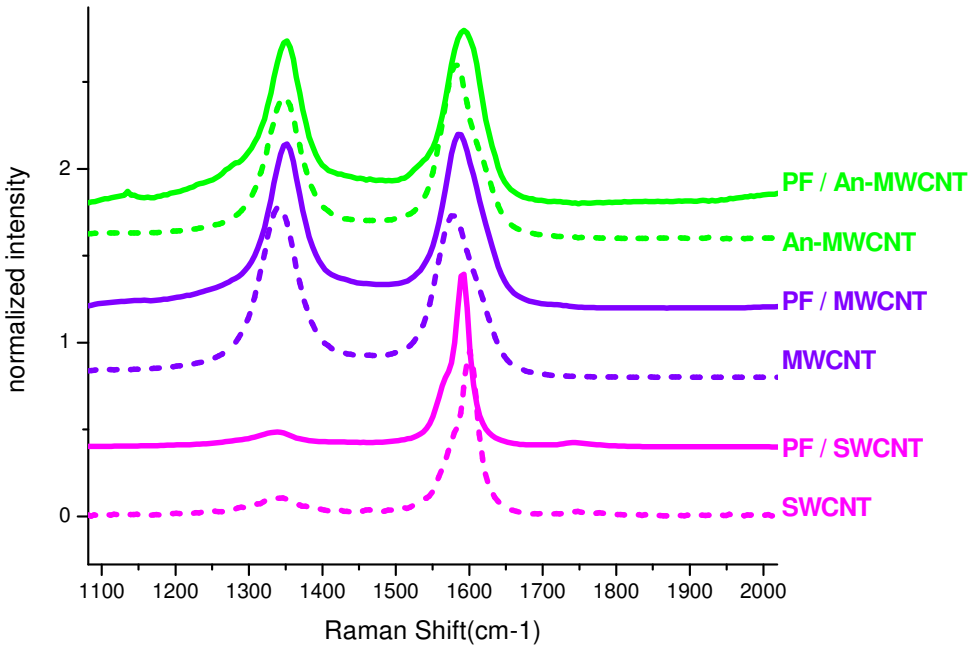

Figure 60. The Raman analysis of the samples Set-4, Set-5, Set-6 interaction with PF and their pristine Raman shift results as a reference.

Table 4. The detailed analysis of the Raman data: D and G peak positions of CNTs with and without interaction PF. The G-D represented as Δ to indicate the shifts at different spectra.

	D (cm-1)	G (cm-1)	Δ (cm-1)
SWCNT	1338.2	1600.9	262.7
PF / SWCNT	1338.7	1592.9	254.2
MWCNT	1343.1	1575.9	232.8
PF / MWCNT	1352.8	1584.4	231.6
An-MWCNT	1347.4	1580.2	232.8
PF /An-MWCNT	1351.8	1592.9	241.1

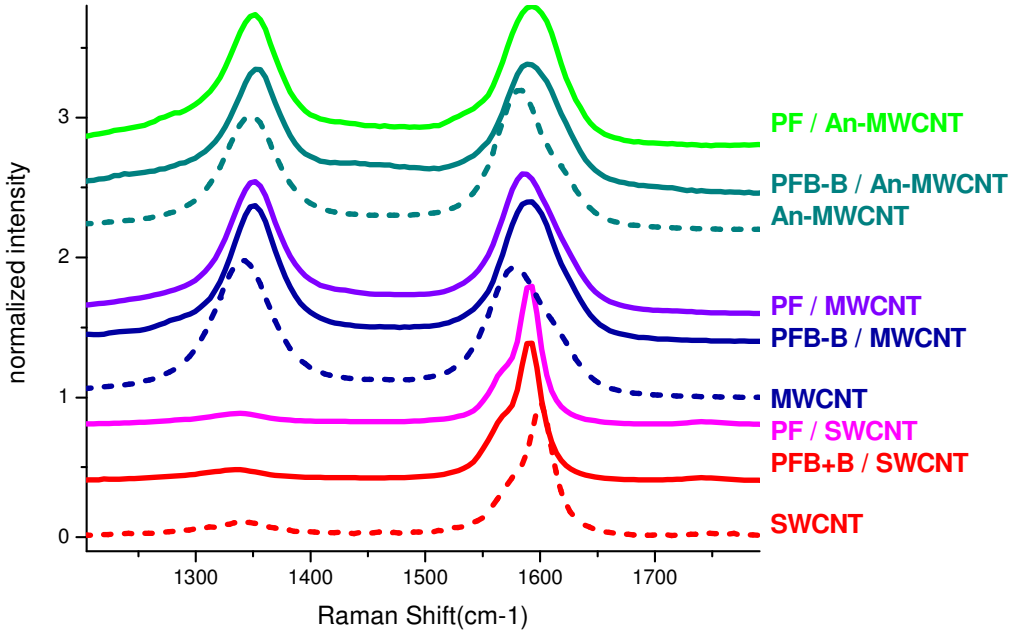

Figure 61. The Raman analysis of the samples Set-1, Set-2, Set-3, Set-4, Set-5, Set-6 interaction with PFB-B, PF and their bare Raman shift results as a reference.

The first order Raman signals shows typical peaks corresponds to SWCNTs and MWCNTs. As the relative intensity of D band (nearly 1360cm^{-1}) with respect to G band (1580 cm^{-1}) is accepted as an indicator for the defect density at the hexagonal network of the CNT sidewalls, the diminished D peak at the Raman signal of SWCNTs can be easily distinguished from MWCNTs. The G versus D peak intensity ratio indicates the defectiveness of the CNTs. Table 5 summarizes the results of the I(G)/I(D) ratios of corresponding PFB-B and PF polymers with different combinations of SWCNT, MWCNT and an-MWCNT.

Table 5. The Raman analysis of the samples Set-1, Set-2, Set-3, Set-4, Set-5, Set-6 interaction with PFB-B, PF and their bare Raman shift results as a reference.

	I(G)/I(D)		I(G)/I(D)		I(G)/I(D)
SWCNT	3.8	MWCNT	0.76	An-MWCNT	0.94
PFB-B / SWCNT	4.3	PFB-B / MWCNT	0.89	PFB-B /An-MWCNT	1.0
PF / SWCNT	4.0	PF / MWCNT	0.87	PF / An-MWCNT	0.73

The indicated I(G)/I(D) ratios are calculated via intensity results of corresponding peak which is achieved by peak-fitting programmer as areal density. As the results in each set of data showed the highest I(G)/I(D) ratio at PFB-B/CNT mixtures, the interaction of the polymer with carbon nanotube surface is enhanced at PFB-B polymer environment.

To summarize, functionalization of CNTs are done by using two different size distributed CPNs. After the interaction of with CPNs, CNTs can be debundled and dispersed in aqueous media. Data achieved from spectroscopic and microscopic techniques evidently confirm the interaction of CPNs with CNTs. As the optical properties of CPNs are not significantly changed after interaction with CNTs, suggest a non-covalent interaction. This feature can open new ways for usage of these CPN attached CNTs as CPNs are fluorescent and be advantageous for many applications such as light emitting diodes, bioimaging and biosensing.

The investigation of the interaction between conjugated polymers and different kind of CNTs are done. From the spectroscopic approach, dissimilar wrapping

mechanisms can be playing role on the interaction of polymer chains with CNT side-walls. The PFB-B polymer is good dispersant for SWCNTs and show total quenching. According to Raman analysis, PFB-B polymer is promising to decrease defect density that refers Br end groups can saturate dangling bonds at the defect sides. For PF case, the interaction with SWCNTs is not enhanced and Raman analysis also indicates the increase at the defect density (an-MWCNT) after the interaction with polymer.

5 CONCLUSIONS

In this work, starting from scratch, a new cheap and effective technique is developed for the synthesis of dense vertically aligned CNT arrays on oxidized Si(100) substrates through AC-CVD.

In this technique, aqueous solutions of the nitrate complex of catalyst metals are applied on the substrates, and left to dry under atmospheric conditions. Various concentrations of γ-Al_2O_3 powder dispersed in water, aluminium nitrate solutions and iron nitrate solutions are used for the preparation of catalyst layers. Two different application techniques are also investigated; spin coating and drop-wise addition using a micropipette. It is found that dense and well-ordered vertical CNT arrays can be synthesized by using aluminium nitrate and iron nitrate aqueous solutions. It is also found that before application of metal nitrate solutions, pre-treatment of the oxidized Si substrate surfaces using a mixture of H_2O:H_2O_2 solution allowed for the wetting of the surface by the nitrate solutions which resulted in a homogeneous coverage of the CNTs. By further optimization of the molarities of the nitrate solutions, large area ($>$ 1 cm^2) synthesis of vertically aligned CNT arrays is achieved. Using the technique developed in this work, dense CNT arrays up to 5 µm in thickness are easily synthesized on oxidized Si substrates and even on various metallic surfaces within 15 minutes.

The structural characterization of synthesized CNT arrays is done by microscopic techniques; SEM and TEM. The Raman signatures, SEM and TEM analysis concluded that the synthesized CNTs are MWCNTs. TEM analysis indicates size diameter of MWCNTs are in the range of 10-30 nm. Dynamic CA measurements done on various samples synthesized by sandwich method concluded that some of them kept super-hydrophobic character even after 30 minutes to water exposure. Hydrophobic properties of CNT arrays are compared against variations at catalyst and base layer concentrations.

The stable dispersion of CNTs synthesised by AC-CVD technique, is achieved by functionalization of them with CPNs in aqueous media. After the interaction between CNTs-CPNs is achieved, stable dispersion of CNTs in water media is enhanced. The investigation of the interactions are done through spectroscopic and microscopic routes. The interaction of CPNs with the side-walls of CNTs is found out from optical properties of CPNs. As there is not a significant change is observed at optical properties of CPNs after interaction with CNTs, non-covalent interection is said to be dominant.

The flourescent property of CPNs are adventageous as they can be used in water based systems with simple detection under UV radiation. They did not show total quenching after interaction with MWCNTs, CPN-CNT mixture turn to blue colored solution under UV radiation. Moreover, attached CPNs on MWCNTs can be detected by this flourescent property of CPNs. The combination of good dispersibility of CNTs in water and attached flourescent nanoparticle to side-walls, may open new routes towars biological and other application areas.

Investigation of possible interaction mechanisms between CNT side-walls and polymers are detected against two type of conjugated polymers as; Br end grouped and alkyl grouped. The interaction types of CPs with CNT side-walls is analysed by PFB-B and PF with respect to three different CNT types (SWCNT, MWCNT and an-MWCNT). The defect sides of CNT side-walls are found to be important factor playing role on nature of interaction between polymers. Also, different polymer types can change the interaction mechanism within CNT-side walls and CPs such as; wrapping of polymer chains around CNTs, extended orientation of polymer chains or not.

6 FUTURE WORK

The synthesis of vertically aligned CNT arrays is succeeded by mentioned methods previously. Besides iron nitrate usage, cobalt nitrate and nickel nitrate aqueous solutions are applied for sandwich method as catalyst layer. The best efficient catalyst is examined by changing only the applied catalyst layer solution type. As a result, Iron nitrate added sample show best vertically alignment and homogenous film formation. In other samples, the CNTs are grown at specific regions on substrate without vertical alignment. The sandwich method is detected towards different transition metal salts as catalyst, according to our conditions with Iron nitrate usage all requirements are achieved for successful VANTA growth. The different spreading and drying mechanisms of transition metals salts on oxidized Si(100) surface can be further worked on by using other transition metal salts or combination of them to have a better catalytic activity for VANTA growth.

As an improvement at catalyst design we have also tried preparation of solution based precursor methods dissolving metal nitrates in non-aqueous media. To detect the wetting and spreading property of applied solutions on Si(100), volatile solvents such as; ethanol, acetone and THF is preferred. In these solvents, equal amounts of iron nitrate and aluminium nitrate salts dissolved. After application of same volume of solutions on substrate, the samples having acetone and THF as solvents crystallize immediately during evaporation. The sample with ethanol solvent leads formation of a thin film of catalyst that is coloured with inhomogeneous drying pattern. As a result of introducing these samples to AC-CVD system, only the sample prepared with ethanol used as solvent resulted with the synthesis of vertically aligned CNT arrays. The high of the vertically aligned CNTs are not homogenous at every point of the sample and the film thickness varies in the range of 4 μm - 8 μm. This solvent effect on catalyst patterning should be studied on. If the mechanism behind inhomogeneous drying pattern is eliminated, by volatile solvents continuous mass production of vertically aligned CNT arrays can be possible.

By obtained good results from usage of ethanol solvent, aluminium nitrate and iron nitrate mixtures are applied on different substrate types such as; titanium and stainless steel 1 inch samples. The resulted CNT array synthesis can be seen in Figure 61, substrates with and without CNT array synthesis on. The same method is then applied on non-planer substrate, on teething rings.

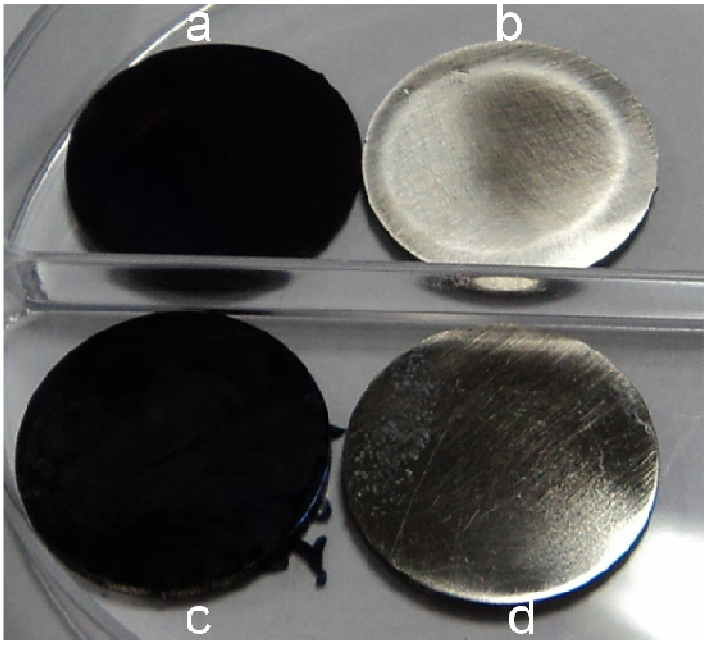

Figure 61. Photographs of titanium and stainless steel samples with and without CNT film; **a)** titanium substrate deposited with CNT arrays, **b)** bare titanium substrate, **c)** Stainless steel substrate deposited with CNT arrays, **d)** bare stainless steel substrate.

According to collaboration studies with Assoc. Prof. Dr. Rengul Çetin – Atalay, growth of CNTs on stainless steel teething ring is tested. The aim of this aspect is to achieve anti-bacterial surface modification by CNT growth. The first part of the work is done by achieving good coverage of CNT on the all the parts of the non-planar, cylindrical architecture of the teething ring. The second part of the work includes the obtaining results from bacterial growth experiments under specified conditions. Unfortunately, the tests are not completed yet. This CNT grown samples are also useful during sterilization steps before the bacterial growth as CNTs are stable up to 600^{o}C. In Figure 62, SEM images of the untreated and CNT grown teething ring surfaces can be seen.

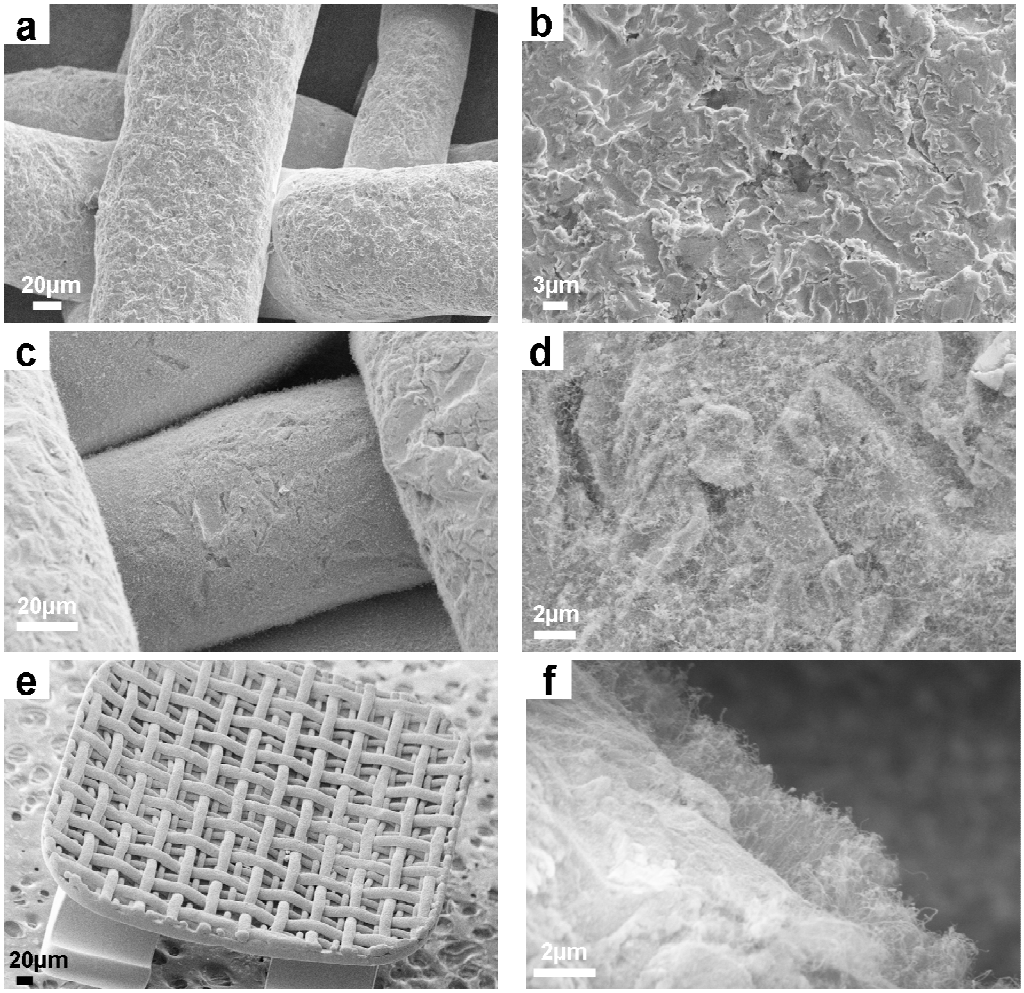

Figure 63. SEM images of; **a)** teething ring, without any treatment, **b)** high magnification SEM image of stainless steel teething ring surface, **c)** after CNT grown on teething ring , **d)** high magnification image of CNTs grown on the cylindrical architecture, **e)** general view of teething ring, **f)** side view image of the CNT arrays that is grown on stainless steel teething ring.

The computational modelling (DFT calculations) of CP-CNT interactions are being worked on by Assoc. Prof. Dr. Oğuz Gülseren. With the computational results, additions to the CP-CNT interactions can be made. Unclear parts of the wrapping mechanism of polymer around side-walls of CNTs can be better understood by DFT calculations.

The investigation of CPN-CNT interaction may open new routes towards toxicity experiments of CNTs. By the fluorescent CPNs the accumulated areas of CPN attached CNTs can be detected. There are limitations against studies as the water solubility of CNTs has not been reached as much as before. Generally organic solvents are used which are cancerogenic. For this reason, introducing of the CPN-CNT mixtures into living organisms can be studied as soon as possible.

REFERENCES

[1] Monthioux M., Kuznetsov V.L., *Carbon*, **2006**, 44, 1621.

[2] Bethune D.S., Kiang C.H., De Vries M.S., Gorman G., Savoy R., *Nature*, **1993,** 363, 605.

[3] Ijima S., Ichihashi T., *Nature*, **1993**, 363, 603.

[4] Jamieson V., *Physics World*, **2000**,13, 6.

[5]Choi W. B., Chung D. S., Kang J. H., Kim H. Y., Jin Y. W., Han I. T., Lee Y. H., Jung J. E., Lee N. S., Park G. S., Kim J. M., *Appl. Phys. Lett*., **1999**, 75, 3129.

[6]Vigolo B., Penicaud A., Coulon C., Sauder C., Pailler R., Journet C., Bernier P., Poulin P., *Science*, **2000**, 290, 1331.

[7]Varghese O. K., Kichambre P. D., Gong D., Ong K. G., Dickey E. C., Grimes C. A.,*Sensors and Actuators B*, **2001**, 81, 32.

[8]Sugie H., Tanemura M., Filip V., Iwata K., Takahashi K., Okuyamab F., *Appl. Phys. Lett.*, **2001**,78, 2578.

[9] Sullivan, Robertson J., Zhou J., Allan O., Coll B., *MRS Symposium Proceedings*, **2000**, 593.

[10] Robertson J., Friedmann T., Geohegan D., Luzzi D., Ruoff R., *MRS Symposium Proceedings*, **2001**, 675.

[11] Hitchman M., Jensen K., *Academic Press*, **1997**.

[12] Barthlott W., Neinhuis C., *Planta*, **1997**, 202, 1.

[13] Patankar N.A., *Langmuir*, **2004**, 20, 8209.

[14] Sethi S., Ge L., Ci L., Ajayan P. M., Dhinojwala A., *Nano letters*, **2008**, 8, 822.

[15] Ausman K.D., Piner R., Lourie O., Ruoff R.S.,*J. Phys. Chem. B*, **2000**, 104, 38, 8911.

[16] Kroto H.W., Heath J.R., O'Brien S.C., Curl R.F., Smalley R.E., *Nature*, **1985**, 318, 162.

[17] Iijima S., *Nature*, **1991**, 354, 56.

[18] Radushkevich L.V., Lukyanovich V.M. *Zurn Fisic Chim*, **1952**, 26, 88.

[19] Hamada N., Sawada S., Oshiyama A., *Phys. Rev. Lett.* **1992**, *68*, 54.

[20] Saito R., Dresselhaus G., Dresselhaus M. S., *Imperial College Press*, **1998**.

[21] Rao A.M., Richter E., Bandow S., Chase B., Eklund P.C., Williams K.A., Fang S., Subbaswamy K.R., Menon M., Thess A., *et al*., *Science*, **1997**,275, 187.

[22] Ajayan P.M., Otto Z., Zhou, *Topics in Applied Physics*, **2001**, 80, 391-425.

[23]Kucukayan G., Ovali R., Ilday S., Baykal B., Yurdakul H., Turan S., Gulseren O. and Bengu E., *Carbon*, **2011**, 49(2), 508.

[24] Ebbesen T. W., Ajayan P. M., *Nature*, **1992**, 358, 220.

[25] Thess A., Lee R., Nikolaev P., Dai H. J., Petit P., Robert J., Xu C.H., Lee Y.H., Kim S.G., Rinzler A.G., Colbert D.T., Scuseria G.E., Tomanek D., Fischer J. E., Smalley R.E., *Science*, **1996**, 273, 483.

[26] Dai H., *Surf. Sci*., **2002**, 500, 218.

[27] Dai H., *Acc. Chem. Res.*, **2002**, 35, 1035.

[28] Dai H., Kong J., Zhou C., Franklin N., Tombler T., Cassell A., Fan S., Chapline M., *J. Phys. Chem.*, **1999**, 103, 11246.

[29] Merkulov V.I., Melechko A.V., Guillorm M.A., Lowndes D.H., Simpson M.L., *Appl. Phys. Lett.*, **2001**, 79, 2970.

[30] Teo K.B.K., Chhowalla M., Amaratunga G.A.J., Milne W.I., Pirio G., Legagneux P., Pribat D., Hasko D.G., *Appl. Phys. Lett.*, **2002**, 80, 2011.

[31] Delzeit L., McAninch I., Cruden B.A., Hash D., Chen B., Han J., Meyyappan M., *J. Appl. Phys.*, **2002**, 91, 6027.

[32] Shiratori Y., Hiraoka H., Takeuchi Y., Itoh S., Yamamoto M., *Appl. Phys. Lett.*, **2003**, 82, 2485.

[33] Wang N., Yao D., *Appl. Phys. Lett.*, **2001**, 78 ,4028.

[34] Dresselhaus M.S., Pimenta, M.A., Eklund, P.C., Dresselhaus G., *Springer*, **2000**, 42, 314-359.

[35] Kastner J., Pichler T., Kuzmany H., Curran S., Blau W., Weldon D.N., Delamesiere M., Draper S., Zandbergen H., *Chemical Physics Letters*, **1994**, 221**,** 53.

[36] Palacin T., Khanh H. L., Jouselme B., Jegou P., Filoramo A., Ehli C., Guldi D.M., Campidelli S., *J. Am. Chem. Soc.*, **2009**, 131, 15394.

[37] Yuan W. Z., Zhao H., Shen X. Y., Mahtab F., Lam J.W.Y., Sun J.Z., Tang B.Z., *Macromolecules*, **2009**, 42, 9400.

[38] Kumar N.A., Kim S. H., Cho B.G., Lim K.T., Jeong Y.T., *Colloid Polym. Sci.*, **2009**, 287, 97.

[39] Park S., Yang H.-S., Kim D., Job K., Jon S., *Chem. Commun.*, **2008**, 2876.

[40] Wong N., Kam S., O'Connell M., Wisdom J.A., Da H., *Proc. Natl. Acad. Sci*., **2005**, 102, 11600.

[41] Lacerda L., Faffa S., Prato M., Bianco A., Kostarelos K., *Nanotoday*, **2007**, 2, 38.

[42] Kang Y.K., Lee O., Deria P., Kim S.H., Park T., Bonnell D.A., Saven J.G., Therien M.J., *Nano Lett*., **2009**, 9, 1414.

[43] Chen J., Liu H., Weimer W.A., Halls M.D., Waldeck D.H., Walker G.C., *J. Am. Chem. Soc.*, **2002**, 124, 9034.

[44] Zou J., Khondaker S. I., Huo Q., Zhai L., *Adv. Funct.Mater.*, **2009**, 19, 479.

[45] Zou J., Liu L., Chen H., Khondaker S.I., McCullough R.D., Huo Q., Zhai L., *Adv. Mater*., **2008**, 20, 2055.

[46] Chen F., Wang B., Chen Y., Li L.J., *Nano Lett*., **2007**, 7, 3013.

[47] Star A., Stoddart J.F., Steuerman D., Diehl M., Boukai A., Wong E.W., Yang X., Chung S.W., Choi H., Heath J.R., *Angew. Chem., Int. Ed*., **2001**, 40, 1721.

[48] Nish A., Hwang J.Y., Doig J., Nicholas R.J., *Nanotechnology*, **2008**, 19, 095603.

[49] Hwang J.Y., Nish A., Doig J., Douven S., Chen C.W., Chen L.C., Nicholas R.J., *J. Am. Chem. Soc.*, **2008**, 130, 3543.

[50] Chen F.M., Zhang W., Jia M., Wei L., Fan X.F., Kuo J.L., Chen Y., Chan-Park M.B., Xia A., Li L.J., *J. Phys. Chem. C* , **2009**, 113, 14946.

[51] Collison C.J., Pellizzeri S., Ambrosio F., *J. Phys. Chem. B*, **2009**, 113, 5809.

[52] Geng J., Kong B.S., Yang S.B., Youn S.C., Park S., Joo T., Jung H.T., *Adv. Funct. Mater.*, **2008**, 18, 2659.

[53] Baykal B., Ibrahimova V., Er G., Bengü E. and Tuncel D., *Chem. Commun.,* **2010**, 46, 6762.

[54] Ajayan P.M., Stephan O., Colliex C., Trauth D., *Science*, **1994**, 265, 1212.

[55] Heer W.A., Chatelain A., Ugarte D., *Science*, **1995**, 270, 1179.

[56] Li W.Z., Xie S.S., Qian L.X., Chang B.H., Zou B.S., Zhou W.Y., Zhao R.A., Wang G., *Science*, **1996**, 274, 1701.

[57] Dresselhaus M.S.; Dresselhaus G., Avouris P., *Springer*, **2001**.

[58] Hata K., Futaba D.N, Mizuno K., Namai T., Yumura M., Iijima S., *Science*, **2004**, 306, 1362.

[59] Saito Y., *Carbon*, **1995**, 33, 979.

[60] Harutyunyan A.R., Mora E., Tokune T., Bolton K., Rosen A., Jiang A., Aisthi N., Curtarolo S., *Appl. Phys. Lett.*, **2007**, 90, 163120/1-163120/3.

[61] Kim N.S., Lee Y.T., Park J.H., Ryu H., Lee H.J., Choi S.Y., Choo J.B., *J. Phys. Chem. B*, **2002**, 106, 9286.

[62] Sinnott S.B., Andrews R., Qian D., Rao A.M., Mao Z., Dickey E.C., Derbyshire F., *Chem. Phys. Lett*, **1999**, 315, 25.

[63] Helveg S., Lopez-Cartes C., Sehested J., HansenP. L., Clausen B.S., Rostrup-Nielsen J.R., Abild-Pedersen F., Norskov J.K., *Nature*, **2004**, 427, 426.

[64] Louchev O.A., Sato Y., Kanda H., *Appl. Phys. Lett*., **2002,** 30, 15.

[65] Jung Y.J., Wei B., Vajtai R., Ajayan P.M., *Nano Lett*., **2003**, 3, 561.

[66] Ng H.T., Chen B., Koehne J.E., Cassell A.M., Li J., Han J., Meyyappan M., *J. Phys. Chem. B*, **2003**, 107, 8484.

[67] Talapatra S., Kar S., Pal S.K., Vajtai R., Ci L., Victor P., Shaijumon M.M., Kaur S., Nalamasu O., Ajayan P.M., *Nature Nanotechnology*, **2006**, 1, 112-116.

[68] Parthangal P.M., Cavicchi R.E., Zachariah M.R., *Nanotechnology*, **2007**, 18, 185005.

[69] Nasibulin A.G., Pikhitsa P.V., Jiang H., Kauppinen E.I., *Carbon*, **2005**, 43, 2251.

[70] Fan S.S., Chapline M.G., Franklin N.R., Tombler T.W., Cassell A.M., Dai H.J., *Science*, **1999**, 283, 512.

[71] Pint C.L., Alvarez N.T., Hauge R.H., *Nano Res*., 2009, **2,** 526.

[72]Chakrabarti S., Kume H., Pan L.J., Nagasaka T., Nakayama Y., *J. Phys. Chem. C*, **2007**, 111, 1929.

[73]Kim H.S., Kim B., Lee B., Chung H., Lee C.J., Yoon H.G., Kim W., *J. Phys. Chem. C*, **2009**, 113, 17983.

[74] Choi G.S., Cho Y.S., Son K.H., Kim D.J., *Microelectron Eng*, **2003**, 66, 77.

[75] Murakami Y., Miyauchi Y., Chiashi S., Maruyama S., *Direct Chem Phys Lett*, **2003**, 377, 49.

[76] Dai H. J., Rinzler A. G., Nikolaev P., Thess A., Colbert D.T., Smalley R.E., *Chem Phys. Lett.* **1996**, *260*, 471.

[77] Maruyama S., Kojima R., Miyauchi Y., Chiashi S., Kohno M., *Chem. Phys. Lett.*, **2002**, 360, 229.

[78]Kimura Y., Numasawa T., Nihei M., Niwano M., *Appl. Phys. Lett*., **2007**, 90, 073109.

[79] Guo Y., Shi D.L., Cho H., Dong Z.Y., Kulkarni A., Pauletti G.M., *Adv Funct Mater*, **2008**, 18, 2489..

[80] Nednoor P., Chopra N., Gavalas V., Bachas L.G., Hinds B.J., *Chem Mater*, **2005**, 17, 3595.

[81] Wang J., Musameh M., *Anal Chem*, **2003**, 75, 2075.

[82] Lin Y.H., Lu F., Tu Y., Ren Z.F., *Nano Lett*, 2004, 4, 191.

[83] Liu Z.M., Han B.X., *Adv Mater*, **2008**, 20, 1.

[84] Yu C., Kim Y.S., Kim D., Grunlan J.C., *Nano Lett*., **2008**, 8(12), 4428.

[85] Serp P., Corrias M., Kalck P., *Appl Catal A*, **2003**, 253, 337.

[86] Pantarotto D., Briand J., Prato M., Pianco A., *Chem Commun*, 2004, 10, 16.

[87] Li P.H., Lim X.D., Zhu Y.W., Yu T., Ong C.K., Shen Z.X., *J Phys Chem B*, **2007**, 111, 1672.

[88] Ebbesen T.W., Hiura H., Bisher M.E., Treacy M.M.J., Shreeve-Keyer J.L., Haushalter R.C., *Adv Mater*, **1996**, 8, 155.

[89] Kakade B., Mehta R., Durge A., Kulkarni S., Pillai V., *Nano Lett*, **2008**, 8, 2693.

[90] Wenzel R.N., *Ind Eng Chem*, **1936**, 28, 988.

[91] Cassie, Baxter S., *Trans Faraday Soc.*, **1944**, 40, 546.

[92] Bico J., Thiele U., Quere D., *Colloids Surf A*, **2002**, 206, 41.

[93] Liu H., Zhaia J., Jiang L., *Soft Matter*, **2006**, 2, 811.

[94] El-Shereafy E., Abousekkina M.M., Mashaly A., El-Ashry M., *J. Radioanal. Nucl. Chem.*, **1998**, 237, 183.

[95] Zhao Y., Huang D., Saito Y., *Nanotechnology*, 2007, **18,** 445608.

[96] Lau K.K.S., Bico J., Teo K.B.K., Chhowalla M., Amaratunga G.A.J., Milne W.I., McKinley G.H., Gleason **K.K**., *Nano Lett.*, **2003**, 3, 1701-1705.

[97] Chakrapani N., Wei B., Carrillo A., Ajayan P.M., Kane R.S., *Proc. Natl. Acad. Sci.*, **2004**, 101, 4009.

[98] Futaba D.N., Hata K., Yamada T., Hiraoka T., Hayamizu Y., Kaku-date Y., Tanaike O., Hatori H., Yumura M., Iijima S., *Nature*, **2006**, 5, 987.

[99] Belin T., Epron F., *Mater. Sci. Eng., B*, **2005**, 119, 105.

[100] Dresselhaus M.S., Dresselhaus G., Saito R., Jorio A., *Phys.Rep*., **2005**, 409, 47.

[101] Antunes E.F., Lobo A.O., Corat E.J., Trava-Airoldi V.J., Martin A.A., Verissimo C., *Carbon*, **2006**, 44, 2202.

[102] DiLeo R.A., Landi B. J., Raffaelle R.P., *J. Appl. Phys*., **2007**, 101, 064307.

[103] Patole A.S., Patole S.P., Yoo J.B., Ahn Y.H., Kim T.H., *J. Polym. Sci., Part A: Polym. Chem.*, **2009**, 47, 1523.

[104] Manuscript being prepared.

[105] Cheng F., Imin P., Maunders C., Botton G., Adronov A., *Macromolecules,* **2008**, 41, 2304.

APPENDIX

Appendix-A: Cold trap design

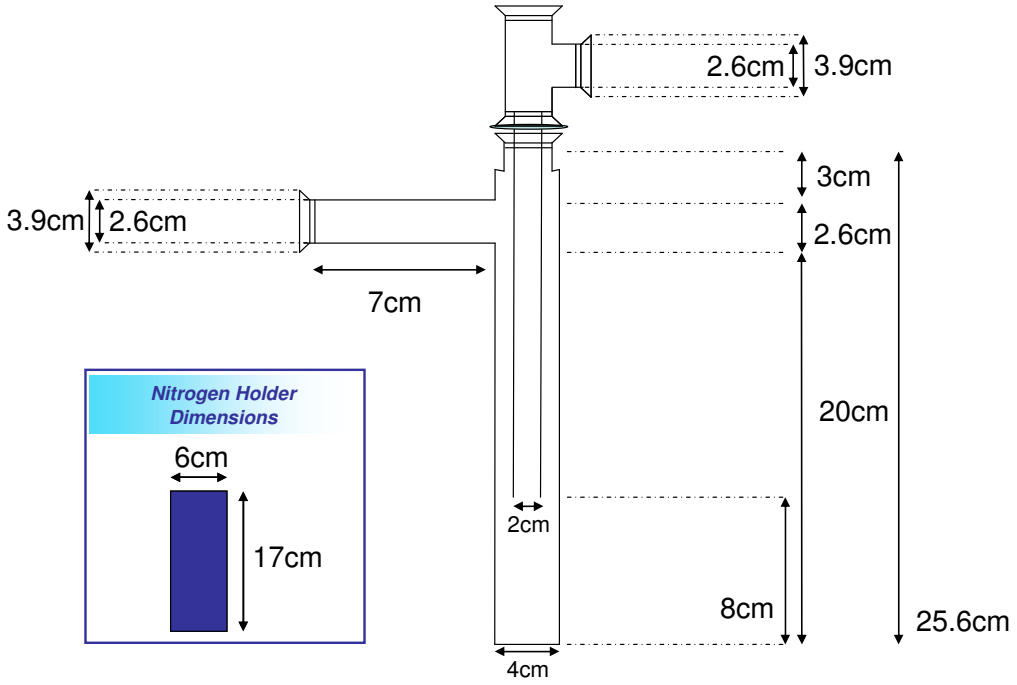

Figure 63. Detailed cold trap design dimensions and indication of liquid nitrogen holder dimensions.

Cold trap design is done according to increase life time of vacuum pump by limiting corrosive gases. Cold trap is stainless steel and the connections with AC-CVD system is done by O-ring. The working principle is collection of gases and decomposed ethanol by condensation at the trap. Liquid nitrogen contained holder is replaced around trap so that the trap is achieved a low equilibrium temperature in this environment. The implementation of the cold trap to AC-CVD system done by the results of test experiments about changed distances from valve, in Figure 64. According to our results, 1st approach, near to valve did not give good results for CNT growth but 2nd approach at middle of valve and pump is did not effect the synthesis conditions. So, the replacement of cold trap is done at the middle distance

between valve and vacuum pump. By this way the synthesized VANTA samples did not effective from the additional equipment at the gas line.

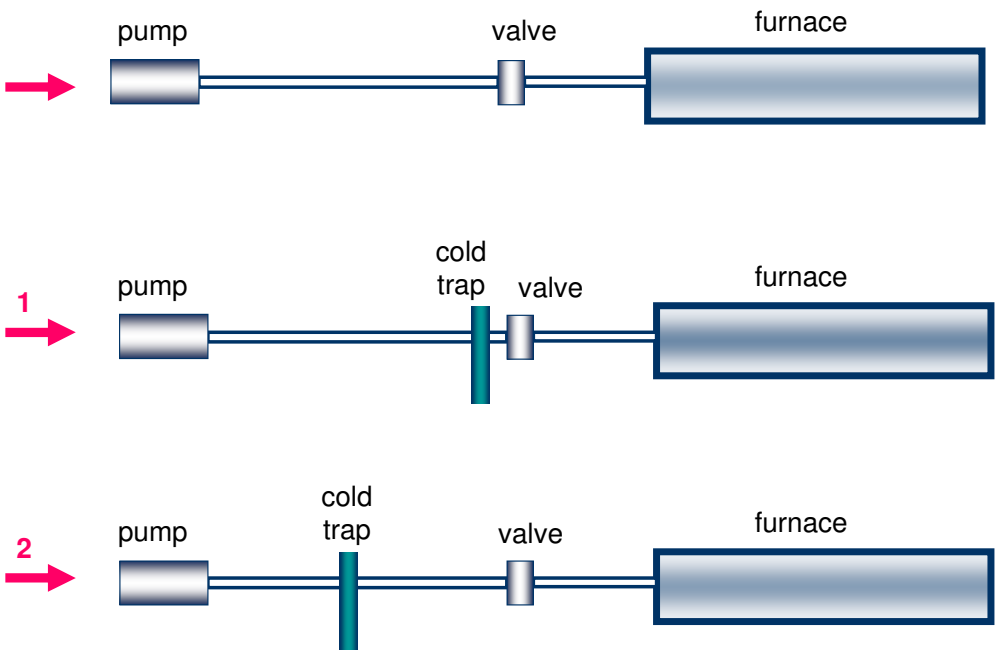

Figure 64. Replacement of cold trap to AC-CVD gas line. At the top initial conditions without cold trap. 1st approach, near to valve, 2nd approach at middle of valve and pump.

Appendix-B: Calculation of the carbon amount at 1x1 VANTA sample

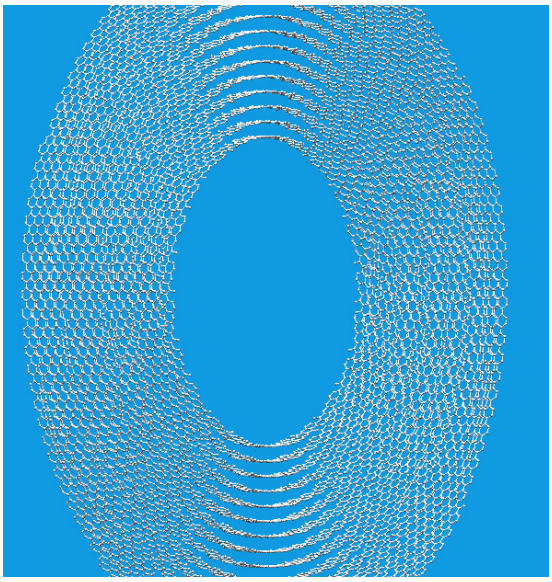

Figure 64. A model of MWCNT 5 Å in length, having 15 side walls is calculated for C atoms. (Nanotube Modeller Programme) As a result 11415 C atoms is computed for 5 Å nanotube cross-section.

As an approximation;

→ 11415 atoms for 5 Å

→ 22930 atoms for 1 nm

→ 22930000 atoms for 1 µm

→ 1.15×10^{8} atoms for 5 µm in length MWCNT

→ 10^{4} nm^{2} includes 1 MWCNT

→ 10^{14} nm^{2} total area of sample

→ 10^{10} MWCNT at that total area

→ 1.15×10^{18} amount of carbon atoms at that area

→ 0.5×10^{-5} mol carbon atoms

→ 6×10^{-5} gr carbon in 1x1 cm^{2} VANTA sample

→ **6×10^{-2} miligram** Carbon in our 1x1 cm^{2} VANTA sample

Some of the figures in this manuscript are used from previous publications and their copyright permissions are presented below.

THE AMERICAN ASSOCIATION FOR THE ADVANCEMENT OF SCIENCE LICENSE TERMS AND CONDITIONS

Jan 08, 2011

This is a License Agreement between Beril Baykal ("You") and The American Association for the Advancement of Science ("The American Association for the Advancement of Science") provided by Copyright Clearance Center ("CCC"). The license consists of your order details, the terms and conditions provided by The American Association for the Advancement of Science, and the payment terms and conditions.

All payments must be made in full to CCC. For payment instructions, please see information listed at the bottom of this form.

License Number	2583031444464
License date	Jan 06, 2011
Licensed content publisher	The American Association for the Advancement of Science
Licensed content publication	Science
Licensed content title	Large-Scale Synthesis of Aligned Carbon Nanotubes
Licensed content author	W. Z. Li, S. S. Xie, L. X. Qian, B. H. Chang, B. S. Zou, W. Y. Zhou, R. A. Zhao, G. Wang
Licensed content date	Dec 6, 1996
Volume number	274
Issue number	5293
Type of Use	Thesis / Dissertation
Requestor type	Other Individual
Format	Print and electronic
Portion	Figure
Number of figures/tables	2
Order reference number	56
Title of your thesis / dissertation	SYNTHESIS OF VERTICALLY ALIGNED CNT ARRAYS USING LIQUID BASED PRECURSORS AND THEIR FUNCTIONALIZATION USING CONJUGATED POLYMERS
Expected completion date	Jan 2011
Estimated size(pages)	100
Total	0.00 USD
Terms and Conditions	

THE AMERICAN ASSOCIATION FOR THE ADVANCEMENT OF SCIENCE LICENSE TERMS AND CONDITIONS

Jan 08, 2011

This is a License Agreement between Beril Baykal ("You") and The American Association for the Advancement of Science ("The American Association for the Advancement of Science") provided by Copyright Clearance Center ("CCC"). The license consists of your order details, the terms and conditions provided by The American Association for the Advancement of Science, and the payment terms and conditions.

All payments must be made in full to CCC. For payment instructions, please see information listed at the bottom of this form.

License Number	2583040216728
License date	Jan 06, 2011
Licensed content publisher	The American Association for the Advancement of Science
Licensed content publication	Science
Licensed content title	Water-Assisted Highly Efficient Synthesis of Impurity-Free Single-Walled Carbon Nanotubes
Licensed content author	Kenji Hata, Don N. Futaba, Kohei Mizuno, Tatsunori Namai, Motoo Yumura, Sumio Iijima
Licensed content date	Nov 19, 2004
Volume number	306
Issue number	5700
Type of Use	Thesis / Dissertation
Requestor type	Other Individual
Format	Print and electronic
Portion	Figure
Number of figures/tables	1
Order reference number	58
Title of your thesis / dissertation	SYNTHESIS OF VERTICALLY ALIGNED CNT ARRAYS USING LIQUID BASED PRECURSORS AND THEIR FUNCTIONALIZATION USING CONJUGATED POLYMERS
Expected completion date	Jan 2011
Estimated size(pages)	100
Total	0.00 USD
Terms and Conditions	

American Association for the Advancement of Science

TERMS AND CONDITIONS

Regarding your request, we are pleased to grant you non-exclusive, non-transferable permission, to republish the AAAS material identified above in your work identified above, subject to the terms and conditions herein. We must be contacted for permission for any uses other than those specifically identified in your request above.

The following credit line must be printed along with the AAAS material: "From [Full Reference Citation]. Reprinted with permission from AAAS."

All required credit lines and notices must be visible any time a user accesses any part of the AAAS material and must appear on any printed copies and authorized user might make.

This permission does not apply to figures / photos / artwork or any other content or materials included in your work that are credited to non-AAAS sources. If the requested material is sourced to or references non-AAAS sources, you must obtain authorization from that source as well before using that material. You agree to hold harmless and indemnify AAAS against any claims arising from your use of any content in your work that is credited to non-AAAS sources.

If the AAAS material covered by this permission is published in Science during the years 1974 - 1994, you must also obtain permission from the author, who may grant or withhold permission, and who may or may not charge a fee if permission is granted. See original article for author's address. This condition does not apply to news articles.

The AAAS material may not be modified or altered except that figures and tables may be modified with permission from the author. Author permission for any such changes must be secured prior to your use.

Whenever possible, we ask that electronic uses of the AAAS material permitted herein include a hyperlink to the original work on AAAS's website (hyperlink may be embedded in the reference citation).

AAAS material reproduced in your work identified herein must not account for more than 30% of the total contents of that work.

AAAS must publish the full paper prior to use of any text.

AAAS material must not imply any endorsement by the American Association for the Advancement of Science.

This permission is not valid for the use of the AAAS and/or Science logos.

AAAS makes no representations or warranties as to the accuracy of any information contained in the AAAS material covered by this permission, including any warranties of

merchantability or fitness for a particular purpose.

If permission fees for this use are waived, please note that AAAS reserves the right to charge for reproduction of this material in the future.

Permission is not valid unless payment is received within sixty (60) days of the issuance of this permission. If payment is not received within this time period then all rights granted herein shall be revoked and this permission will be considered null and void.

In the event of breach of any of the terms and conditions herein or any of CCC's Billing and Payment terms and conditions, all rights granted herein shall be revoked and this permission will be considered null and void.

AAAS reserves the right to terminate this permission and all rights granted herein at its discretion, for any purpose, at any time. In the event that AAAS elects to terminate this permission, you will have no further right to publish, publicly perform, publicly display, distribute or otherwise use any matter in which the AAAS content had been included, and all fees paid hereunder shall be fully refunded to you. Notification of termination will be sent to the contact information as supplied by you during the request process and termination shall be immediate upon sending the notice. Neither AAAS nor CCC shall be liable for any costs, expenses, or damages you may incur as a result of the termination of this permission, beyond the refund noted above.

This Permission may not be amended except by written document signed by both parties.

The terms above are applicable to all permissions granted for the use of AAAS material. Below you will find additional conditions that apply to your particular type of use.

FOR A THESIS OR DISSERTATION

If you are using figure(s)/table(s), permission is granted for use in print and electronic versions of your dissertation or thesis. A full text article may be used in print versions only of a dissertation or thesis.

Permission covers the distribution of your dissertation or thesis on demand by ProQuest / UMI, provided the AAAS material covered by this permission remains in situ.

If you are an Original Author on the AAAS article being reproduced, please refer to your License to Publish for rules on reproducing your paper in a dissertation or thesis.

Gratis licenses (referencing $0 in the Total field) are free. Please retain this printable license for your reference. No payment is required.

If you would like to pay for this license now, please remit this license along with your payment made payable to "COPYRIGHT CLEARANCE CENTER" otherwise you will be invoiced within 48 hours of the license date. Payment should be in the form of a check or money order referencing your account number and this invoice number RLNK10908953. Once you receive your invoice for this order, you may pay your invoice by credit card. Please follow instructions provided at that time.

Make Payment To:

Copyright Clearance Center

Dept 001
P.O. Box 843006
Boston, MA 02284-3006

If you find copyrighted material related to this license will not be used and wish to cancel, please contact us referencing this license number 2583031444464 and noting the reason for cancellation.

Questions? customercare@copyright.com or +1-877-622-5543 (toll free in the US) or +1-978-646-2777.

ELSEVIER LICENSE
TERMS AND CONDITIONS

Jan 08, 2011

This is a License Agreement between Beril Baykal ("You") and Elsevier ("Elsevier") provided by Copyright Clearance Center ("CCC"). The license consists of your order details, the terms and conditions provided by Elsevier, and the payment terms and conditions.

All payments must be made in full to CCC. For payment instructions, please see information listed at the bottom of this form.

Supplier	Elsevier Limited The Boulevard,Langford Lane Kidlington,Oxford,OX5 1GB,UK
Registered Company Number	1982084
Customer name	Beril Baykal
Customer address	Bilkent University Main ANKARA, other 06800
License number	2584410892179
License date	Jan 08, 2011
Licensed content publisher	Elsevier
Licensed content publication	Carbon
Licensed content title	Who should be given the credit for the discovery of carbon nanotubes?
Licensed content author	Marc Monthioux, Vladimir L. Kuznetsov
Licensed content date	August 2006

Licensed content volume number	44
Licensed content issue number	9
Number of pages	3
Start Page	1621
End Page	1623
Type of Use	reuse in a thesis/dissertation
Intended publisher of new work	other
Portion	figures/tables/illustrations
Number of figures/tables /illustrations	1
Format	both print and electronic
Are you the author of this Elsevier article?	No
Will you be translating?	No
Order reference number	18
Title of your thesis/dissertation	SYNTHESIS OF VERTICALLY ALIGNED CNT ARRAYS USING LIQUID BASED PRECURSORS AND THEIR FUNCTIONALIZATION USING CONJUGATED POLYMERS
Expected completion date	Jan 2011
Permissions price	0.00 USD
Value added tax 0.0%	0.0 USD / 0.0 GBP
Total	0.00 USD
Terms and Conditions	

INTRODUCTION

1. The publisher for this copyrighted material is Elsevier. By clicking "accept" in connection with completing this licensing transaction, you agree that the following terms and conditions apply to this transaction (along with the Billing and Payment terms and conditions established by Copyright Clearance Center, Inc. ("CCC"), at the time that you opened your Rightslink account and that are available at any time at http://myaccount.copyright.com).

20. Thesis/Dissertation: If your license is for use in a thesis/dissertation your thesis may be submitted to your institution in either print or electronic form. Should your thesis be published commercially, please reapply for permission. These requirements include permission for the Library and Archives of Canada to supply single copies, on demand, of the complete thesis and include permission for UMI to supply single copies, on demand, of the complete thesis. Should your thesis be published commercially, please reapply for permission.

Gratis licenses (referencing $0 in the Total field) are free. Please retain this printable license for your reference. No payment is required.

If you would like to pay for this license now, please remit this license along with your payment made payable to "COPYRIGHT CLEARANCE CENTER"

otherwise you will be invoiced within 48 hours of the license date. Payment should be in the form of a check or money order referencing your account number and this invoice number RLNK10910335.
Once you receive your invoice for this order, you may pay your invoice by credit card. Please follow instructions provided at that time.

Make Payment To:
Copyright Clearance Center
Dept 001
P.O. Box 843006
Boston, MA 02284-3006

If you find copyrighted material related to this license will not be used and wish to cancel, please contact us referencing this license number 2584410892179 and noting the reason for cancellation.

Questions? customercare@copyright.com or +1-877-622-5543 (toll free in the US) or +1-978-646-2777.